Soft Wearable Robotics for Ankle and Lower Body Gait Rehabilitation: Design, Modeling, and Implementation of Fabric-Based Actuators to Assist Human Locomotion

by

Carly Thalman

A Dissertation Presented in Partial Fulfillment
of the Requirements for the Degree
Doctor of Philosophy

Approved April 2021 by the
Graduate Supervisory Committee:

Hyunglae Lee, Co-Chair
Panagiotis Artemiadis, Co-Chair
Thomas Sugar
Wenlong Zhang

ARIZONA STATE UNIVERSITY

May 2021

ABSTRACT

This work presents the design, modeling, analysis, and experimental characterization and testing of soft wearable robotics for lower limb rehabilitation for the ankle and hip. The Soft Robotic Ankle-Foot Orthosis (SR-AFO) is a wearable soft robot designed using multiple pneumatically-powered soft actuators to assist the ankle in multiple degrees-of-freedom during standing and walking tasks. The flat fabric pneumatic artificial muscle (ff-PAM) contracts upon pressurization and assists ankle plantarflexion in the sagittal plane. The Multi-material Actuator for Variable Stiffness (MAVS) aids in supporting ankle inversion/eversion in the frontal plane. Analytical models of the ff-PAM and MAVS were created to understand how the changing of the design parameters affects tensile force generation and stiffness support, respectively. The models were validated by both finite element analysis and experimental characterization using a universal testing machine. A set of human experiments were performed with healthy participants: 1) to measure lateral ankle support during quiet standing, 2) to determine lateral ankle support during walking over compliant surfaces, and 3) to evaluate plantarflexion assistance at push-off during treadmill walking, and 4) determine if the SR-AFO could be used for gait entrainment. Group results revealed increased ankle stiffness during quiet standing with the MAVS active, reduced ankle deflection while walking over compliant surfaces with the MAVS active, and reduced muscle effort from the SOL and GAS during 40 - 60% of the gait cycle with the dual ff-PAM active. The SR-AFO shows promising results in providing lateral ankle support and plantarflexion assistance with healthy participants, and a drastically increased basin of entrainment, which suggests a capability to help restore the gait of impaired users in future trials. The ff-PAM actuators were used in an X-orientation to assist the hip in flexion and extension. The Soft Robotic Hip Exosuit (SR-HExo) was evaluated using the same set of actuators and trials with healthy participants

showed reduction in muscle effort during hip flexion and extension to further enhance the study of soft fabric actuators on human gait assistance.

DEDICATION *I dedicate this work to my brother, Joe, who helped me through the hardest of times and pulled me through to the light in even the darkest moments.*

ACKNOWLEDGMENTS

I would like to thank the wonderful mentors that I have had through this journey in both life and academia. I would like to thank Dr. Hyunglae Lee, who always helped motivate me and help me grow regardless of the circumstances. I want to thank him for showing me how to lead with respect and integrity, and to push me to be the best I could be. I would also like to thank Panagiotis Artemiadis, who also served as a valuable mentor to me in turbulent times and helped me learn and grow in my confidence professionally. I am grateful for you both in your fantastic leadership, critical mentoring roles, and kindness that you showed me throughout my research. I would also like to thank the amazing peers in my lab that have helped me grow and supported me every step of my journey. I would like to thank my fellow students Marielle Debeurre, Tiffany Hertzell, Varun Nalam, Omik Save, and Lily Baye-Wallace for the endless support, contributions, and motivation. Your company, positive attitudes, and welcoming nature made working with you a pleasant and important aspect of my degree. I would also like to acknowledge Panagiotis Polygerinos for initial mentorship and introducing me to the field of soft robotics in my undergraduate years. Finally, I would like to thank my closest friends and family for their endless encouragement and support, and my husband Cody Van Cleve for being my anchor.

TABLE OF CONTENTS

CHAPTER Page

CHAPTER Page

CHAPTER Page

CHAPTER Page

LIST OF TABLES

LIST OF FIGURES

Chapter 1

INTRODUCTION

A new and rapidly growing topic of research in wearable technologies is soft robotics. Over the past decade, assistive soft wearable robotic (SWR) devices have been advancing at an exponential rate, branching into numerous categories such as: mobility assistance achieving activities of daily living (ADL), robot-facilitated therapy, and human augmentation; to name a few. In robotics, the term "soft" is typically used to describe materials that conform to existing surroundings and are compliant when exposed to external forces or interact with objects of unknown geometries. The use of materials that are inherently soft is conducive to the development of robotic systems that have demonstrated potential for safer, more comfortable, and lower-cost alternatives when compared to rigid counterparts (Wehner *et al.*, 2013; Schiele and van der Helm, 2009). Research on soft robotics has proven that using such systems is effective for human-robot interaction, improved durability, and increased user comfort (Majidi, 2013). It is a field with much promise and many novel technologies that are quickly beginning to change the way we think about wearable, assistive mechanisms (Bao *et al.*, 2018; Majidi, 2013).

Soft mechatronic technologies have become more reliable, effective, and well known over the last decade, and have become an attractive solution for wearable robotic technologies (Bao *et al.*, 2018). There has been a gradual advancement from rigid exoskeletons with isolated compliant methods of actuation towards a paradigm of entirely soft, garment-like wearables that feel nearly transparent to the user (Granberry *et al.*, 2017). Wearable robotic devices made from soft, compliant materials have been gaining momentum in both academic and commercial settings over the past

decade (Bao *et al.*, 2018; Cianchetti *et al.*, 2018). The lightweight, low-cost characteristics of garment-like devices forgo heavy, bulky, and rigid components in favor of inherently soft and compliant materials such as silicone elastomers, fabrics, and other forms of flexible materials (Coyle *et al.*, 2018). This helps to alleviate issues with joint alignment that can be observed in some rigid exoskeletons (Schiele and van der Helm, 2009), and provide safer interaction with people and the environment around the robotic system. The compliance of the materials can easily conform to its surroundings, the user's joints, or the objects with which it interacts(Galiana *et al.*, 2012). Soft robotics offers an unmatched level of flexibility and versatility, resulting in systems that mold easily to their surroundings and the user for increased comfort, safety, and ease of use.

Some SWRs are entirely soft, monolithic, garment-like wearable devices, made from soft actuators, fabric, and other compliant materials; while other applications include minimal or reduced amount of rigid components as mounting points for the soft actuators. Categories of wearable robots can be simplified into four main groups as defined by Wearable Robotics Association (2015) and Exoskeleton Report (ExR) (2020): 1) Military, 2) Industrial, 3) Consumer, and 4) Medical. Most wearable devices aim to either provide assistance or augmentation. In this review, assistance is defined as an SWR with a goal of restoring a more "natural" movement of biomechanical behavior (Awad *et al.*, 2017b), and serves a role in accomplishing activities of daily living (ADL) (Spector and Fleishman, 1998). Augmentation is defined as an SWR that applies active external forces to a healthy user to increase the capability, strength and/or endurance of said user.

In this manuscript, SWRs are analyzed and sorted into upper body (UB) wearables, or lower body (LB) wearables categories. This review evaluates multiple types of actuator designs and approaches that provide active assistance. While the follow-

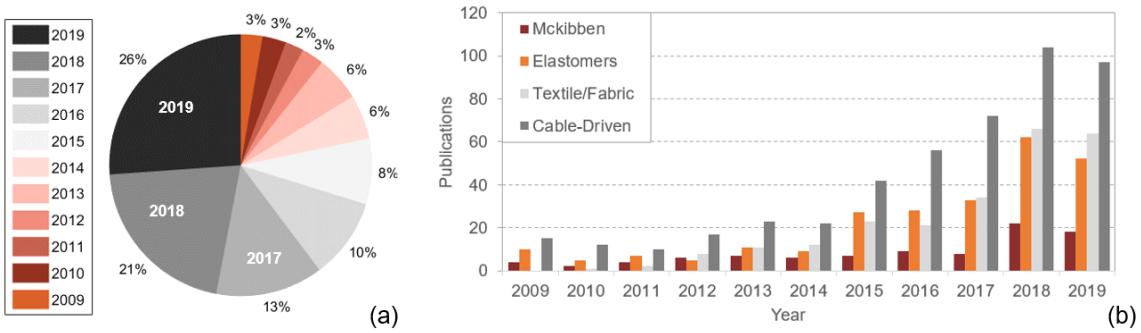

Figure 1.1: (a) Highlights the number of publications found on IEEE Xplore, including conference and journal publications, for research related to SWR between 2009 and 2019. Over the last decade, 57% of the existing research in SWR has been published in the span of the last three years. (b) Indicates the Number of publications found on IEEE Xplore, including conference and journal publications, for research related to SWR between 2009 and 2019. Papers are refined according to type of actuation.

ing sections briefly highlight the prevalence of passive types of assistance, this review focuses only on looking at SWRs that utilize active actuator assistance and therefore will exclude thorough examination or discussion regarding SWRs that rely on passive assistance. This review analyzes the two most prevalent, and rapidly expanding methods of providing active power, actuation, and assistance in SWRs: Cable-driven systems and fluidic actuation. While there are many other types of soft actuators being developed (as discussed in Section 3.4), this review aims to break down and analyze some of the most widely explored actuator designs, methods, and applications for SWR for cable-driven and fluidic actuation. Fluidic actuators are organized into subcategories based on the materials used in fabrication: McKibben/PAMs, Elastomers, and textiles/fabric-based actuators. Each aforementioned actuator design will be discussed in greater detail in Section 3.

1.1 Growing Trends in Assistive SWRs Over the Decade

In order to determine just how rapidly the interest in this sub-field of soft robotics has begun to grow, a meta-analysis of publications in this category is performed to

analyze the rate of expansion. IEEE Xplore is used as the primary search engine, and all meta-data is searched for the specified conditions to determine the number of publications that fit the selected criteria. For this search, only peer reviewed articles published as part of IEEE conference proceeding and journals listed in the IEEE Xplore search engine were included for the final publication count. The search was limited by year for each search, and the total number of publications was recorded from years spanning from 2009 to 2019, to obtain a record of relevant publications across the last decade. This data was collected on January $9th$ of 2020. The search parameters were limited articles that included the terms "soft" and "robot" in the title or main text, and also containing the words "wearable" and "assist" in the metadata of the publications. The resulting information of the meta-analysis is shown in Fig. 1.1a, which highlights that 60% of all publications on IEEE Xplore fitting the aforementioned criteria were published across 2019, 2018, and 2017, the last 3 years since this search was performed. This data indicates visible trends which show that soft robotics itself a rapidly growing field, and additionally that research into SWR has begun to expand at exponential rates in recent years. The last year evaluated (2019 from Fig. 1.1a), shows the highest number of publications fitting within the confines of the refined search criteria, with 26% of the search results appearing in the most recent year.

To further evaluate the trends across SWRs published during this time, each search was refined in the respective year of publication by the actuation methods used (Fig. 1.1b). These actuation methods, the pros and cons of each, as well as a more in-depth look are included in the following sections. The increasing trend in publications and research interest can also be observed for each of the following actuation types, though it is notable that while cable-driven systems appear to remain predominant in most years, textiles and passive SWRs have begun to gain more popularity among published

research. Where there were no notable SWR publications in 2009, these actuation method made up 16% of published work since 2017, and nearly 20% of the published SWR research in 2019.

A push for rapid advancement in wearable technologies in the early 2010s may be partially attributed to military and government-funded projects in the field of robotics for more simplistic, lower cost, and lighter wearable devices to enhance human performance. Some of these major projects started with funding from DARPA and NASA grants with the Warrior Web (Asbeck *et al.*, 2013) and the Armstrong (Kadivar *et al.*, 2017). These exosuits aimed to reduce the overall metabolic cost to soldiers, who walk prolonged distances while carrying heavy loads, as well as reduce ergonomic issues and increase prevention of work-related injuries for astronauts.

Chapter 2

REVIEW OF SOFT WEARABLE ROBOTICS

Soft mechatronic technologies have become more reliable, effective, and well known over the last decade, and have become an attractive solution for wearable robotic technologies (Bao *et al.*, 2018). There has been a gradual advancement from rigid exoskeletons with isolated compliant methods of actuation towards a paradigm of entirely soft, garment-like wearables that feel nearly transparent to the user (Granberry *et al.*, 2017). Wearable robotic devices made from soft, compliant materials have been gaining momentum in both academic and commercial settings over the past decade (Bao *et al.*, 2018; Cianchetti *et al.*, 2018). The lightweight, low-cost characteristics of garment-like devices forgo heavy, bulky, and rigid components in favor of inherently soft and compliant materials such as silicone elastomers, fabrics, and other forms of flexible materials (Coyle *et al.*, 2018). This helps to alleviate issues with joint alignment that can be observed in some rigid exoskeletons (Schiele and van der Helm, 2009), and provide safer interaction with people and the environment around the robotic system. The compliance of the materials can easily conform to its surroundings, the user's joints, or the objects with which it interacts(Galiana *et al.*, 2012). Soft robotics offers an unmatched level of flexibility and versatility, resulting in systems that mold easily to their surroundings and the user for increased comfort, safety, and ease of use.

Some SWRs are entirely soft, monolithic, garment-like wearable devices, made from soft actuators, fabric, and other compliant materials; while other applications include minimal or reduced amount of rigid components as mounting points for the soft actuators. Categories of wearable robots can be simplified into four main groups

as defined by Wearable Robotics Association (2015) and Exoskeleton Report (ExR) (2020): 1) Military, 2) Industrial, 3) Consumer, and 4) Medical. Most wearable devices aim to either provide assistance or augmentation. In this review, assistance is defined as an SWR with a goal of restoring a more "natural" movement of biomechanical behavior (Awad *et al.*, 2017b), and serves a role in accomplishing activities of daily living (ADL) (Spector and Fleishman, 1998). Augmentation is defined as an SWR that applies active external forces to a healthy user to increase the capability, strength and/or endurance of said user.

2.1 Actuation Methods and Materials for SWR

Fluidic actuators have been simplified and broken down into sub categories: McKibben/PAMs, Elastomers, and textiles/fabric-based actuators. The pros and cons of each aforementioned actuator design will be discussed in greater detail in the following sections.

2.1.1 Development in Fluid-Driven Soft Actuators for SWR

One of the earlier soft actuator design, and most commonly implemented method of actuation used in the soft robotics field is the fluid-driven approach (Yariott, 1972; Petersen and Shepherd, 2018). This method uses fluidic pressurization of specific cavities within the soft actuators to entice some kind of motion or generate force, and can be traced back to initial designs from the 1970s and early 2000s (Yariott, 1972; Noritsugu, 2005). Pneumatically powered systems use compressible fluids to generate variable stiffness within specific actuators. Compressed air is most commonly used due to low viscosity, high compressibility, accessibility, and low cost (Ding *et al.*, 2014b). However, pneumatic systems have suffered from issues with latency and controllability when expected to interact or react to the user's kinematic or surrounding

feedback (Malcolm *et al.*, 2013; Ding *et al.*, 2014b). This review analyzes methods of soft actuation when applied to wearable devices, which are discussed in the following sections for McKibben/PAMs, Elastomers, and textiles/fabric-based actuators.

2.1.2 Pneumatic Artificial Muscles / McKibben (Fig. 2.1a)

The pneumatic artificial muscle (PAM) is one of the earliest developments in soft actuators for wearable devices, dating back as far as the 1970s for initial documentation (Yariott, 1972; Klute *et al.*, 1999). PAM actuators are typically characterized by a uniaxial contraction force upon actuator pressurization, which can be used to apply high tensile forces that closely resemble the mechanisms of human muscles contracting (Noritsugu, 2005). When unactuated, PAMs have an intrinsic compliance from the soft materials that is nearly transparent to the user's natural kinematics in comparison to a rigid exoskeleton.

The McKibben muscle (or braided PAM) is a well-known PAM actuator (Yariott, 1972; Klute *et al.*, 1999; Davis *et al.*, 2003) that began introducing the concept of using soft materials to create a robotic actuator for human assistance in the early 2000s (Noritsugu, 2005; Kobayashi *et al.*, 2007). McKibben muscles consist of a cylindrical shell (often a type of braided mesh) that is capable of radial expansion and becomes inextensible at a maximum threshold (Sasaki *et al.*, 2005b; Klute *et al.*, 1999). The shell contains an airtight, thin-walled rubber tube with hyperelastic properties, and is capped on both ends with an inlet for pressurization (Yariott, 1972). Once pressurized, the tube expands the radius of the shell, inducing an overall contraction in the PAM actuator and an increasing tensile strength (Majidi, 2013). McKibben muscles have a high force-to-weight ratio which makes them a popular choice when assisting human joints that require high torque (Teng *et al.*, 2012; Wehner *et al.*, 2013). McKibben muscles can have low bandwidth for certain human movements

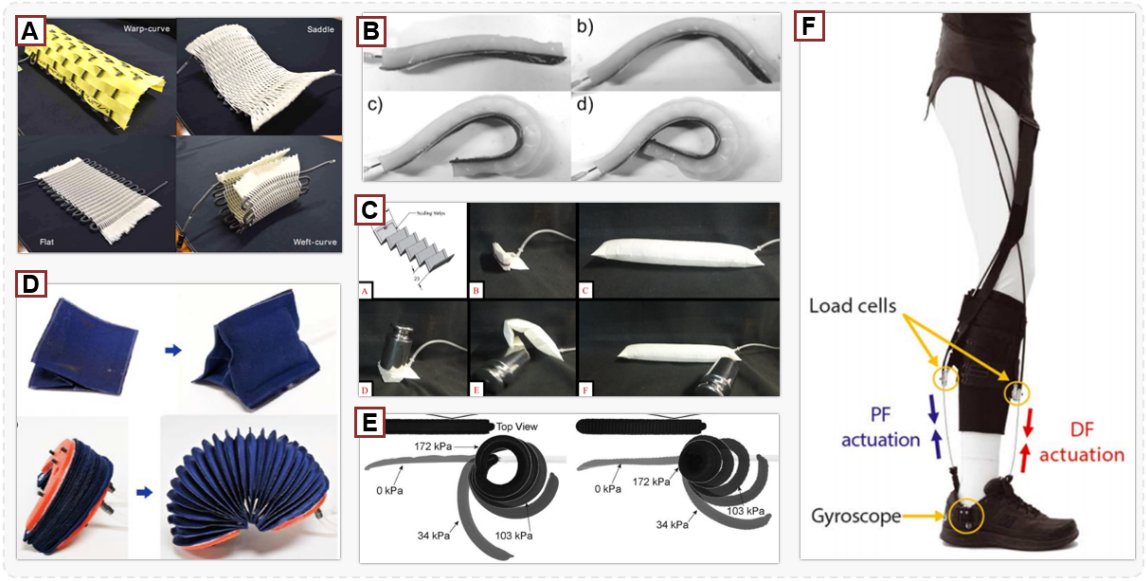

Figure 2.1: This figure provides a brief overview of different actuation methods used in soft exosuits: A) Improved McKibben type actuators braided into a mesh for higher contraction, lower profile, and a wider range of bending mechanics (Hiramitsu *et al.*, 2019), B) An elastomeric actuator that can be mechanically programmed to achieve different types of bending (Yap *et al.*, 2015a), C) A stiffening beam textile actuator designed to resisted bending and buckling (Miller-Jackson *et al.*, 2019), D) new fabrication methodologies to create fabric based inflatable actuators (Yang and Asbeck, 2018), E) shows fabric based inflatables based on fiber reinforcement to induce different types of motions (Cappello *et al.*, 2018a), F) A cable-driven SWR device using Bowden cables to provide assistance (Awad *et al.*, 2017b)

(Wehner *et al.*, 2012) and can cause discomfort related to friction from the constantly varying surface area when in contact with the body (Davis *et al.*, 2003).

Some PAM actuators address these issues, by decreasing the overall size for more effective operation (Hiramitsu *et al.*, 2019), and increasing the types of motions that the actuators can achieve (Hassanin *et al.*, 2017; Sasaki *et al.*, 2005a; Funabora, 2018). These new approaches are opening doors to biologically-inspired exosuits that have the high force-to-weight ratio of a McKibben muscle (Bilodeau *et al.*, 2018), but with less weight, bulk, lower operating pressures and a higher degree of transparency and flexibility for the user (Abe *et al.*, 2018; Hiramitsu *et al.*, 2019).

2.1.3 Elastomeric Fluidic Actuators (Fig. 2.1b)

Wearable robotics began to embrace new types of soft actuators made from hyperelastic elastomers and other polymers shortly after the McKibben Muscle began attracting researchers to using compliant actuators (Noritsugu *et al.*, 2004; Noritsugu, 2005). Elastomers and soft robotics were already a field of research that was well in the process of becoming an emerging field, but it was not until the early 2010s that elastomeric actuators started maintaining a presence in the wearable robotics community (Petersen and Shepherd, 2018). Initial investigations into using hyperelastic materials for actuator designs revealed functional implementation of using the actuators to assist the human hand (Noritsugu *et al.*, 2004). Elastomeric actuators are forgiving when interacting with surroundings of a complex or unknown geometry (Galloway *et al.*, 2013). The major advantage to systems of such high compliance is the simplistic, underactuated nature of the actuator, and successful examples in human assistance in the mid 2010s for rehabilitation have been showcased featuring silicone-based actuators (Polygerinos *et al.*, 2015; Wilkening *et al.*, 2015; Oguntosin *et al.*, 2015). Due to the generally lower force output from fluidic elastomer actuators, a wide majority of applications have focused on assisting the hand or wrist, but some focused on lower limbs (Park *et al.*, 2014c).

Pneu-Net actuators became a popular design choice for many researchers in SWR following the launch of the open-source instructional website "Soft Robotics Toolkit" (Holland *et al.*, 2014) which was released by Harvard University in 2014. This design hosts several individual hollow units or chambers formed in a single plane, connected by a central cavity to allow pressurization of all chambers (Mosadegh *et al.*, 2014; Yap *et al.*, 2015b). Strain-limiting material is embedded in the base of the actuator. Upon pressurization, the chambers begin to expand, and due to the difference in strain at

the top of the expanding chambers, and the constrained layer along the base, the actuator begins to curl (Polygerinos *et al.*, 2015) Recent advancements utilizing elastomeric actuators centers around applications where low forces and high compliance are needed. Elastomeric actuators in more recent designs have integrated multimaterial properties into a single actuator during the fabrication process of casting and curing silicone molds to generate a wide variety of actuator designs (Polygerinos *et al.*, 2017). Other materials have been used to generate a wide range of motions and actions for each actuator, such as contraction (Han *et al.*, 2018; Wirekoh and Park, 2017; Low *et al.*, 2016), bending or curling (Li *et al.*, 2020), and expansion (Zhang *et al.*, 2019a) for rehabilitative purposes generally focused on the hand, wrist, or a weakened ankle.

2.1.4 Fabric-Based Inflatables and Textiles (Fig. 2.1c-e)

Many actuators used in SWR designs in recent years have switched to a fabric-based methodologies, using soft actuators made from fabrics and other forms of textiles and thin films to make soft exosuits more garment-like with reduced form-factors (Park *et al.*, 2019b; Granberry *et al.*, 2017). Research has been conducted with fabric-based soft actuators since the early 2000s (Noritsugu *et al.*, 2008; Yang, 2017), even before the concept became widely popular to the SWR community. Thin walled, air-tight bladders made from binding two or more layers of the material together to form a pouch (Niiyama *et al.*, 2015). Fabrics have been used to make soft actuators by using materials that bind together chemically with adhesive, thermally, or with ultrasound welding processes (Yap *et al.*, 2017). The fabrics often do not possess the same hyperelastic properties as the silicone-based actuators, and so design considerations often revolve more heavily around geometric programming of materials (Khin *et al.*, 2017). The benefits of using a single layer of thin film or textile is the simplic-

ity in the final design, as well as the low profile the resulting actuator will possess when at atmospheric pressure. When depressurized, most textiles return to a state in which there is minimal volume or thickness in the actuator, which prevents the body of the actuator from becoming a hindrance to the movement of the user more so than rigid robotic counterparts (Chung *et al.*, 2018). A combination of material properties, textiles, and basic geometric configurations of bladders is used to achieve the desired motion and force output (Cappello *et al.*, 2018a; Felt *et al.*, 2018).

New developments in fabric based inflatable textiles have allowed for the implementation of new materials that can achieve a high variety of deformations and force translations (Cappello *et al.*, 2018a; Realmuto and Sanger, 2019). Fabric based actuators have also been created to mimic the behavior of a bellows to create a bending or rotary motion, similar in mechanical principles to the Pneu-Net actuator (Yang and Asbeck, 2018; Felt *et al.*, 2018; Thalman *et al.*, 2018; Miller-jackson *et al.*, 2019a; Khin *et al.*, 2017). Similar to fiber-reinforcing elastomers, design and characterization of fabric actuators can be performed by combining inextensible fabrics with extensible fabrics, such as spandex or neoprene to obtain the desired actuator behavior (Cappello *et al.*, 2018a; Realmuto and Sanger, 2019). Other common methods of fabrication include heat welded thermoplastic polyurethane (Niiyama *et al.*, 2015) and fabric based inflatables made from weather-proof nylon or women mesh (Thalman *et al.*, 2019; Abrar *et al.*, 2019; Yap *et al.*, 2017). Some fabric-based designs and textiles are striving to create smart garments, and have developed sheets of fabric controlled through pneumatics (Funabora, 2018; Hiramitsu *et al.*, 2019)

2.1.5 Cable Driven (Fig. 2.1f)

Designing new, lighter weight, lower profile wearable robots began to converge towards mainstreamed popularity around the early 2010s as the term “exosuit” became

more well-known and defined (Asbeck *et al.*, 2014). While PAM actuators had been effective in providing assistance, SWRs rapidly gained attention from researchers with the introduction of cable-driven mechanisms, which aimed to address several issues observed in early developments of fluidic SWRs (Galiana *et al.*, 2012; Asbeck *et al.*, 2013). Cable-driven actuation (Fig.2.1f) can easily mimic behaviors of the human musculoskeletal system to assist specific motions (In *et al.*, 2015; Asbeck *et al.*, 2014; Awad *et al.*, 2017b; Zhang *et al.*, 2019b). These systems have developed significantly in the past decade and are still one of the more prevalent actuation methods used. Extensive research has been done in controllability (Ding *et al.*, 2018), anchor points for applied loads (Yandell *et al.*, 2020), and design (Kwon *et al.*, 2019) to create high performing exosuits.

The cables (or tendons) are affixed to a point on the exosuit (typically a strap or tab made from inextensible synthetic fabrics or lightweight plastics) which interfaces with the human body to allow for proper force transmission to the targeted joint (In *et al.*, 2015; Awad *et al.*, 2017a; Asbeck *et al.*, 2014). The cable is routed along the body and fed to a motor which, when activated, winds the cables to apply a tensile force to the anchor point to mimic the musculoskeletal behaviors of specified joint or area (Awad *et al.*, 2017b). Selecting an ideal anchor point is critical to ensuring the forces are translated to the body safely and effectively, as misalignments can cause the SWR to under-perform (Galiana *et al.*, 2012; Asbeck *et al.*, 2014). Actuator power is transmitted to the direct point of contact (Yandell *et al.*, 2017) by engaging the motors or pulley system to provide varying levels of tension and movement on each cable. Sheathing is often used to help reduce friction of the cables moving across the skin and reduce overall friction (Nilsson *et al.*, 2012). The interface that attaches the cable to the user must avoid slippage, allow for predictable torque generation when the cable is tensioned, and be comfortable to the wearer (Asbeck *et al.*, 2015b;

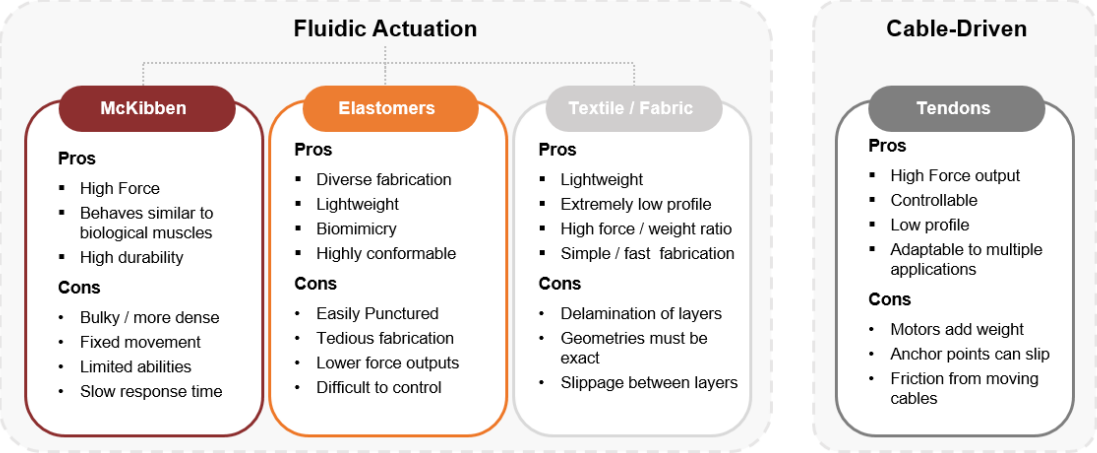

Figure 2.2: Brief overview of different actuation methods used in soft exosuits and the benefits / disadvantages of the listed types

In *et al.*, 2015). This method of actuation can produce high torques at a bandwidth higher than that of other methods of soft robotic actuation (Asbeck *et al.*, 2014). As a result, cable-driven systems are a popular approach for augmentation of performance (Quinlivan *et al.*, 2015). However, such high tensile forces applied at singular points on the body can cause discomfort (Schiele, 2009; Baltrusch *et al.*, 2018; Quinlivan *et al.*, 2015).

2.1.6 Comparison and Critical Evaluation of Actuation Methods in SWRs

Each type of actuator has benefits and drawbacks depending on the application and the user. Designing an effective SWR means being able to select the materials and methods needed for the chosen application, and ensure the selection will sufficiently meet the need. Listed in this section is a summarized overview of some of the pros and cons of each type of actuator. The highlights of each section are outlined in Fig. 2.2, which categorizes the actuation methods discussed in the previous sections.

- **Pros: Pneumatic Artificial Muscles (McKibben)** - McKibben muscles have a higher force / weight ratio and are able to withstand and generate higher

forces during pressurization than other pneumatic designs. The actuators behave similarly to the human muscle, which simplifies design conceptualization and can easily provide assistance (Wehner *et al.*, 2013). The lightweight and flexible nature of the inactive actuator makes it easy to integrate onto a person without adding excessive weight to the users. The design of the braided mesh McKibben muscles is durable and can withstand the wear and tear of daily and repeated use.

- **Cons: Pneumatic Artificial Muscles (McKibben)** - McKibben actuators face some issues with bulkiness and anchoring points (Kobayashi *et al.*, 2007). Some McKibben muscles can be large in diameter to facilitate the needed force output, and the anchoring point of the point load from the actuator must be securely fixed on the user in order function as anticipated.

- **Pros: Elastomeric Fluidic Actuators** - Elastomeric actuators can achieve high degrees of freedom with a single input, and are forgiving against complicated joints or surfaces. Elastomers are less impacted by misalignment between the actuator and joint when subjected to an injection of pressurization, and conform easily to their surroundings without additional input. Actuators are made from lightweight materials that have hyperelastic properties, and expand and interact over larger surface areas against the body to avoid anchor point issues. This is useful for assistance to joints where additional bulkiness or anchor points may restrict user movement. These actuators can also reach a high degree of biomimicry which can be helpful when designing actuators to perform a specific biological or kinematic task.

- **Cons: Elastomeric Fluidic Actuators** - Elastomeric actuators begin to see a disadvantage in the aspect of controllability, due to the nonlinear behaviors

exhibited upon pressurization and the general lack of sensing capabilities for position or control. Slower actuation time can be a limiting factor in the final application, and higher force output can lead to inevitable structural failure, which would not be ideal for tasks that require higher force or cyclical repetition during assistance (i.e. heavy lifting or walking). Tethers to the pneumatic source may also be limiting to user motions or system portability.

- **Pros: Fabric-Based Inflatables and Textiles** - Textile-based actuators have similar benefits to elastomeric alternatives, however, textiles are even lighter weight and can achieve a nearly undetectable profile when not pressurized (Yang and Asbeck, 2018). Textile actuators can achieve higher force output at elevated pressure levels with inextensible fabrics, which increases the strength of the material properties to match the most durable inextensible layers. Textile or fabric actuators motion is pre-determined by the materials and the corresponding material properties selected during fabrication (Cappello *et al.*, 2018a). Fabrication techniques are easily accessible and simple, and design possibilities are limited mainly by the materials present or readily available for development (Yang and Asbeck, 2018).

- **Cons: Fabric-Based Inflatables and Textiles** - Textile based actuators face the same limitations as the aforementioned fluidic actuators with power source portability and latency. Other disadvantages can arise from mechanical fragility or failure, delamination of layers creating fluidic chambers, and slippage between layers of fabric and the human (Cappello *et al.*, 2018a).

- **Pros: Cable Driven** - The pros of cable-driven systems are low profile, lightweight, high torque and increased controllability when compared to fluidic actuators. Highly complex motions can be achieved with a simple and

underactuated input (Asbeck *et al.*, 2013). This is beneficial for joints such as the hand or the shoulder, or assisting multiple joints in series, such as LB limbs during walking. High torque is also easily achievable and controlled through fine-tuned input to the actuator motors, which allows for fast response time at precise and specified values. Cable-driven systems do not require a tether and are highly portable which is helpful to ADL tasks dealing with locomotion.

- **Cons: Cable Driven** - Some drawbacks of cable-driven systems are friction, backlash hysteresis, nonliniarities (Dinh *et al.*, 2017), and force translation to anchor point on the user (Galiana *et al.*, 2012). Force and torque translation from the tendons to the joints relies on applying a point load to a soft or flexible interface (often garment-like exosuits or braces) which can result in slippage or hysteresis (Dinh *et al.*, 2017). Slippage can often be observed between the skin and the fabrics, which can cause discomfort or inaccurate actuation based on non-observable discrepancies with this displacement. The user typically must support the weight of the motors and other supporting hardware on their body (Asbeck *et al.*, 2013).

2.1.7 Other Types of Actuation for SWRs

The following are actuation methods and designs that are beginning to be of more interest in the field of SWRs but have not yet become as effective or thoroughly investigated at this stage. These actuation methods have proven highly effective when implemented properly and are therefore worth noting. However, these actuator designs and methodologies are not within the scope of the review paper and will not be discussed in depth beyond this section.

Origami-inspired actuators are made from very thin, lightweight materials and designed to fold or bend in ways that mimic soft materials (Sedal *et al.*, 2018; Li

et al., 2017). Actuators can be controlled via small motors or are sometimes placed inside sealed thin film structures. Negative pressure can then be applied to remove the air from the thin film casing, forming a reinforced, folded structure encased inside the vacuum chamber contained in the thin film. Negative pressure can often be used just as effectively as positive pressure (Felt *et al.*, 2018), which can be used in combination with other soft materials (i.e. foam, sand, paper etc.) which occupy a certain volume at atmospheric pressure, and compress and become stiff when subjected to negative pressure (Robertson and Paik, 2017). Another form of actuation method used is the shape-memory alloy (SMA) actuator, which use electrical current to affect the behavior, shape, and/or length of a material used in designing an actuator (Park and Park, 2019). Another method is passive assistance from flexible or relatively soft materials. These actuators use materials with some intrinsic compliance or elasticity, to provide passive assistance to the user (Higuma *et al.*, 2017; Lee *et al.*, 2017b).

2.2 Actuator Design for SWR

Initial characterization of functional constraints for SWRs design requires initial identification of the actuation methods selected, which joint(s) will be assisted, and how the forces will be translated from the actuator to the user to provide effective, comfortable, and predictable assistance (Yandell *et al.*, 2020). In most cases the actuator is designed around a particular type of assistance that is needed at a selected joint on the human body or motion that is targeted for improvement. This can be done by utilizing actuators with different types of functionality (Wang, 2016; Connolly *et al.*, 2015). Throughout some of the most commonly seen SWRs, there are themes of the actuator designs designated for particular types of motion assistance and deformation methods. These were touched on briefly in previous sections, but were more specific to elastomeric actuator design as an isolated concept. This section

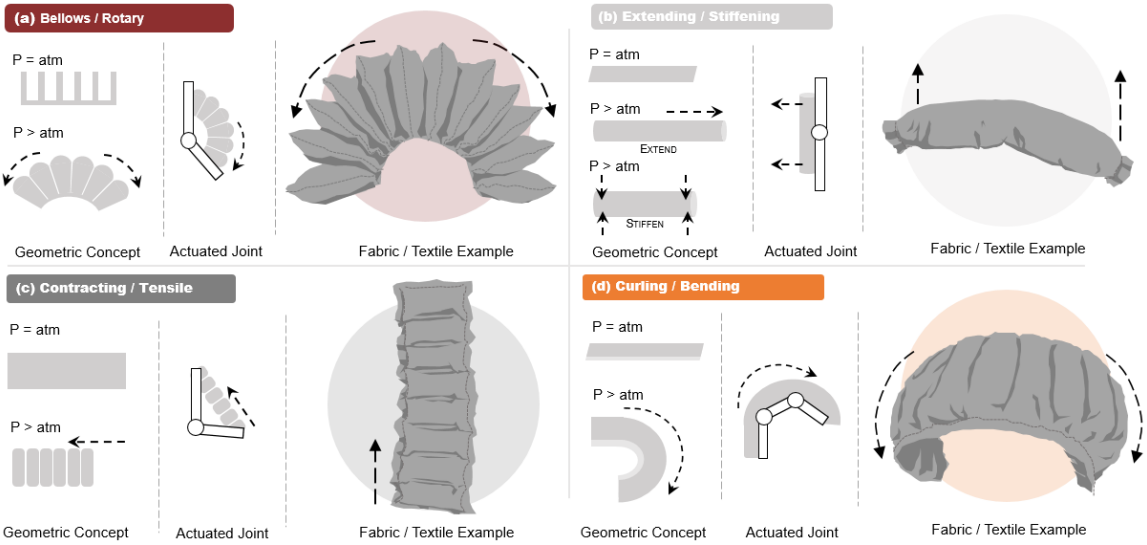

Figure 2.3: This figure provides an overview of the most commonly used actuator designs in SWRs and the driving mechanical principles behind the motions supported by each listed category. Categories have been broken down into (a) Bellows / Rotary, (b) Extending / Stiffening, (c) Contracting / Tensile, and (d) Curling / Bending designs. Each design is illustrated as a geometric representation of the actuator before and after injection of pressurized air, the actuator acting on a conceptual joint, and an illustration of a fluidic textile representation of these actuators for reference

aims to highlight overarching themes of soft actuator designs commonly used in SWR, specifically focused on fluidic actuators. These actuator designs have been categorized as shown in Fig. 2.3 by 1) Bellows / Rotary, 2) Extending / Stiffening, 3) Contracting / Tensile, and 4) Curling / Bending designs.

2.2.1 Bellows / Rotary (Fig. 2.3a)

The first design in Fig. 2.3a builds upon the Pneu-Net actuators, such as works presented at Harvard University (Polygerinos *et al.*, 2015) and Arizona State University (Thalman *et al.*, 2018), for elastomeric and textile based actuators, respectively. This design utilizes individual chambers or pockets that expand when inflated, as shown in Fig. 2.3a. The base has a strain-limiting layer while the top is free to move. This allows for expansion across the top surface, while expansion is restricted at the base. Each chamber expands and exerts a contact force against adjacent chambers,

which results in an effect that resembles a bellows and generates a rotational motion (Miller-jackson *et al.*, 2019b). This actuator design is effective for assisting joints in a single degree of freedom, and has been commonly used in flexion of joints (such as the elbow or a finger).

2.2.2 Extending / Stiffening (Fig. 2.3b)

A design that forms a straight beam-like shape which will either stiffen or extend depending on the exact design and intended purpose (Fig. 2.3b). Creating a beam of variable stiffness can allow for corrections in kinematics and support based the torque and stiffness provided by the beam (Miller-Jackson *et al.*, 2019). This actuator design can provide variable stiffness as seen in the elastomeric design from National University of Singapore (Koh *et al.*, 2017), where the inherent stiffness and recoiling effect of the beam is used to push the elbow into extension. Another example is the ExoBoot from Harvard Univeristy (Chung *et al.*, 2018), which uses an inflatable textile beam to push the foot into plantarflexion. The beam design is beneficial when either placed laterally across a joint to serve as a split or pull into alignment when activated (Natividad and Yeow, 2016), or is placed in acute angle of a joint to push the joint to straighten as the beam inflates and extends (Miller-jackson *et al.*, 2019b). This design is most commonly used in joint extension or joint bending prevention (e.g. finger or shoulder).

2.2.3 Contracting / Tensile (Fig. 2.3c)

This actuator design is the most common in exosuits, mainly because it includes Cable-driven systems by nature, as well as McKibben muscles. Actuators that generate tensile forces mimic concentric contraction of human muscles, which provides many design concepts for SWRs that behave similarly to natural biological functions.

Cable-driven actuation functions similarly to tendons in teh body, and fluidic contracting actuators are designed to contract like muscles when an internal pressure is applied as depicted in Fig. 2.3c. Researchers at Carnegie Mellon developed an elastomeric version of a PAM that generates a tensile force when pressurized (Wirekoh and Park, 2017), and a fabric-based contracting actuator was developed from Arizona State University (Thalman *et al.*, 2019). Contracting actuators are the most widely seen design and support joints in all motions from flexion to extension, and are commonly seen assisting multiple joints in series (ankle + hip, fingers + hand, etc.).

2.2.4 Curling / Bending (Fig. 2.3d)

This design (depicted in Fig. 2.3d) is in a separate category from the bellows / rotary design to distinguish the different methods in which this motion is achieved. Specifically, the materials used and the properties that interact when subjected to internal pressure or load will generate the resulting deformation. The top layer is made from a hyperelastic or highly extensible material, while the base layer is made from or constrained with an inextensible material. This difference in extensibility will cause the actuator to curl around the inextensible layer when pressurized (Noritsugu *et al.*, 2008). The benefit of an actuator that can curl rather than rotate about a point is the forgiving nature, which can easily form around complex joints with a single input. This design is commonly placed on the outside of a joint, such as the finger to assist flexion. This is seen in the three discussed fluidic actuation methods with modified McKibben muscle from University of Salford (Hassanin *et al.*, 2017), elastomeric design from (Yap *et al.*, 2015a), and fabric-based design from Harvard University (Cappello *et al.*, 2018b)

2.3 Fabrication Methods for SWR Actautors

The McKibben muscle (or braided PAM) is a durable soft actuator that is made from a single hollow tube, which is impermeable to air(Yariott, 1972; Klute *et al.*, 1999). This tube is inserted into a braided mesh tube of a slightly larger diameter. The braided mesh moves is able to slide and expand radially up until a certain point where it becomes inextensible. This braided mesh restricts the inner tube from over-expanding or weakening/bursting if over inflated. It also allows for the inner tube to inherit the material properties of the braided mesh when fully radially expanded which increases the strength of the actuator (Sasaki *et al.*, 2005b; Klute *et al.*, 1999). The ends of the layered tubes are capped with a metal ring or other air tight fitting that allows for a tube to connect. When pressurized, the tube expands inside the braided mesh, which experiences a radial expansion that results in a reduction in overall actuator length (Yariott, 1972). This is the governing principle behind the McKibben Muscle actuator, and it is a design that has managed to stay relevant through the past decade due to the versatility, low cost, and easy of fabrication (Noritsugu, 2005).

Elastomers (or elastic polymers) typically have a low Young‘s modulus. A metric to measure the hardness of these materials is commonly identified using the Shore Hardness Scale, which can help determine how inertly stiff or flexible a material will be prior to actuator fabrication and during analytic and Finite Element Analysis modeling (Holland *et al.*, 2017). Elastomeric, fluidically actuated technologies have an extremely versatile range of motions, in categories of deformation types such as a) bending, b) expanding, c) contracting, d) elongating, and e) twisting (Wang, 2016; Connolly *et al.*, 2015; Schmitt *et al.*, 2018). These movements can be mechanically programmed into the actuator during the fabrication process (Galloway *et al.*, 2013).

Inextensible components are embedded within the elastomer to limit the strain at certain points and restrict expansion of the material during fluidic pressurization (Wirekoh and Park, 2017; Heung *et al.*, 2019). Fiber-reinforcement provides predictable, programmable motions depending on the orientation and positioning of the inextensible fibers (Connolly *et al.*, 2015; Galloway *et al.*, 2013). Strain limiting layers such as mesh or fabrics can be cured within the casting process to achieve a similar programmable motion (Polygerinos *et al.*, 2015). For silicone-based elastomers specifically, there is a casting process that allows for complete customization and has been thoroughly explained and detailed for research groups and individuals to attempt independently (Holland *et al.*, 2014).

Fabrics and textile-based actuator designs typically involve creating a specified, predetermined shape for a chamber, and thermally or chemically bonding two or more layers of material together to form an air-tight seal with a net-shape of the desired chamber (Niiyama *et al.*, 2015). Some actuators use only one type of material to achieve complete actuator fabrication (Yang and Asbeck, 2018). They can be constructed from a heat-sealable material such as thermoplastic polyurethane (TPU), which forms an air-tight seal when consistent pressure and heat is applied to form a thermal bond between layers (Ang and Yeow, 2019; Niiyama *et al.*, 2015; Thalman *et al.*, 2018). Actuators may be formed from just TPU (or other heat-sealable thin films) layers (Niiyama *et al.*, 2015), or they may use a fabric coated on one or both sides with a layer of heat-sealable film (Abrar *et al.*, 2019; Park *et al.*, 2019b; Yang and Asbeck, 2018; Miller-jackson *et al.*, 2019b; Thalman *et al.*, 2019). As soft components are ideally lightweight and compact, actuators are designed to produce the highest forces possible with the smallest associated volumes (Coyle *et al.*, 2018; Cappello *et al.*, 2018a). New manufacturing methods optimize this process and reduce the time and level of complexity involved in fabrication (Miller-jackson *et al.*, 2019b). Finite

Element Analysis (FEA) studies have shown promise in providing realistic models for actuator design and optimization by simulating the behavior of soft materials (Holland *et al.*, 2017; Coyle *et al.*, 2018). This can allow for easier material selection and geometric optimization for mechanical programming of soft materials (Polygerinos *et al.*, 2015). Automated methods of manufacturing are being developed utilizing custom 3D printers for additive manufacturing using soft materials, and CNC methods of heat sealing textiles to increase complexity and accuracy of actuator designs while simplifying the labor-intensive portions of actuator fabrication (Niiyama *et al.*, 2015; Park *et al.*, 2019b; Ang and Yeow, 2019). Another method of creating these seams between layers is by using ultrasonic welding, which has successfully produced fabric-based actuators in previous work (Yap *et al.*, 2017).

2.4 Upper Body Soft Assistive Robots

Upper Body (UB) assistance often focuses more on stationary rehabilitation, assistance in achieving the activities of daily living (ADL), or injury and fatigue prevention (Maciejasz *et al.*, 2014). Figure 2.4 presents a brief look at some successful upper body soft robots assisting various joints, and Tables 6.1 and 2.2 provide a more comprehensive list of some of the more recently developed technologies listed in this section. The UB has a high level of complexity and many DoF isolated to specific joints in concentrated areas that are easily affected by additional weight (such as the hand). The benefits of using SWRs for UB assistance avoid placing heavy components or restricting joint alignments on the user's arms or torso. Many of these SWR for the UB are outlined in the following sections to discuss several types of assistance in more detail.

Figure 2.4: A brief survey of recent SWR technologies for each of the following upper body joints: A) a soft robotic hand developed at Harvard University at the Wyss Institute for Biologically Inspired Engineering (Cappello *et al.*, 2018b), B) a soft assistive device for the wrist made from fabric materials (Realmuto and Sanger, 2019), C) a soft elbow exosuit designed at Arizona State University (Thalman *et al.*, 2018), D) Shoulder assistive device also from Harvard University at the Wyss Institute for Biologically Inspired Engineering (O'Neill *et al.*, 2017), E) Trunk Orthosis from the Reconfigurable Robotics Lab at Ecole Polytechnique Fédérale de Lausanne (Robertson, 2019; Robertson and Paik, 2016), and F) an upper body device that assists multiple joints via cable-driven actuation (Lessard, 2018)

2.4.1 Head and Neck

There are limited studies of soft robotics application above the shoulders. However, there are studies on how soft robotics can help with basic facial motor functions. So far this area of research is minimal, though could pose promise for future studies due to the bio-mimicry often seen in many SWRs. Due to limited or sufficient data on this particular joint, it is omitted from the final list of considered (real) options.

Table 2.1: This chart illustrates the correlation between existing SWRs for the upper body, showing the most prevalent method of actuation used related to the specific type of assistance provided at each joint of the upper body and the respective degrees of freedom that are assisted.

Joint	Year	Soft Wearable Robot	Actuation	Method	Design	DoF	Motion*
a. Shoulder	2008	Balasubramanian *et al.* (2008)	Pneumatic	McKibben	Contraction	2	Ab, C
	2019	Abe *et al.* (2019)	Pneumatic	McKibben	Contraction	1	F
	2012	Galiana *et al.* (2012)	Cable-Driven	Bowden Cables	Tensile	1	Ab/Ad
	2014	Koo *et al.* (2014)	Pneumatic	Textile / Fabric	Rotary	1	Ab
	- -	- -	Cable-Driven	Bowden Cables	Tensile	1	F/E
	2016	Natividad and Yeow (2016)	Pneumatic	Textile / Fabric	Stiffening Beam	1	Ab
	2017	Kobayashi *et al.* (2007)	Pneumatic	McKibben	Contraction	3	F/E, Ab/Ad, C
	2017	O'Neill *et al.* (2017)	Pneumatic	Textile / Fabric	Rotary	2	Ab/Ad
	- -	- -	Pneumatic	Textile / Fabric	Stiffening Beam	2	F/E
	2017	Lessard *et al.* (2017)	Cable-Driven	Bowden Cables	Tensile	2	F/E, Ab/Ad
	2018	Abe *et al.* (2018)	Pneumatic	McKibben	Contraction	2	F/E, Ab/Ad
	2018	Han *et al.* (2018)	Pneumatic	Elastomeric	Extension	2	F, Ab
	2018	Lessard (2018)	Cable-Driven	Bowden Cables	Tensile	2	F/E, Ab/Ad
b. Trunk	2015	Ohno *et al.* (2015)	Pneumatic	McKibben	Contraction	1	E
	2016	Inose *et al.* (2016)	Pneumatic	McKibben	Extension	1	E
	- -	- -	- -	Textile / Fabric	Stiffening	1	E
	2016	Robertson and Paik (2016)	Pneumatic	Elastomeric	Bending	2	F/E, LF
	2017	Cho *et al.* (2017)	Pneumatic	McKibben	Extension	1	E
	- -	- -	- -	Textile / Fabric	Stiffening	1	E
	2019	Yang *et al.* (2019)	Cable-Driven	Bowden Cables	Tensile	1	F
c. Elbow	2005	Noritsugu (2005)	Pneumatic	McKibben	Contraction	1	F
	- -	- -	- -	McKibben	Bending	1	E
	2005	Aragane *et al.* (2008)	Pneumatic	Textile / Fabric	Bending	1	F/E
	2014	Koo *et al.* (2014)	Cable-Driven	Bowden Cables	Tensile	1	F
	2015	Nycz *et al.* (2015)	Cable-Driven	Bowden Cables	Tensile	1	F/E
	2015	Wilkening *et al.* (2015)	Pneumatic	Elastomeric	Rotary	1	F/E
	2017	Xiloyannis *et al.* (2017)	Cable-Driven	Bowden Cables	Tensile	1	F/E
	2017	Koh *et al.* (2017)	Pneumatic	Elastomeric	Bending	1	F
	–	- -	- -	Textile / Fabric	Stiffening Beam	1	E
	2018	Tripanpitak *et al.* (2018)	Pneumatic	McKibben	Contraction	1	F
	2018	Gao *et al.* (2018)	Pneumatic	Elastomeric	Bending	1	F
	2018	Thalman *et al.* (2018)	Pneumatic	Textile / Fabric	Rotary	1	F
	2018	Chiaradia *et al.* (2018)	Cable-Driven	Bowden Cables	Tensile	1	F/E
	2018	Li *et al.* (2018)	Cable-Driven	Bowden Cables	Tensile	1	F/E
	2018	Lessard (2018)	Cable-Driven	Bowden Cables	Tensile	1	F/E
	2019	Irshaidat *et al.* (2019)	Pneumatic	McKibben	Contraction	1	F
	2019	Abrar *et al.* (2019)	Pneumatic	Textile / Fabric	Extending Beam	1	E
	- -	- -	Cable-Driven	Tendons	Contraction	1	F
	2019	Miller-jackson *et al.* (2019b)	Pneumatic	Textile / Fabric	Rotary	1	F
	- -	- -	- -	Textile / Fabric	Stiffening Beam	1	E
	2019	Abe *et al.* (2019)	Pneumatic	McKibben	Contraction	1	F

***Legend**: F = Flexion E = Extension Ab = Abduction Ad = Adduction C = Circumduction LF = Lateral Flexion

2.4.2 Shoulder (Table 2.1a)

The shoulder joint is comprised of a combination of DoF and motions that become coupled during certain movements and remain separate entirely for other motions, which creates a particularly complex location to provide assistance with wearable devices. The shoulder maintains several rotational DoF that intersect and do not have perfectly perpendicular axes, as well as another DoF that moves as a translation of the center of the joint itself. This level of complexity has made the shoulder a difficult joint to assist with rigid robots, and many early designs required the user to be seated with their torso fixed in order to utilize the device.

Initial research into SWRs for the shoulder can be observed in the turn of the century, when McKibben actuators were the more common approach (Kobayashi *et al.*, 2007; Balasubramanian *et al.*, 2008). Initial designs were lighter than rigid counterparts and less complex, however, because McKibben muscles could only apply tensile forces the DoF assisted were limited. Significant issues with slippage were observed, and the translation of forces to the human body was not always comfortable for the user (Kobayashi *et al.*, 2007). As cable-driven systems became more common in the 2010s, shoulder assistance with SWR shifted away from McKibben and fluidic actuators and focused more on using tendons to manipulate the joint (Galiana *et al.*, 2012; Kesner *et al.*, 2011). These systems were far less bulky and conformed more easily to the joint, with less limitation on tensile force or contraction ratio which could support the full RoM, and also facilitate placement to allow support in more DoF (Galiana *et al.*, 2012; Kobayashi *et al.*, 2007). Development for shoulder SWRs became a more active research topic in the later 2010s as NASA began to invest in the "Armstrong", a wearable suit for astronauts that used tendons to assist the shoulder (Kadivar *et al.*, 2017). It was around the time of this development that increasingly

advanced textile actuators emerged in the field (Natividad and Yeow, 2016; O'Neill *et al.*, 2017) and McKibben muscles showed more sophisticated and effective designs (Abe *et al.*, 2018). The shoulder has proven to be a difficult joint to assist, and some of the most prevalent SWRs tackling this goal are still seeking to find actuators that most closely resemble human muscle functions and placements (Abe *et al.*, 2019).

2.4.3 Back and Trunk (Table 2.1b)

These SWRs are commonly seen to help prevent injuries before they occur when dealing with the back or trunk of the user (Table 2.1b), and usually focus on posture and lifting assistance (Babič *et al.*, 2017). This is especially critical for factory or industrial workers, or other individuals who do repetitive heavy lifting (Lamers *et al.*, 2018; Babič *et al.*, 2017). Several soft systems utilize passive methods of actuation such, as pretensioned elastic bands or pulley systems that help support the back at opportune moments for injury (Cho *et al.*, 2017; Yang *et al.*, 2019). The benefit of actuation that uses tension in-line with the spine is the ability to store and release energy during lifting with the flexion and extension of the trunk. Since the human trunk can be heavy, actuation methods to actively assist movement can be difficult when locating anchor points that do not impede motion or translate forces to become burdensome to other joints.

2.4.4 Elbow (Table 2.1c)

SWRs for elbow assistance range from a focus in rehabilitation to injury prevention (Table 2.1c). These systems began in a consistent and similar methodology as wearable robots for the shoulder. The initial introduction of the McKibben muscle led to development emerging to design systems in robotics that would facilitate elbow rehabilitation without restricting movement of the user (Noritsugu *et al.*, 2008).

McKibben muscles quickly became an issue when translating tensile force to torque at the elbow joint, and with cable-driven systems gaining popularity in LB SWRs, designing cable-driven systems for the UB became a focus for SWRs (Koo *et al.*, 2014). With only a single degree of freedom to maneuver at the elbow, it became more common to integrate designs for assisting both joints simultaneously with underactuation (Abe *et al.*, 2018). Cable-driven systems provide assistance that mimics the biological function of the muscles in the upper arm to enact flexion and extension (Chiaradia *et al.*, 2018; Xiloyannis *et al.*, 2017). By attaching cables to the base of the forearm and running them up to an anchor point at the shoulder, they can be controlled to provide flexion and extension assistance at the elbow joint (Xiloyannis *et al.*, 2017; Li *et al.*, 2018).

Fluidic actuation approaches specific to the elbow begun to emerge in the 2010s with other pneumatic SWRs, and varied stylistically to match the specific need the exosuit is trying to fulfill (Abe *et al.*, 2018). Some used a bellows-type design to push the elbow into extension and pull it into flexion from the armpit area (Oguntosin *et al.*, 2015), while others designed for rotary actuators placed on the exterior side of the elbow joint to apply a rotational torque to induce flexion assistance (Aragane *et al.*, 2008; Thalman *et al.*, 2018; Noritsugu *et al.*, 2008). Elbow assistance is still a topic of high interest. It is less commonly seen as an isolated SWR for the particular joint. The elbow is commonly designed to be assisted as a part of a larger upper body system as factors such as posture and weight/load distribution become more critical.

2.4.5 Wrist and Hand (Table 2.2d - f)

SWRs are effective for the human hand due to their ability to easily follow complex motion and utilize the compliance for an underactuated mechanism (Sasaki *et al.*, 2005b). Table 2.2d - f lists several successful executions of SWRs for assistance to the

Table 2.2: Continuation of Table 1, showing SWR for the upper body, specifically focused on the hand and wrist as this is an area that has been thoroughly explored by the listed groups using the actuation types specified in the following table.

Joint	Year	Soft Wearable Robot	Actuation	Method	Design	DoF	Motion*
d. Wrist	2005	Noritsugu (2005)	Pneumatic	McKibben	Bending	1	Ab/Ad
	2005	Sasaki *et al.* (2005a)	Pneumatic	McKibben	Contraction	2	F/E, Ab/Ad
	2008	Balasubramanian *et al.* (2008)	Pneumatic	McKibben	Bending	2	E, Su
	2017	Lessard *et al.* (2017)	Cable-Driven	Bowden Cables	Tensile	1	Su/Pr
	2017	Hassanin *et al.* (2017)	Pneumatic	McKibben	Bending	1	Ab/Ad, Su/Pr
	–	–	–	–	Contraction	1	Ab/Ad
	2017	Zhu *et al.* (2017)	Pneumatic	Textile / Fabric	Bending	1	F/E
	2018	Lessard (2018)	Cable-Driven	Bowden Cables	Tensile	1	Su/Pr
	2018	Li *et al.* (2018)	Cable-Driven	Bowden Cables	Tensile	1	Su/Pr
	2019	Ang and Yeow (2019)	Pneumatic	Elastomeric	Rotary	1	F/E, Su/Pr
	2019	Park *et al.* (2019b)	Pneumatic	Textile / Fabric	Contraction	1	Su/Pr
	2019	Realmuto and Sanger (2019)	Pneumatic	Textile / Fabric	Bending / Curling	1	Su/Pr
e. Hand	2004	Noritsugu *et al.* (2004)	Pneumatic	McKibben	Bending	1	F
	–	–	Pneumatic	McKibben	Extension	1	E
	2008	Noritsugu *et al.* (2008)	Pneumatic	Textile / Fabric	Bending	1	F
	2012	Nilsson *et al.* (2012)	Cable-Driven	Bowden Cables	Tensile	1	F
	2014	Lee *et al.* (2014b)	Cable-Driven	Tendons	Tensile	1	F/E
	2015	Yap *et al.* (2015b)	Pneumatic	Elastomeric	Rotary	1	F
	2015	Yap *et al.* (2015a)	Pneumatic	Elastomeric	Bending	1	F/E
	2015	In *et al.* (2015)	Cable-Driven	Bowden Cables	Tensile	1	F/E
	2015	Nycz *et al.* (2015)	Cable-Driven	Bowden Cables	Tensile	1	F/E
	2015	Polygerinos *et al.* (2015)	Pneumatic	Elastomeric	Bending	1	F
	2016	Borboni *et al.* (2016)	Cable-Driven	Bowden Cables	Tensile	1	F
	2016	Zhao *et al.* (2016)	Pneumatic	Elastomeric	Tensile	1	F/E
	2017	Meeker *et al.* (2017)	Cable-Driven	Bowden Cables	Tensile	1	E
	2017	Xiloyannis *et al.* (2017)	Cable-Driven	Bowden Cables	Tensile	1	F/E
	2018	Cappello *et al.* (2018b)	Pneumatic	Textile / Fabric	Bending	1	F/E
	2018	Kang *et al.* (2018)	Cable-Driven	Bowden Cables	Tensile	1	F/E
	2018	Park *et al.* (2018)	Cable-Driven	Bowden Cables	Tensile	1	E
	2018	Jiang *et al.* (2018)	Pneumatic	Elastomeric	Bending	1	E
	2019	Heung *et al.* (2019)	Pneumatic	Elastomeric	Rotary	1	F/E
	2019	Shiota *et al.* (2019)	Pneumatic	Elastomeric	Bending	1	F
	2019	Heung *et al.* (2019)	Pneumatic	Elastomeric	Bending	1	F
	2019	Zhang *et al.* (2019a)	Pneumatic	Elastomeric	Stiffening	1	F
f. Thumb	2004	Noritsugu *et al.* (2004)	Pneumatic	McKibben	Contraction	1	Ab/Ad
	2010	Connelly *et al.* (2010)	Pneumatic	Textile / Fabric	Bending	1	Ad
	2014	Maeder-York *et al.* (2014)	Pneumatic	Elastomeric	Bending	1	F
	2014	Lee *et al.* (2014b)	Cable-Driven	Bowden Cables	Tensile	1	Ab/Ad
	2015	Yap *et al.* (2015a)	Pneumatic	Elastomeric	Bending	1	Ab
	2018	Kim and Park (2018)	Cable-Driven	Bowden Cables	Tensile	1	Ab/Ad
	2019	Shiota *et al.* (2019)	Pneumatic	Elastomeric	Bending	1	Ab/Ad

Ledgend: F = Flexion, E = Extension, Ab = Abduction, Ad = Adduction, Su = Supnation, Pr = Pronation

hand and wrist. Underactuated SWRs use limited inputs for each segment of the hand and allow for reduced computing power and simplified control (Yap *et al.*, 2015b). The goal for these technologies is to restore basic hand movement and functionality to regain independence and achieve ADL (Connelly *et al.*, 2010). There has been a variety of adaptations of soft hand exosuits for rehabilitation over the past decade, and the hand in particular is an assistance location that has draw a significant amount of attention from the SWR community. Some notable applications of soft robotics on the hand and wrist can be seen as far back as the early 2000s, utilizing the principles of McKibben muscles to modify the existing mechanical behavior to generate new and more helpful actuator performance (Noritsugu *et al.*, 2004; Sasaki *et al.*, 2005b).

Despite major shift of McKibben actuators and expanding capabilities, other avenues of soft actuation were being explored to provide assistance to the the human hand. As cable-driven SWR gained popularity, This strategy actuation that is effective as it mimics the natural mechanics of the hand and tendons, and often have a low-profile, though often requires motors being places somewhere on the arm or wrist. PAMs (Sasaki *et al.*, 2005b,a), fluidic elastomers (Shiota *et al.*, 2019; Zhao *et al.*, 2016; Polygerinos *et al.*, 2015; Jiang *et al.*, 2018), and fabric-based inflatable (Zhu *et al.*, 2017; Realmuto and Sanger, 2019; Noritsugu *et al.*, 2008) actuation methods have been used achieve various levels of assistance, are are typically all actuated using pneumatics, which pose similar uses of needed tubing and a pneumatic source. Fabric-based pneumatics have shown promise to avoid some of the issues of bulkiness observed in PAMs and elastomers. There is newly emerging research on soft exosuits for the wrist joint with focus on preventative assistance, as well as supporting forearm pronation and supination (Park *et al.*, 2019b; Realmuto and Sanger, 2019).

Figure 2.5: A brief survey of lower body SWRs, focused on each joint listed in Section VI. A) Shows an exosuit developed by the Wyss Institute to support the hip (Lee *et al.*, 2017a). B) shows and exosuit with a combination of cables and passive elastic bands used to assist the hip and knee joints (Schmidt *et al.*, 2017). C) provides an example of a soft knee exosuit using elastomeric PAMs (Park *et al.*, 2014c), and D) an ankle device using cable-driven mechanisms to support multiple degrees of freedom from Carnegie Mellon University (Kwon *et al.*, 2019). E) Shows the ExoBoot, which uses fabric-based inflatables for ankle plantarflexion (Chung *et al.*, 2018)

2.5 Lower Body Soft Assistive Robots

Lower Body (LB) assistive devices are commonly designed with the purpose of assisting or augmenting the human gait. Assistance is typically aimed at restoring a natural gait pattern to an impaired individual with abnormal gait adaptations. Augmentation is aimed at either increasing walking capabilities for a faster pace or reducing the metabolic cost for walking/running. Using SWRs for LB limbs is a major advancement that allows The user to interface with a LB robot without adding additional weight to their legs (Siviy *et al.*, 2017). Adding weight to the limbs during walking increases the inertia of the limb while in motion which can cause unnatural gait adaptations and safety concerns with balance for increased risk of trips and falls (Browning *et al.*, 2007). In the following sections, each joint will be discussed separately, even if particular devices span across assistance for multiple joints. Figure 2.5 shows a few of these devices. Tables 2.3 and 2.4 provide a comprehensive list of referenced work, specifying the works observed for each section and joint location for assistance.

Table 2.3: This table lists of some of the most cited and prevalent works in SWR for the lower body over the past decade, focused on the hip and knee joint. Each research group included below has been sorted by the joint assisted and actuation method used.

Joint	Year	Soft Wearable Robot	Actuation	Method	Design	DoF	Motion*
g. Hip	2013	Wehner *et al.* (2013)	Pneumatic	McKibben	Contraction	1	F/E
	2013	Kawamura *et al.* (2013)	Pneumatic	McKibben	Contraction	1	F
	2015	Asbeck *et al.* (2015c)	Cable-Driven	Bowden Cables	Tensile	1	E
	2015	Quinlivan *et al.* (2015)	Cable-Driven	Bowden Cables	Tensile	1	E
	2015	Asbeck *et al.* (2015a)	Cable-Driven	Bowden Cables	Tensile	1	F
	2015	Wu *et al.* (2015)	Cable-Driven	Bowden Cables	Tensile	1	F
	2016	Lee *et al.* (2016)	Cable-Driven	Bowden Cables	Tensile	1	F
	2016	Ding *et al.* (2016a)	Cable-Driven	Bowden Cables	Tensile	1	E
	2017	Schmidt *et al.* (2017)	Cable-Driven	Bowden Cables	Tensile	1	E
	2017	Ding *et al.* (2017)	Cable-Driven	Bowden Cables	Tensile	1	F
	2017	Karavas *et al.* (2017)	Cable-Driven	Bowden Cables	Tensile	1	F
	2018	Thakur *et al.* (2018)	Pneumatic	Elastomeric	Contraction	1	F
	2018	Poliero *et al.* (2018)	Cable-Driven	Bowden Cables	Tensile	1	E
	2019	Di Natali *et al.* (2019)	Cable-Driven	Bowden Cables	Tensile	1	E
	2019	Park *et al.* (2019a)	Cable-Driven	Bowden Cables	Tensile	1	E
	2019	Panizzolo *et al.* (2019)	Cable-Driven	Bowden Cables	Tensile	1	E
	2019	Fraiszudeen and Yeow (2019)	Pneumatic	Textile / Fabric	Tensile	1	E
h. Knee	2012	Teng *et al.* (2012)	Pneumatic	McKibben	Contraction	1	F/E
	2013	Wehner *et al.* (2013)	Pneumatic	McKibben	Contraction	1	F
	2013	Baiden and Ivlev (2013)	Pneumatic	McKibben	Contraction	1	F
	2014	Park *et al.* (2014c)	Pneumatic	Elastomeric	Contraction	1	E
	2017	(Schmidt *et al.*, 2017)	Cable-Driven	Bowden Cables	Tensile	1	E
	2018	Thakur *et al.* (2018)	Pneumatic	Elastomeric	Contraction	1	E
	2019	(Park *et al.*, 2019a)	Cable-Driven	Bowden Cables	Tensile	1	E
	2019	Miller-jackson *et al.* (2019b)	Pneumatic	Textile / Fabric	Rotary	1	E
	2019	Fraiszudeen and Yeow (2019)	Pneumatic	Textile / Fabric	Stiffening	1	E
	2019	Ezzibdeh *et al.* (2019)	Pneumatic	Textile / Fabric	Rotary	1	E

***Legend**: F = Flexion E = Extension Ab = Abduction Ad = Adduction Su = Supnation Pr = Pronation

2.5.1 Hip (Table 2.3g)

The human hip is a critical joint that allows for the transmission of force from the grown to the torso. The hips also assist in standing, balancing, postural, and sitting tasks, and hip joint actuation with SWRs (shown in Table 2.3g) primarily relies on cable-driven actuation, due to the high torque output from the tension forces of the cables as shown in (Asbeck *et al.*, 2015c; Ding *et al.*, 2018; Di Natali *et al.*, 2019; Lee *et al.*, 2017a; Wu *et al.*, 2015; Ding *et al.*, 2016a), though recent work has shown how fluidic actuators done by groups (Thakur *et al.*, 2018; Kawamura *et al.*, 2013) and

passive actuation methods seen in (Lee *et al.*, 2017b) can be used in hip assistance. Hip assistance from SWRs can be used for both stationary sit-to-stand tests or during corrective gait therapy (Abouhossein *et al.*, 2018; Fraiszudeen and Yeow, 2019).

2.5.2 Knee (Table 2.3h)

SWRs have been designed to help assist in both knee flexion and extension, as well as to provide stability to the knee joint to prevent buckling at the knee as shown in Table 2.3h. SWRs for the knee are often seen as stationary systems designed to be worn to address issues with gait symmetry (Elliott *et al.*, 2013). This can be done by helping assist the knee in either flexion or extension for executing the swing phase, or providing support during the weight shift in the stance phase (Teng *et al.*, 2012). Many designs are cable-driven systems that pull the knee into both flexion and extension (Asbeck *et al.*, 2013; Di Natali *et al.*, 2019). Other research has been done on using fluidic actuators for knee assistance (Teng *et al.*, 2012; Park *et al.*, 2014c; Miller-jackson *et al.*, 2019b; Ezzibdeh *et al.*, 2019). Issues with pneumatic knee assistance are found in the latency in the actuators firing. Other methods include passive elastic elements to provide preventative micro-corrections (Elliott *et al.*, 2013).

2.5.3 Ankle and Foot (Table 2.4i)

Prior to advancements in portable, wearable robotics, most ankle rehabilitation robots focused on seated therapies on robotic platforms that would adjust or orient the ankle into various positions. Designing wearable robots for the ankle joint has been difficult until recent years, as rigid robots can be heavy and adding excessive weight to the ankle joint can lead to increased risk of trips or slowed gait due to higher inertia at the foot while walking (Browning *et al.*, 2007). The ankle joint has two major degrees of freedom, the dorsiflexion/plantarflexion (DP) axis, and the inversion/eversion (IE)

axis (Perez-Ibarra *et al.*, 2017; Hong *et al.*, 2017). During walking, the DP axis plays a major role in assisting in forward locomotion and foot ground clearance (toe up and toe down), while IE assists in ankle stability and resilience to external perturbations during movement (lateral ankle rotation) (Siviy *et al.*, 2017; Hong *et al.*, 2017).

A few early instances of soft actuators seen for ankle rehabilitation consisted of a McKibben actuator affixed to a rigid orthosis. Issues with latency and weight were still prevalent however, and as more opportunities became available with DARPA and other funding sources, there was a noticeable shift toward one of the most common approaches for SWRs for the ankle: Cable-driven systems or other forms of contracting actuation methods have been widely seen in use ankle assistance, likely due to similarities with the tendon and muscle groups that control the foot (Park *et al.*, 2011; Ren *et al.*, 2017; Iwata *et al.*, 2018). This can be attributed to the high complexity and torque requirements for the ankle joint, specifically plantarflexion, during walking (Teng *et al.*, 2012; Murphy *et al.*, 2014; Chung *et al.*, 2018). There is extensive research on using cable-driven systems to assist ankle function, both through calculated torque generation and metabolic cost reduction experimentation (Chin *et al.*, 2009; Chung *et al.*, 2018; Yandell *et al.*, 2019). Cable-driven ankle SWRs tend to switch between both assistance and augmentation, with applications ranging from warfighter assistance to post-stroke rehabilitation during walking (Bae *et al.*, 2015; Sovero *et al.*, 2016; Siviy *et al.*, 2017; Kwon *et al.*, 2019). Fluidic actuation methods for the ankle are relatively popular, with some of the most notable contributions using PAM Mckibben type actuators (Sovero *et al.*, 2016; Bowers *et al.*, 2017; Murphy *et al.*, 2014; Wehner *et al.*, 2012), with a select few fabric-based inflatable devices (Chung *et al.*, 2018; Thalman *et al.*, 2019; Thalman and Lee, 2020). Some applications seek simply to add stability and prevent trips and falls using the user's body weight to distribute pressure through different chambers based on where the user is applying their body

Table 2.4: This table is a continuation of the previous table for SWR for assisting the lower body, detailing work done on the ankle joint. This is another heavily researched area and the worked cited below are some of the most well known and exemplary works sorted by the assisted degree of freedom and actuation method used.

Joint	Year	Soft Wearable Robot	Actuation	Method	Design	DoF	Motion*
i. Ankle	2006	Gordon *et al.* (2006)	Pneumatic	McKibben	Contraction	1	P
	2006	Ferris *et al.* (2006)	Pneumatic	McKibben	Contraction	1	D/P
	2011	Park *et al.* (2011)	Pneumatic	McKibben	Contraction	2	P, I/E
	2012	Teng *et al.* (2012)	Pneumatic	McKibben	Contraction	1	D/P
	2012	Wehner *et al.* (2012)	Cable-Driven	Bowden Cables	Tensile	1	P
	2013	Asbeck *et al.* (2013)	Cable-Driven	Bowden Cables	Tensile	1	P
	2013	Wehner *et al.* (2013)	Pneumatic	McKibben	Contraction	1	D/P
	2014	Murphy *et al.* (2014)	Pneumatic	McKibben	Contraction	2	D/P, I/E
	2014	Park *et al.* (2014b)	Pneumatic	McKibben	Contraction	2	D/P, I/E
	2015	Bae *et al.* (2015)	Cable-Driven	Bowden Cables	Tensile	1	D/P
	2015	Low *et al.* (2015)	Pneumatic	Elastomeric	Contraction	1	D
	2015	Asbeck *et al.* (2015a)	Cable-Driven	Bowden Cables	Tensile	1	P
	2016	Low *et al.* (2016)	Pneumatic	Elastomeric	Contraction	1	D
	2016	Sovero *et al.* (2016)	Pneumatic	Textile /Fabric	Rotary	1	P
	2016	Lee *et al.* (2016)	Cable-Driven	Bowden Cables	Tensile	1	D/P
	2017	Awad *et al.* (2017b)	Cable-Driven	Bowden Cables	Tensile	1	D/P
	2017	Ding *et al.* (2017)	Cable-Driven	Bowden Cables	Tensile	1	P
	2017	Yandell *et al.* (2017)	Cable-Driven	Bowden Cables	Tensile	1	P
	2017	Siviy *et al.* (2017)	Cable-Driven	Bowden Cables	Tensile	1	P
	2017	Karavas *et al.* (2017)	Cable-Driven	Bowden Cables	Tensile	1	P
	2017	Hong *et al.* (2017)	Pneumatic	McKibben	Contraction	1	P
	2017	Bowers *et al.* (2017)	Pneumatic	McKibben	Contraction	1	D/P
	2018	Chung *et al.* (2018)	Pneumatic	Textile /Fabric	Stiffening Beam	1	P
	2018	Iwata *et al.* (2018)	Pneumatic	McKibben	Contraction	1	D
	2019	Thalman *et al.* (2019)	Pneumatic	Textile /Fabric	Contraction	1	D
	2019	Di Natali *et al.* (2019)	Cable-Driven	Bowden Cables	Tensile	1	D/P
	2019	Kwon *et al.* (2019)	Cable-Driven	Bowden Cables	Tensile	1	D/P
	2019	Zhang *et al.* (2019b)	Pneumatic	McKibben	Contraction	1	D/P
	2020	Thalman *et al.* (2020b)	Pneumatic	Textile /Fabric	Contraction	1	P
	2020	Thalman and Lee (2020)	Pneumatic	Textile /Fabric	Stiffening Beam	1	I/E

***Legend**: D = Dorsiflexion P = Plantarflexion I = Inversion E = Eversion

weight to their foot (Babu *et al.*, 2018).

2.6 Current Work and Future Scope of Research

This review of past literature presents an examination of SWR devices for human assistance. A survey of actuation methods used in wearable devices, fabrication advancements, and applications is presented to provide a comprehensive overview of trends with the field. Soft robotics is an effective approach to providing wearable

robotic technologies with lightweight, low cost, and comfortable adaptations, while pushing the boundaries of material science and sensing technology. The rapidly growing field is challenging the way that roboticists have thought about wearable assistive devices, and is providing new pathways to enabling users to have wearable assistive robotics that are nearly transparent to their movement.

Soft robotic actuators have many benefits, however there are areas where improvements are still needed to further enhance the field. Potential areas for growth and current issues that are seen across most wearable robots in general is the power source for actuation. Pneumatic systems require some method of obtaining pressurized fluid to perform actuation, which is usually done by tethering the SWR to a compressor and regulating the resulting output pressure (Sasaki *et al.*, 2005b; Wang, 2016; Ding *et al.*, 2014b). The ideal system would be a standalone electro-pneumatic system, giving the user unconstrained mobility (Manfredi and Cuschieri, 2019), however portable pneumatic sources typically have struggled to provide sufficient flow rate or volume for most adult users without excessive weight (Wehner *et al.*, 2012; Thalman *et al.*, 2018). Latency issues resulting from pneumatic power sources is common in soft robotics (Malcolm *et al.*, 2013). This can be mitigated somewhat with the higher flow rates that can be achieved from directly connecting to air supply lines in existing infrastructure or tubing with larger diameter (Ding *et al.*, 2014b). Cable-driven systems use battery powered motors and control boards to induce actuation, which can be easily implemented into a hip mounted pouch or a backpack to house all control components (Bae *et al.*, 2015). Actuation motors are commonly mounted on the body to ensure the cables remain routed along the path needed to produce desired torques. While advantageous to have all hardware easily portable, a disadvantage is that the weight is often borne by the user.

The compliant and extremely variable positioning and behaviors of materials used

can cause difficulties when higher levels of flexibility are introduced to the core foundation of the device. Control of compliant actuation methods is usually based on oversimplified models based on pressure, volume, simplified geometries, constant-curvature or basic deformation (Petersen and Shepherd, 2018). While cable-driven system control has been more widely investigated, control of fluidic or extremely compliant actuator bodies has created interest in the soft robotics community posed as a free-form, open ended question: how can soft-bodied actuators be controlled? Open loop control is often times not sufficient, and so closed loop control is attempted using these simplified models. Bang-bang control is a common control strategy, using pressure or bending/curvature sensors to trigger pressurization at defined intervals (Petersen and Shepherd, 2018).

Soft robotics poses as a safe method to provide robotic assistance to individuals who may have unpredictable behaviors or movements patterns, without a noticeable amount of weight or bulk (Polygerinos *et al.*, 2017). LB assistive robotics are typically focused on gait training, and restoring some form of symmetry to an otherwise abnormal gait pattern, or offloading muscle effort for a gait with reduced strain to the user (Kawamura *et al.*, 2013). These exosuits can be used to actively prevent compensatory gait mechanics, provide additional support and stiffness, or to encourage proper gait mechanics (Abouhossein *et al.*, 2018). Some assistive devices, especially those focused on UB systems and the hand, aim to help impaired user regain independence and achieve ADL (Maciejasz *et al.*, 2014; Morales *et al.*, 2011). With preventative assistance, SWRs alleviate strain to particular parts of the body by offloading or translating pressure and stress from the user. This can help prevent injuries caused by heavy lifting, repetitive tasks, and poor ergonomics. Human augmentation can be achieved with wearable devices by providing high amounts of torque and force, while some SWRs can assist users carrying extremely heavy loads over long distances, lift

at higher capacities, run faster with a lower metabolic cost, and even increase sports performance (Lee *et al.*, 2017a; Roam, 209).

Review of existing SWRs presented in this manuscript shows a trend that is beginning to favor actuator designs that can be easily embedded into the user's clothing with minimal interference to normal range of motion and increased comfort. Observations from current devices and prevalence in the field based on publication records suggest that assistive soft robots are still in their infancy. This leaves ample opportunity for the field to begin to further explore how fabric-based actuators can be integrated together with other efforts toward functional garments to advance the way that rehabilitative robotics is approached for UB and LB assistance.

Chapter 3

DESIGN, MODELING, ANALYSIS, CHARACTERIZATION, AND FABRICATION OF SOFT ACTUATORS

Human locomotion is one of the most critical physical tasks for an individual to maintain independence and achieve the average activities of daily living (Spector and Fleishman, 1998). The human ankle joint is a critical point of rotation and weight translations, and is one of the major contributing factors to assist in forward locomotion and postural stabilization (Sawicki and Ferris, 2009; 201, 2018; Mueller *et al.*, 1995). Two major contributors to successful forward locomotion are plantarflexion and medial/lateral ankle stability for balance throughout walking. Ankle plantarflexion is responsible for 45% of the power behind moving the body forward during walking (Winter, 1983; Farris and Sawicki, 2011). Push-off is the stage of human gait where the heel lifts, which is a major contributor to forward propulsion during walking, and occurs at roughly between 45% and 60% of the gait cycle (Winter, 1980, 1983; Winter and Sienko, 1988). There are many factors that can impact an individual's ability to achieve natural and comfortable mobility. Among the most common factors are injuries sustained from trips or falls, neuromuscular conditions, and neurological disorders, and many of those with a history of ankle injury (or injuries) face an increased risk of reoccurring injuries (Yeung *et al.*, 1994). Chronic ankle instability is a common ankle impairment that affects the medial/lateral stability and increases the risk of future ankle injuries and sprains (Garrick, 1977; Venesky *et al.*, 2006). Ankle sprains usually occur when there is a sudden instance of inversion due to unanticipated lateral ankle buckling (Garrick, 1977; Venesky *et al.*, 2006).

Ankle-foot orthoses (AFOs) are the most commonly-used orthoses available to

Figure 3.1: This is the concept illustration of a soft robotic ankle-foot orthosis (SR-AFO) that helps impaired users walk again through active plantarflexion assistance, as well as support for lateral ankle buckling for prevention of trips and falls.

patients, accounting for as many as 26% of all orthoses provided to patients in the United States (Lusardi *et al.*, 2013; Whiteside *et al.*, 2007). In particular, AFOs are commonly prescribed for stroke victims suffering from hemiparesis, which affects around 80% of stroke survivors (Lusardi *et al.*, 2013; Sankaranarayan *et al.*, 2016; Cogollor *et al.*, 2018). According to the 2002 World Health Report, around 15 million people suffer from strokes each year, yielding potentially as many as 8 million survivors affected by hemiparesis (Organization, 2002; Center, 2020). While there are many versions of AFOs available on the market, they are largely made out of rigid materials like plastics and carbon fiber (Lusardi *et al.*, 2013; Whiteside *et al.*, 2007). With the rise in popularity of the wearable robotic industry, new robotic devices are being created to replace existing rehabilitative technology (Shi *et al.*, 2019; Kwon *et al.*, 2019; Chung *et al.*, 2018; Park *et al.*, 2014a; Lee *et al.*, 2016; Ren *et al.*, 2017). The

field of assistive soft robotics has gained popularity within the wearable robotics community (Bao *et al.*, 2018; Thalman and Artemiadis, 2020). Previous works have made significant advancements to substantiate the recent popularity of the use of soft, compliant materials to create wearable robots that are lightweight, comfortable, and effective at providing assistance to the user (Malcolm *et al.*, 2017; Kwon *et al.*, 2019; Chung *et al.*, 2018; Thalman *et al.*, 2019). Integrating textiles and fabrics into a wearable robot can help to eliminate some of the drawbacks seen with rigid exoskeletons such as size, weight, and cost (Malcolm *et al.*, 2017; Park *et al.*, 2014a; Asbeck *et al.*, 2013). This is especially critical when assisting a joint such as the ankle, where gait dynamics can be heavily affected by even slight changes to external conditions (Browning *et al.*, 2007).

This paper presents the Soft Robotic Ankle Foot Orthosis (SR-AFO) exosuit, which integrates soft, pneumatic actuators made from garment-like fabrics. The SR-AFO utilizes principles of soft robotics to help alleviate troublesome attributes of other traditional AFO solutions. It integrates two novel soft actuators and operates in multiple degrees-of-freedom (DoF), providing both assistance in ankle plantarflexion in the sagittal plane and support in inversion-eversion in the frontal plane during walking. The SR-AFO is designed to provide safe, active assistance at the precise intervals where it is needed without impacting the comfort or range of motion of the wearer. The paper presents the design, modeling, analysis, characterization, and control of the two soft actuators and human trials with the SR-AFO exosuit.

Applications of soft robotics specifically designed to treat chronic ankle instability and other long-term gait-impairing disabilities are limited. Our original actuator designs are therefore at the forefront of innovation in assistive wearable robotics, and particularly make use of the aforementioned advantages of soft robotics versus traditional wearable robotics and exosuits. As a design within the rapidly expanding

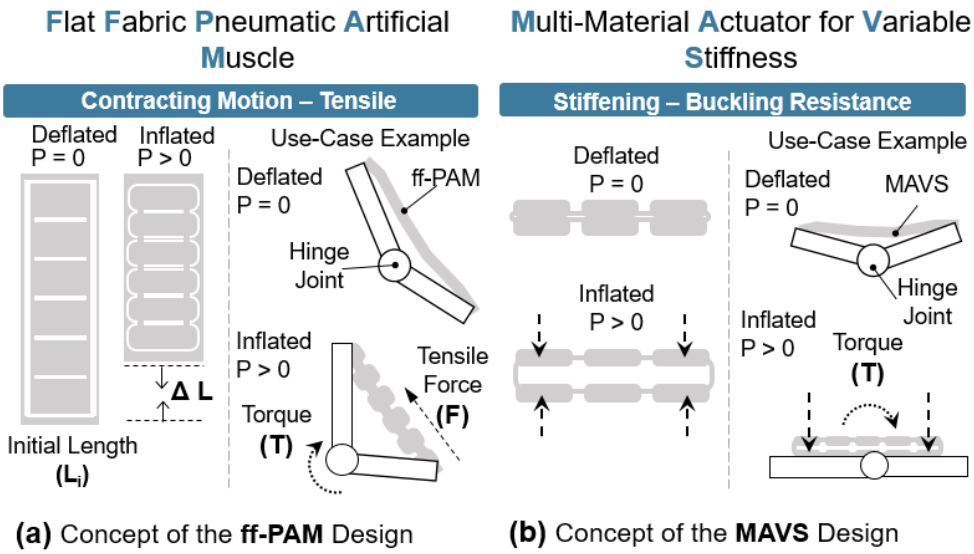

Figure 3.2: The concept illustration of (a) the flat fabric pneumatic artificial muscle (ff-PAM) actuator design and (b) multi-material actuator for variable stiffness (MAVS) design and their use cases.

field of soft robotics, our soft wearable robotic AFO has been optimized in a variety of ways, including actuator design optimization.

The first iteration of this work investigated the use of soft actuators for lateral ankle support (Thalman and Lee, 2020) and plantarflexion assistance (Thalman *et al.*, 2020b). Observations made based on previous publications suggest that assistive soft robots are in their infancy, yet the field is still rapidly expanding and gaining momentum (Thalman and Artemiadis, 2020). This leaves ample opportunity for the field to begin to further explore how fabric-based actuators can be integrated together to advance the way that rehabilitative robotics is approached for lower extremity assistance.

3.1 Design and Modeling of Soft Actuators

The SR-AFO is a soft, wearable ankle robot that is comprised entirely of fabric materials such as neoprene, spandex, and nylon. The combination of these materials forms a pattern that creates the main body of the SR-AFO, which can be worn over

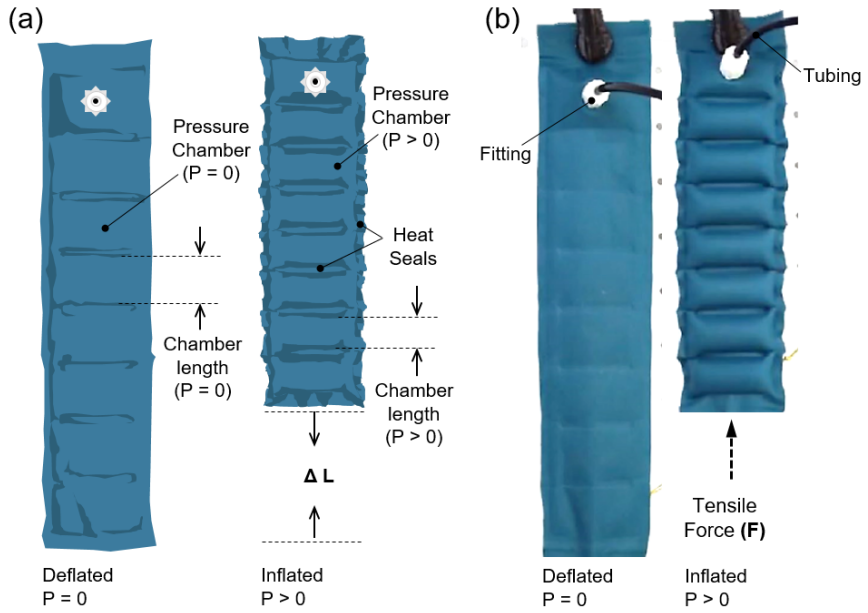

Figure 3.3: (a) The concept illustration of the ff-PAM actuator in the deflated and inflated states. (b) A fabricated ff-PAM before and after inflation to show the contraction and motion of the actuator.

the user's athletic shoe and can accommodate most adult shoe sizes. The SR-AFO exosuit comprises two sets of soft actuators which serve different primary functions in the overall performance of the soft exosuit.

The first actuator is the flat fabric pneumatic artificial muscle (ff-PAM), located at the posterior end of the foot and anchored to the knee brace just below the knee joint. The ff-PAM contracts when pressurized to create a tensile force. This tensile force pulls at the base of the heel to assist ankle plantarflexion.

The second set of actuators is the multi-material actuator for variable stiffness (MAVS). The MAVS are made from a combination of soft and rigid materials and can resist bending in various capacities depending on the fabrication techniques and applied pressure levels. The MAVS are placed on the medial and lateral sides of the ankle within the SR-AFO, running from a placement above the joint down to the base of the 1^{st} and 5^{th} metatarsal. When pressurized, the MAVS provide additional stiffness and support to the ankle in inversion-eversion to help prevent ankle buckling

in the frontal plane.

The theoretical models for ff-PAM and MAVS actuators were created using the geometric programming of materials, which has been shown to be a useful approach to modeling textile-based soft pneumatic actuators (Thalman *et al.*, 2019). The fixed set of assumptions used in the inextensible textile-based actuator modeling consist of: 1) soft materials are inextensible, 2) soft materials assume common geometric shapes when inflated, and 3) fully inflated soft segments assume a 'rigid' behavior at maximum pressure.

3.1.1 Design and Modeling of Flat Fabric PAM (ff-PAM)

The model used to represent the ff-PAM is governed by the following set of equations (Fig. 3.4) (Niiyama *et al.*, 2015):

$$F(\theta) = L_i w P \frac{cos(\theta)}{\theta}, \tag{3.1}$$

$$L_\epsilon = \frac{L_i - L(\theta)}{L_i} = 1 - \frac{sin(\theta)}{\theta} \tag{3.2}$$

where F is the tensile force, L_i is the original length of each chamber, $L(\theta)$ is the length of each chamber after inflation, L_ϵ is the contraction ratio of the actuator, P is the supply pressure, and w is the width of the actuator. Estimation of force output is based on the laws of conservation of energy. A relation between the supplied pressure and resultant force output can be expressed as:

$$-FdL = PdV \tag{3.3}$$

where V is the internal volume of the pneumatic chamber. Both V and L can be expressed as a function of θ and the expression can be written as

$$F(\theta) = -P \frac{\frac{dV}{d\theta}}{\frac{dL}{d\theta}} \tag{3.4}$$

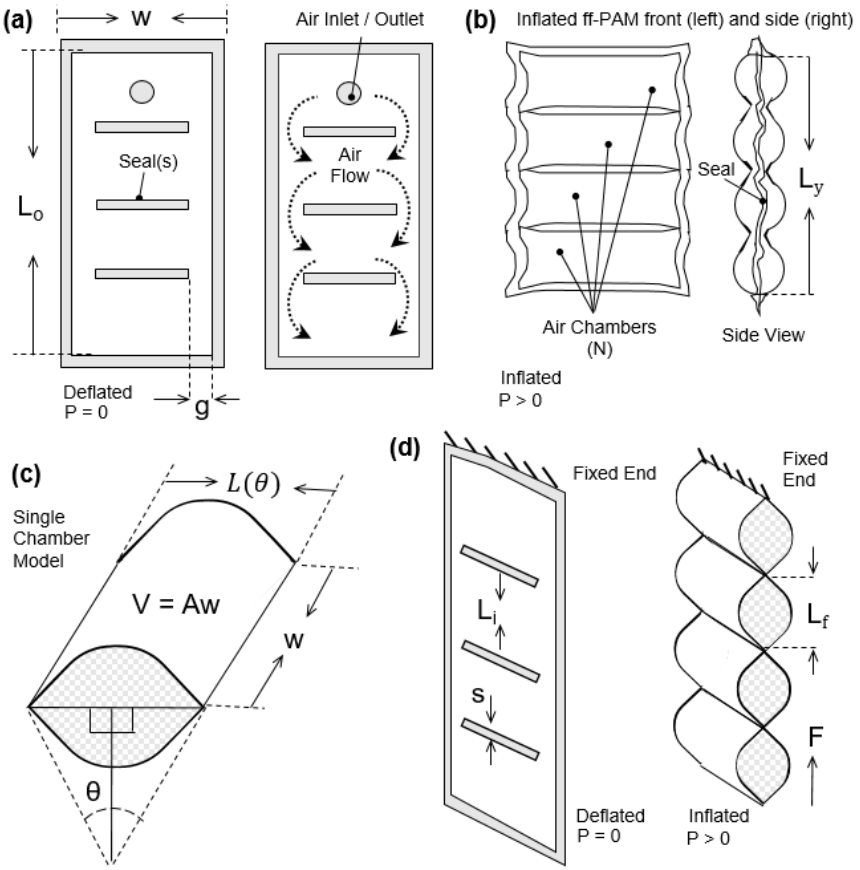

Figure 3.4: (a) A simplified frontal view representation of the ff-PAM at P =0, which indicates the simplified geometries of the actuators, and the path of airflow within the chambers. (b) The frontal view of ff-PAM at P >0 where the length and geometries are altered as a result of pressurization. (c) A cross-section of a single chamber inspired by previous model iteration of inflatable pouches (Niiyama *et al.*, 2015). (d) An isometric view of the ff-PAM in a deflated and inflated state for a comparative view of the active and inactive actuator states, where L_i and L_f are the initial and final lengths of $L_(\theta)$ respectively.

In order to determine the contraction in terms of strain (L_ϵ), a corrected version of L_ϵ is used ($L_{\epsilon C}$),

$$L_{\epsilon C} = L_\epsilon(1 + \frac{d\pi}{\pi - 2}) - d \tag{3.5}$$

where d is a correction coefficient as described in (Niiyama *et al.*, 2015) to account for some of the flexibility and compliance of the soft, thin textiles used to fabricate the actuator, which can affect the resulting strain. The length of the entire actuator, including all chambers of the actuator, with all chambers of the actuator was later

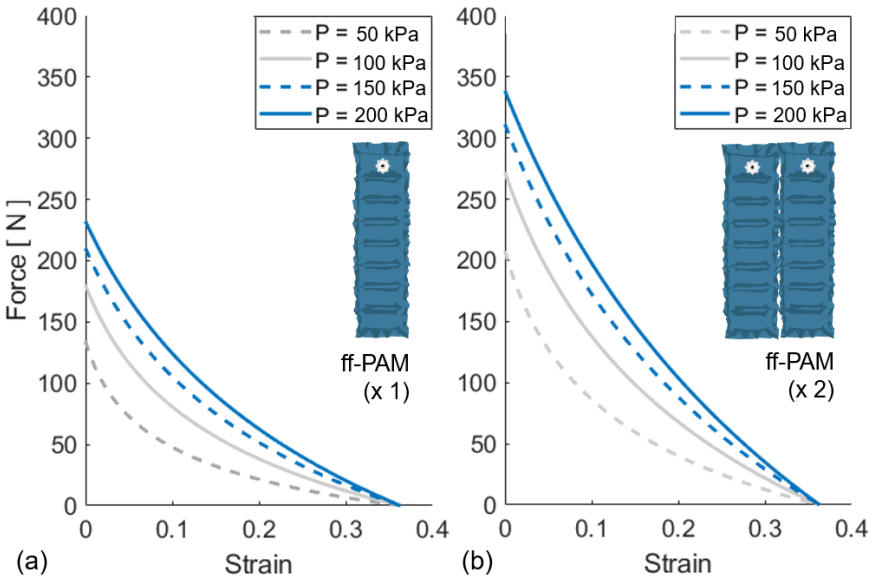

Figure 3.5: (a) The tensile force/strain curve for a single ff-PAM actuator for pressure levels of $P = 50$, 100, 150, and 200 kPa. (b) The force/strain curve for two parallel ff-PAM actuators for pressure levels of $P = 50$, 100, 150, and 200 kPa.

optimized via finite element analysis (FEA) using the following conditions:

$$L_y = (N-1)s + NL(\theta), \tag{3.6}$$

where L_y is the total length of the ff-PAM, s is the distance between each chamber created by the heat seal, and N is the total number of chambers.

For this work, 8 chambers ($N = 8$) have been selected to achieve desired contraction. The stress/strain curves for the ff-PAM design with $N = 8$ is indicated in Fig. 3.5 for both a single ff-PAM actuator and two parallel ff-PAM actuators. Each model is evaluated at four pressure levels (50, 100, 150, and 200 kPa), which show that the tensile force of the ff-PAM increases with increasing P in both the single and dual ff-PAM configurations. The single ff-PAM and the dual ff-PAM actuators were predicted to reach 220 N and 307 N, respectively, at the theoretical point $L_{\epsilon C} = 0$ at 100 kPa. While the dual actuator configuration increased the total volume of the active ff-PAM setup, the increase in force output throughout the duration of actuator contraction was considered valuable for the application of plantarflexion and push-off

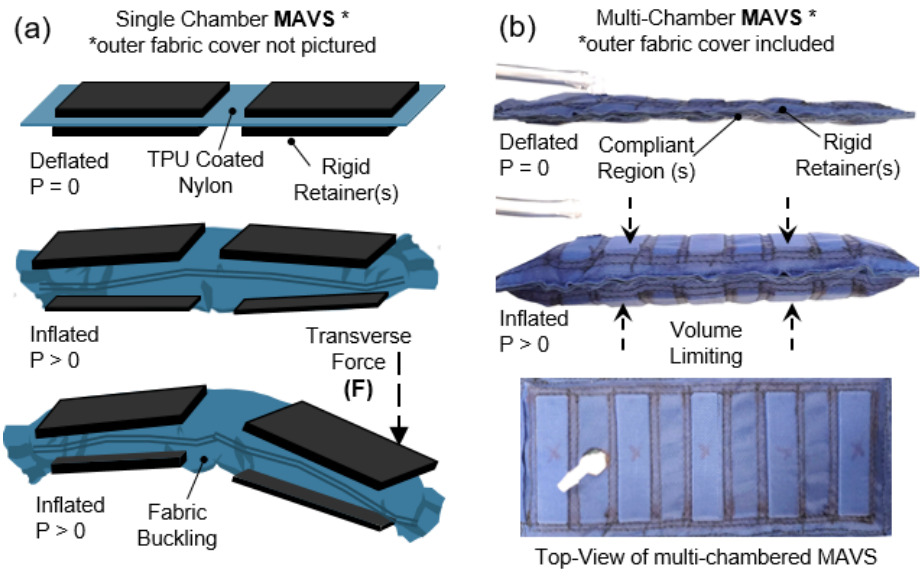

Figure 3.6: (a) The concept illustration of the MAVS actuator in a deflated state, inflated state, and buckled state after being subjected to a transverse load. (b) An image of the MAVS actuator from the side view in a deflated state and inflated state, and from the top view.

assistance. The SR-AFO exosuit used the dual ff-PAM configuration, which was the focus of the evaluation performed on the ff-PAM actuator in the following sections. This design was selected due to its high predicted force output at 348.3 N of tensile force at 200 kPa, which produced an increase of nearly 100 N for the resulting tensile force compared to the single ff-PAM actuator.

3.1.2 Design and Modeling of Multi-Material Actuator for Variable Stiffness (MAVS)

The second actuator introduced in the SR-AFO was the multi-material actuator for variable stiffness (MAVS), which utilized the integration of rigid components into a soft, fabric-based actuator. The rigid components are small, thin pieces of custom 3D printed Polylactic Acid (PLA), embedded into the soft actuator fabric layers during the sewing stages of the fabrication process. The rigid materials limit vertical expansion of the actuator when pressurized and restrict physical internal volume by

(a) Example MAVS Set

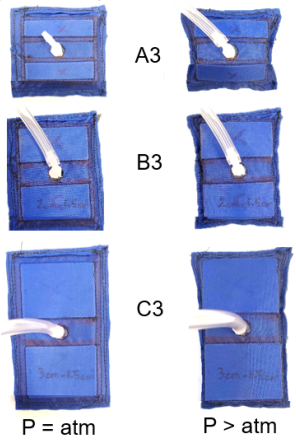

(b)

L_g (cm)	L_r (cm) 1	2	3
0.5	A1	B1	C1
1	A2	B2	C2
1.5	A3	B3	C3
2	A4	B4	C4
2.5	A5	B5	C5
3	A6	B6	C6

Figure 3.7: (a) A visual of the different iterations of the MAVS when deflated and inflated. (b) The different gaps and rigid retainer lengths used in the different design iterations represented by a letter and number label. L_g is the width of gap of exposed soft actuator between rigid retainers, and L_r is the width of the rigid retainer.

limiting the cross-sectional area of the MAVS. The rigid retainers are placed along the length of the actuator and alternate with sections of exposed fabric, providing the MAVS with varying levels of compliance. By alternating segments of soft and rigid-bound cross sections, the MAVS can obtain varying levels of lateral stiffness that can be adjusted during fabrication or pressurization (Fig. 3.6). This is done for various sizes and combinations of ratios of the MAVS actuator.

The rigid retainers were tested in three sizes, labeled A - C for each size. The gap length was denoted by the numerical value assigned. Based on previous analysis presented in (Thalman *et al.*, 2020a), the A2 MAVS was selected from the table in Fig. 3.7 for the SR-AFO. This was because the selected ratio between rigid and soft materials allowed for the highest stiffness when pressurized (inflated) without becoming overly stiff when inactive (deflated).

Inspiration for the integration of multi-segment, multi-material use for the MAVS was drawn from several previous works, such as the sliding layer laminate actuator design presented in works by Jiang and Gravish (Jiang and Gravish, 2018). This

design focused on a three-layer laminate actuator that varies stiffness based upon the ratio of the size of each exposed material when subjected to transverse load. The stiffest condition was achieved when there was a total misalignment of the layers, where the exposed soft material was minimized. Similarly, the smallest stiffness was achieved when the layers were stacked in perfect alignment, where the exposed soft material was maximized. The MAVS design was implemented with these physical characteristic behaviors in mind. The rigid retainers were placed on the outside of the layer of inflatable actuator. The design created for the MAVS integrated this idea by having an inflatable actuator secured between two layers of rigid pieces embedded in fabric. The rigid pieces were aligned on the top and bottom of the actuator. A single segment of the MAVS weighs only between 31.2 - 89.3 g, depending on the configuration used. A similar design to the MAVS incorporates rigid pieces into an inflatable actuator designed for contraction (Kwon *et al.*, 2020).

The MAVS actuator was modeled as a cantilever beam, fixed and pinned in place across one half of the actuator, with the other half free to move. The cross-section of each segment of the MAVS was accounted for in the final equation for deflection of the free end. The total deflection $V_t(L_t)$ of the MAVS was calculated by:

$$V_t(L_t) = N(V_{PLA} + V_{Nylon}) + V_{PLA} \tag{3.7}$$

for an actuator with N segments of alternative materials. These material types were denoted by the variables V_{PLA} and V_{Nylon}, which indicate the deflections using the material properties of PLA and Nylon, respectively. Segments for PLA ($E_1 I_1$) and Nylon ($E_2 I_2$) respond differently when subjected to external loads, due to differences in material properties. These were accounted for individually for both V_{PLA} and V_{Nylon} using the Young's elastic modulus (E) and moment of inertia (I) of each segment. Each of the rigid (PLA) and soft (Nylon) segments was modeled as a simply

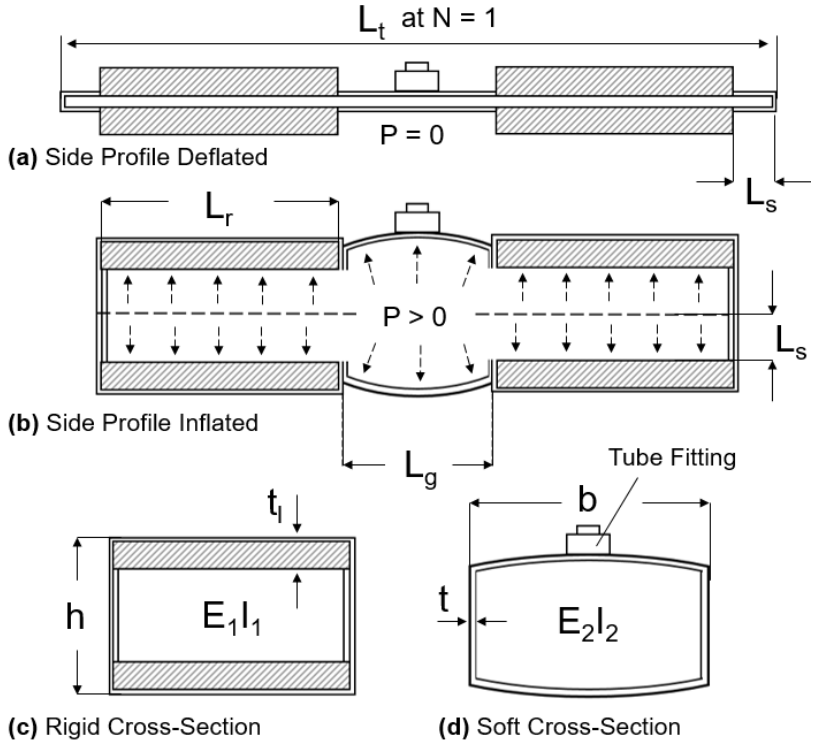

Figure 3.8: (a) The MAVS actuator when deflated. (b) The MAVS actuator when inflated with the main components of the actuator specified. (c) A cross-section view of the rigid part. (d) A cross-section view of the soft part.

supported cantilever beam with a single point load at the free end and using Timoshenko's theory (Wielgosz and Thomas, 2002; Thomas and VANa, 2019; Wielgosz *et al.*, 2008). Applying this theory, the deflection of each segment ($V(x)$) can be modeled as:

$$V(x) = \frac{F}{(E + P/S_o)I_o}\left(\frac{{L_{r,g}}^2 x}{2} - \frac{x^3}{6}\right) + \frac{Fx}{(P + kGS_o)} \tag{3.8}$$

where $L_{r,g}$ is the length of each segment (L_r for the rigid segment and L_g for the soft segment), which can be calculated at a length x away from the fixed end $x = 0$. The beam was subject to an internal pressure P and a transverse force F at the free end, where $x = L_t$. The second moment of inertia, I_o, was determined by the shape of the cross-sectional area and the axis about which the actuator was being deflected. The shear coefficient was represented by kGS_o, where S_o is the cross-sectional area,

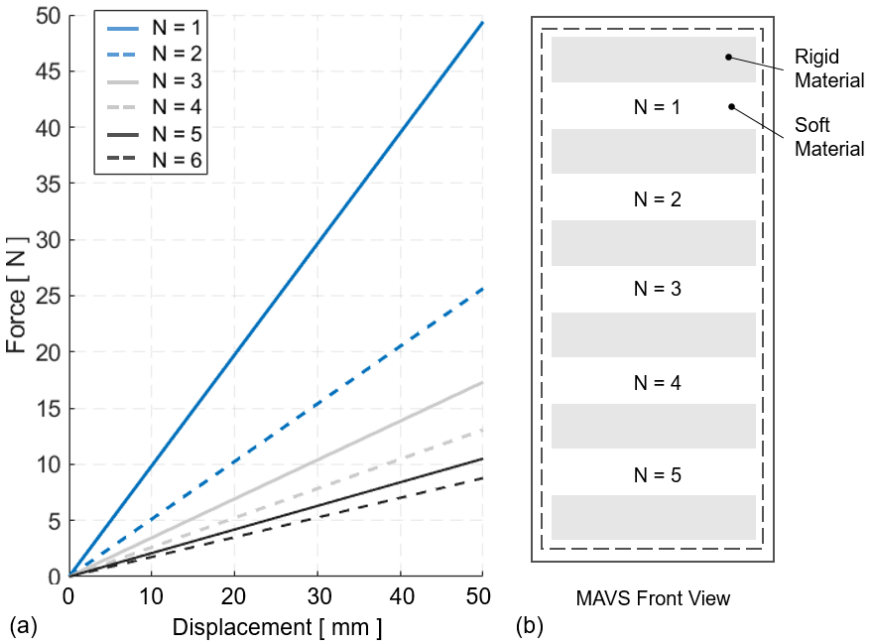

Figure 3.9: (a) The stiffness outputs of the MAVS for various values of N, which denotes the quantity of exposed soft actuators segments in MAVS design $A2$. (b) A front view of the MAVS-A2 design is illustrated with multiple segments of N.

G is the shear modulus of the material, and k was determined by the cross-sectional shape and Cowper's formulation (Cowper, 1966). From Cowper's formulation of a thin-walled box section, k was calculated as:

$$k = \frac{10(1+\nu)(1+3m)^2}{(12+72m+150m^2+90m^3)} + ...$$

$$\frac{10(1+\nu)(1+3m)^2}{\nu(11+66m+135m^2+90m^3)+10n^2((3+\nu)m+3m^2)} \tag{3.9}$$

where

$$m = \frac{bt_l}{ht} \tag{3.10}$$

and

$$n = \frac{b}{h} \tag{3.11}$$

The shear modulus was calculated for the PLA rigid retainers (E_1) and Nylon fabric (E_2) with the equation,

$$G = \frac{E}{2(1+\nu)} \tag{3.12}$$

where ν is the Poisson's ratio, which is determined by the material properties. The maximum deflection was calculated with $x = L_t$, (Wielgosz and Thomas, 2002), which reduces Eq. (3.8) to,

$$V(L_t) = -\frac{F}{2Pbh}L_t - \frac{FL_t^3}{3Ebh^2} \tag{3.13}$$

where b is the base length of the cross-sectional area (which was kept constant at 4 cm), h is the height of the actuator when inflated, and L_t is the total length of the MAVS actuator. The length L_t of the actuator was calculated as:

$$L_t = 2L_s + N(L_r + L_g) + L_r \tag{3.14}$$

where L_s is the length added by the seam, L_r is the length of the rigid piece, and L_g is the length of the gap between rigid pieces where the soft actuator was exposed (Fig. 3.8). The number of exposed sections of the soft actuator was represented by N to account for varying lengths of the MAVS. The effects of varying N are shown in Fig. 3.9, where applied transverse load vs. tip deflection are shown for varying N conditions.

3.2 Finite Element Analysis

In order to investigate the behavior of each actuator prior to fabrication, simulations were performed using FEA. The analysis predicted the accuracy of the analytical models, validated the behavior of the soft and integrated materials, and optimized the

geometric parameters of the design. The FEA simulation was performed using a FEA software (ABAQUS, Dassault Systems, Vlizy-Villacoublay, France) in a dynamic explicit environment. The TPU coated nylon was simulated using the Young's Modulus of $E = 498.9\ MPa$, the Poisson's ratio of $\nu = 0.35$, and the material thickness of 0.15 mm as found in previous works (Thalman *et al.*, 2019). For each actuator design, the air chambers were modeled by creating a 2D homogeneous thin shell with the net shape of a single layer of the TPU coated nylon. Partitions were created where the heat seals were placed.

Two layers of these thin shells were stacked in an assembly, and the innermost facing surfaces of each seam partition were bound using a tie constraint. The innermost facing surfaces of the air chambers were designated at a load-bearing face, and a uniform pressure load was applied outward from the initial plane of the fabric in both directions to simulate pressure. This was done for both the ff-PAM and MAVS actuators, which are described in more detail in the following sections.

3.2.1 FEA Analysis of ff-PAM

An FEA model was created for the ff-PAM using two layers of TPU coated nylon stacked and tied at the seams. Two different types of simulation were performed: (1) simulation investigating force vs. displacement at one constant pressure level (200 kPa); and (2) simulation investigating force vs. pressure at a fixed displacement (0 mm). These are standard practices used to evaluate pneumatic contracting actuators such as McKibben Muscles (Ching-Ping and Hannaford, 1996; Doumit *et al.*, 2009). In the first simulation (Fig. 3.10a), the force-contraction relation was measured, when the pressure was held at a constant level of 200 kPa and applied uniformly across each step of the simulation. The force and displacement at the free end were evaluated throughout pressurization until the actuator had reached full contraction.

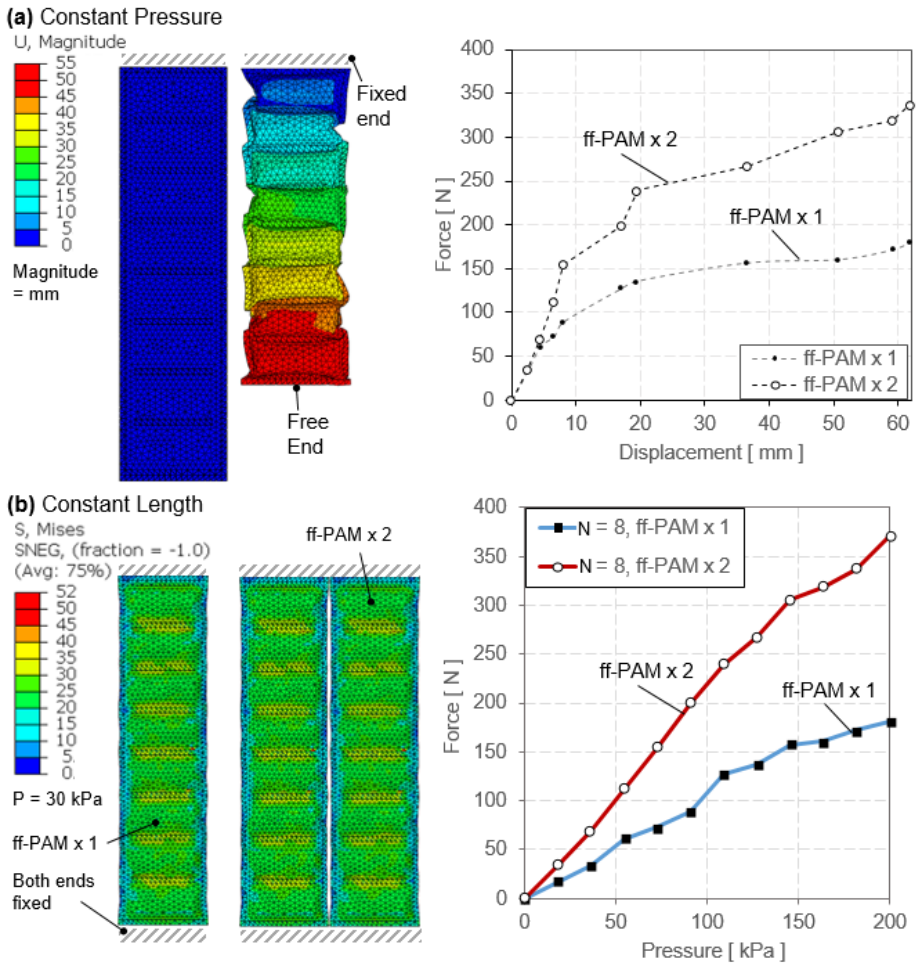

Figure 3.10: (a) Constant pressure simulation results for the single and dual ff-PAM actuators, where one end of the actuator is free to move and the contraction is measured as the total displacement, with the color-map showing the displacement in the vertical direction (mm). (b) Constant displacement simulation results for the single and dual ff-PAM actuators, with both ends fixed and the pressure is varied to obtain the maximum force at each level. The colors map shows the stress across the surface of the actuator to show a uniform loading of the internal pressure force. A sample result at 30 kPa is shown.

The total force output for the single and dual ff-PAM actuators was 180.2N and 337.5N, respectively, both at the contraction rate of 28.9%.

In the second simulation (Fig. 3.10b), actuator vertical displacement at each end was held constant and the pressure was varied. The constant displacement condition was intended to estimate the theoretical maximum force output of the actua-

tors, which occurs when displacement of the actuator was fixed at its original length (Ching-Ping and Hannaford, 1996). This simulation was run in a quasi-static, isometric contraction evaluation, where both ends of the actuator were fixed and pressure was incremented with each simulation until the model stabilized and a final maximum force value was obtained. One end was fixed in all directions while the other was fixed vertically and used to evaluate the reaction forces across its surface to estimate the force. The forces in the vertical direction were summed along the width of the top of the actuator to estimate the tensile force generated from the actuator. This was done for varying pressure levels (0 - 200 kPa), as well as for the single and dual ff-PAM actuators.

For the same level of pressure, the dual actuators always exhibited a higher output force than the single actuator (Fig. 3.10b). At the maximum pressure level tested (i.e., 200 kPa), the peak force was 180.2N and 337.5N for the single and dual actuators, respectively. Simulation results of maximum force obtainable at each pressure level can be used to estimate the behavior of the actuator prior to fabrication.

3.2.2 FEA Analysis of MAVS

The MAVS was modeled using a combination of simulated materials for both the soft actuator and rigid retainers. Thin 2D homogeneous shells were used in the shape of a hollow rectangle to create the pneumatic chamber, with the length and width of the rectangle the same dimensions as that of the MAVS width and length. The rigid retainers were modeled using solid 3D homogeneous extrusions, and assigned a material property for PLA 3D printed material, which was modeled using material properties with the Young's Modulus of 3600 MPa and the Poisson's ratio of 0.3 as used in previous works (Thalman *et al.*, 2019).

The pneumatic pouch was sealed by tying the edges of the thin shells around

the perimeter of the rectangular parts. The rigid pieces were placed on the top and bottom faces of the rectangular shell, parallel to the face and spaced according to which MAVS variation was simulated. An additional 2D homogeneous shell of nylon fabric was placed to encase the stacked soft actuator and rigid retainers. The outward faces of the rigid pieces were tied to the outer shell and a global interaction property for surface-surface contact was applied to the assembly. A solid 3D homogeneous clamp was created with the PLA material property and fixed to hold the actuator at a fixed point for the cantilever beam example modeled in the previous section. The major benefit of being able to model the MAVS was to show the interaction between multiple layers of several material types, thicknesses, and properties. This allowed the internal chambers of the MAVS to be observed and studied as done in other works with variable stiffness actuators (Sun *et al.*, 2020).

Two loads were applied to the model: (1) a uniform pressure load to the internal faces of the thin shells of the actuator, and (2) a transverse load applied at a fixed point at the end of the actuator. A total of three steps were run for the simulation: (1) pressurization, (2) stabilization, and (3) point loading as depicted in Fig. 3.11a. The deflection of the MAVS was measured by fixing one half of the MAVS and applying a perpendicular force to the free end. Transverse loads of 5, 10, 15, and 20 N were applied at a fixed point on the free end of the actuator, which was inflated to 100 kPa. This was done for the three highest performing MAVS designs ($A1 - A3$) predicted by the analytical model. The deflection at the end of the actuator was measured along the direction of the transverse load. Simulation results showed that stiffness of the MAVS decreased as L_g increased (Fig. 3.11a). However, since the MAVS-A2 was selected as the primary MAVS actuator for the SR-AFO, the MAVS-A2 design was evaluated in further detail using FEA to analyze the behavior of the actuator at varying lengths and values of N.

The MAVS-A2 actuator was modeled in the FEA simulation as a cantilever beam as done in the previous simulation. One end of the MAVS was constrained between two infinitely stiff, fixed blocks which held the end in place. The other end of the MAVS was subjected to a transverse point load at the end of the actuator perpendicular to the top surface as shown in Step 3 of Fig. 3.11a. The tip deflection of the MAVS was recorded for loads of 5, 10, 15, and 20 N. The value of N was also increased after each set of point loads were applied from $N = 1$ to 5 with the internal pressure of the MAVS fixed at a constant 50 kPa for each simulation.

Simulation results showed the least deflection with $N = 1$ across all loading conditions, likely due to the small net size of the actuator. However, as N increased more than 2, the degree of deflection was comparable for each loading condition. This result helps to validate that, even at longer lengths, the MAVS-A2 actuator can maintain relatively constant stiffness and resist deflection against medial and lateral loads. This is a critical point as a single MAVS-A2 chamber is not long enough to cross the length of the human ankle, whereas a MAVS-A2 at $N = 5$ is able to cross the joint effectively.

3.3 Actuator Characterization

A universal testing machine (UTM) (Instron 5565, Instron Corp., High Wycombe, United Kingdom) was used to experimentally characterize both the ff-PAM and MAVS actuators of the SR-AFO exosuit and evaluate their performance.

3.3.1 Characterization of ff-PAM

Three different types of experiments were performed to evaluate (1) tensile force vs. contraction (or displacement) at varying pressure levels; (2) tensile force vs. pressure at a fixed displacement at 0 mm (i.e., zero contraction); and (3) dynamic

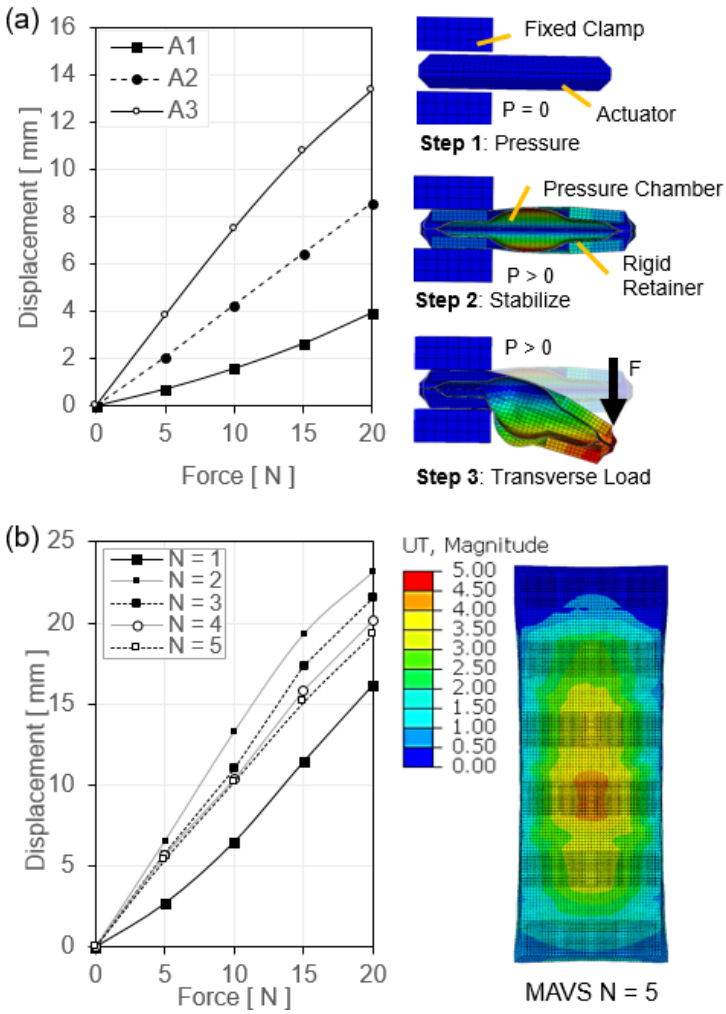

Figure 3.11: (a) The force-displacement output of a single MAVS actuator is evaluated with FEA for the MAVS-A1, A2, and A3. Various loads are applied to the free end of the MAVS while in a cantilever orientation and the resulting displacement is recorded. (b) shows the results of an FEA simulation of the same sequence of steps as (a), with the MAVS-A2 actuator, varying the number of segments, N for each simulation to calculate the total displacement of the free end.

response of tensile force generation.

In the first quasi-static experiment, the output tensile force vs. actuator contraction (or displacement) relation was evaluated under varying pressure levels. The experiment was performed at five different pressure levels (20, 60, 100, 160, and 200 kPa) with five repetitions per each pressure condition. The UTM was programmed to induce a controlled vertical translation and measure actuator force vs. displacement.

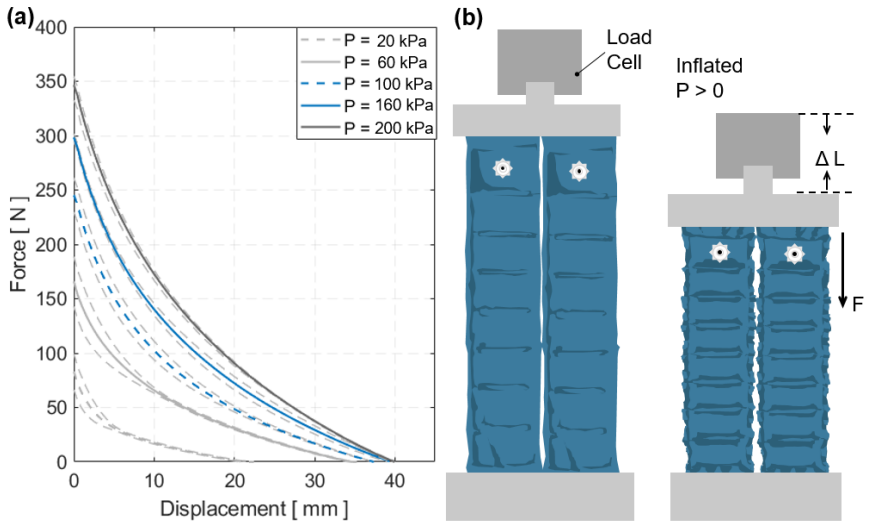

Figure 3.12: (a) The force output of the dual ff-PAM setup using a constant pressure test protocol, evaluated across 5 selected pressure levels, was averaged across 5 trials. (b) The test conditions and setup of the ff-PAM in the UTM before and after the UTM performs the vertical translation.

Each measurement was completed once the load cell reading was 0 N indicating full actuator contraction. The load cell increased the uniaxial compression at 5 mm/s until it read 0 N of force. The load cell was returned to the zeroed position and the test was run cyclically for five repetitions. The average result (mean and mean $\pm$ standard deviation (std)) and the test condition are shown in Fig. 3.12.

Tensile force of the ff-PAM was maximized when the actuator length was maximized (zero contraction) and the force approached 0 N as the actuator fully contracted. In addition, as the pressure level increased, the force output was more repeatable and accurate. At 200 kPa, the maximum force output was 346.5 $\pm$ 1.4 N, while at 100 kPa it was 245.4 $\pm$ 15.8 N, decreasing the output by 100 N and decreasing the repeatability drastically. Following this trend, at 20 kPa the maximum force output was 83.0 $\pm$ 16.5 N. The variability was close to that at 100 kPa, yet the force dropped drastically. The analytical model predicted a maximum force output of 337.5 N at 200 kPa, which fell within 10 N of the value predicted from the analytical model.

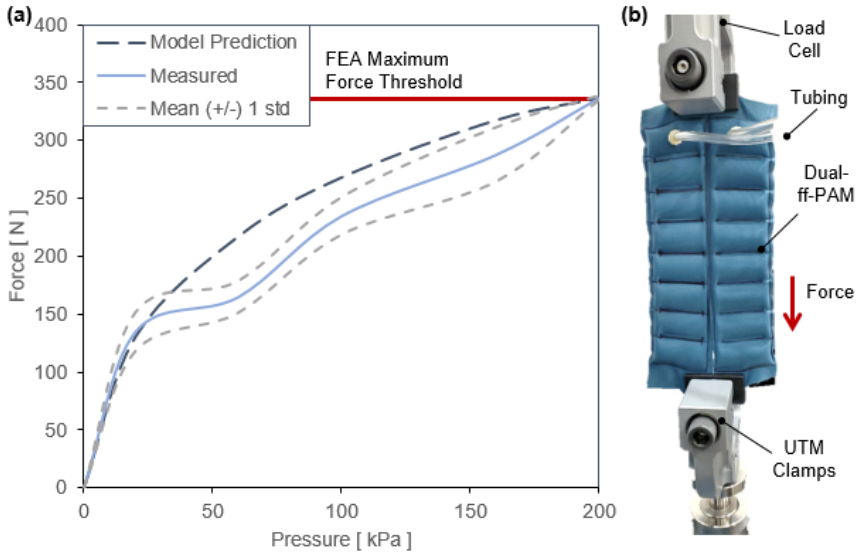

Figure 3.13: (a) The experimental results of the dual ff-PAM actuators are compared to the model prediction to show their similar behavior pattern. (b) The test setup for experimental characterization is shown with the ff-PAM fixed in the vice clamp of the UTM.

In the second static experiment, the output tensile force vs. pressure relation was evaluated when displacement was fixed at 0 mm. This relation was compared with the predictions from the analytical model and the FEA simulated maximum threshold. The dual ff-PAM was placed in a vice clamp as shown in Fig. 3.13b, with the UTM displacement fixed at 0 mm. The pressure increased quasi-statically from 0 to 200 kPa in fixed increments of 10 kPa until a stable load could be read from the UTM. Three repeated measurements were performed. The final maximum tensile force output of the ff-PAM actuator at 200 kPa measured by the UTM was 337.1 $\pm$ 1.4 N, which fell within a threshold $< 0.5\%$ error from the predicted value from the analytical model (336 N) and FEA simulation result (337.5 N).

In the third experimental characterization, a dynamic test was performed to obtain a force-time relation to measure how quickly the actuator reacts to pressurized input. The dynamic response was initiated by rapidly opening a 3-way, 2-channeled solenoid valve (320-12 VDC, Humphrey, USA) to quickly deliver pre-set pressure to

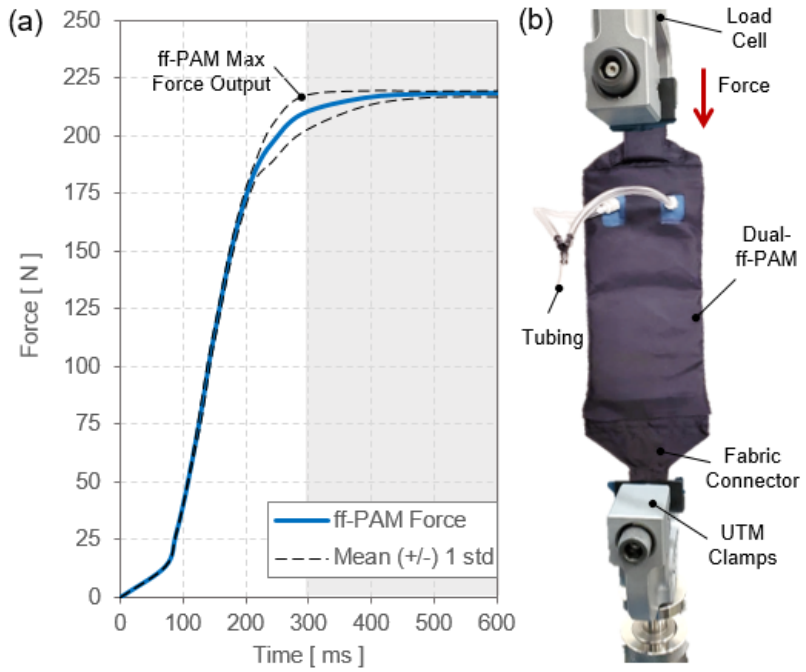

Figure 3.14: (a) The dynamic response of the dual ff-PAM actuators, while clamped at maximum length in the UTM interface. The response is measured for the time required to achieve maximum force output at 150 kPa. (b) The test setup and conditions of the ff-PAM connected to the UTM with fabric connectors.

the internal air chambers of the ff-PAM. This characterization is important since the ff-PAM actuator is designed to provide a tensile force through uniaxial contraction to the posterior end of the foot during plantarflexion at the push-off phase of human gait, and the actuator must be able to provide sufficient force output within a time window that allows the user to feel each controlled perturbation.

A fabric connector was affixed to the top and bottom of the ff-PAMs to secure both actuators together with a tapered fabric component used to transfer the force from pressurization to a single point as shown in Fig. 3.14b. By allowing the actuator to interface with a fabric anchor, it is assumed that a more realistic force output can be measured to represent the behavior of the actuator when worn on the SR-AFO exosuit. After increasing the tubing diameter used in the valves to 1/4 inch outside diameter tubing, the new force-time curves were obtained at a fixed pressure of 150

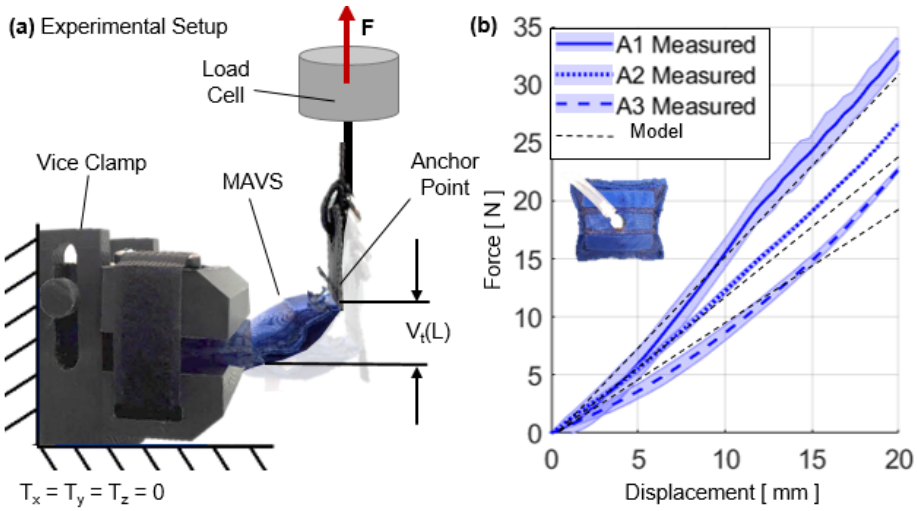

Figure 3.15: (a) The test setup with the UTM is shown from the side view, with the custom 3D printed clamp and MAVS fixed to the load cell. (b) The resulting measured force/deflection relationship for the A1, A2, and A3 MAVS actuators for a single unit for a maximum 20 mm deflection at 50 kPa. The force required to deflect the same distance (20 mm) is shown in with the actuator model.

kPa, and the valve was opened to provide rapid pressurization. The actuator was able to provide 212.3 $\pm$ 7.7 N of tensile force in 0.29 sec.

3.3.2 Characterization of MAVS

Three MAVS actuators (A1-A3) were tested at varying pressures from 0 to 100 kPa in increments of 10 kPa. A custom clamp was fabricated to fix the MAVS in place while being subjected to deflection testing. The MAVS had a tab sewn into the free end to interface with the clamps paired with the load cell of UTM as seen in Fig. 3.15a. This allowed for the UTM to apply a point load to the MAVS while it is fixed in a cantilever position. The UTM pulled the free end of the MAVS upward 20 mm. The tab acted as a constant point of contact so that the lever arm distance did not change. To keep the most consistent point load location, the tabs were used to deflect the MAVS upward. Each iteration was deflected upward and the force was measured so that the stiffness of each MAVS could be determined.

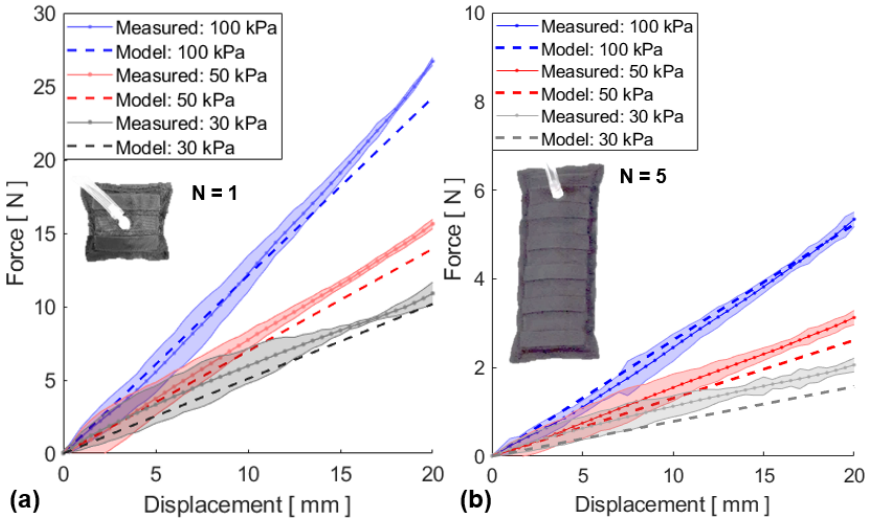

Figure 3.16: The characterized force/deflection relationship of the MAVS-A2 at three pressure levels (30, 50, and 100 kPa) in comparison to the analytical model results for (a) $N = 1$, (b) $N = 5$.

The trends of each MAVS followed closely to the model predictions for each evaluated condition. MAVS-A1 required the highest force to reach a 20 mm deflection, reaching 32.6 $\pm$ 1.4 N with calculated stiffness of 1,629.4 N/m, which fell within 4.5% of the model predictions (Fig. 3.15b). MAVS-A2 was the second highest stiffness values observed at 100 kPa, reaching 26.7 $\pm$ 0.1 N with calculated stiffness of 1,335.5 N/m and fell within 9.1% of the model predictions. The third highest stiffness MAVS was MAVS-A3, which obtained 22.7 $\pm$ 0.2 N, with calculated stiffness of 1,137.0 N/m, and fell within 11.1% of the predicted value.

The MAVS-A2 actuator was further evaluated for various pressure levels in the cantilever orientation and compared to the analytical model. The pressures evaluated were 30, 50, and 100 kPa. The rationale for these pressure level selections was based on two factors (1) accuracy of higher pressures, and (2) comfort of the user. With the MAVS actuator integrated into the SR-AFO design, user feedback indicated pressure levels above 100 kPa were not comfortable during walking.

The MAVS-A2 was tested at these three pressure levels using the test setup pre-

viously described and shown in Fig. 3.15a. This evaluation was performed for the original MAVS-A2 design where $N = 1$, and performed a second time for MAVS-A2 for $N = 5$, the latter of which is the version of the MAVS-A2 actuator embedded into the SR-AFO exosuit. The MAVS-A2 actuator experienced 20 mm of deflection with an applied load of 12.1 $\pm$ 0.2 N, 15.6 $\pm$ 0.1 N, and 26.7 $\pm$ 0.1 N at 30, 50, and 100 kPa, respectively.

It was observed that as pressure decreased, so did the applied load required to reach the fixed displacement threshold. The deviation increased with lower pressures, though this was anticipated as lower pressure would result in higher changes of buckling at unpredictable locations. Increasing the length to $N = 5$ showed similar trends. While the overall deflection has less resistance to bending observed than $N = 1$ condition, this was an expected result since the MAVS-A2 had an increased length. The $N = 5$ MAVS-A2 required 2.4 $\pm$ 0.2 N, 3.1 $\pm$ 0.2 N, and 5.3 $\pm$ 0.2 N, for 30, 50, and 100 kPa, respectively.

3.3.3 SR-AFO Hardware Design

The SR-AFO is designed to be worn in a variety of applications. The hardware used to control the exosuit is housed within a lightweight fabric belt, which can be adjusted to be worn on the hips, or worn as a bareback depending on the user preference. The cables are long enough to allow the hardware to be set aside and placed next to the test platform if on-board hardware is not ideal for the test conditions. The table-top version of the design was the orientation used in the results of this manuscript.

The hardware logic controller used an Arduino Mega 2560 Rev3, which connects all analog inputs and digital outputs of the SR-AFO to monitor the status of the system. These I/O are categorized by the force-sensitive resistor (FSR) sensors (In-

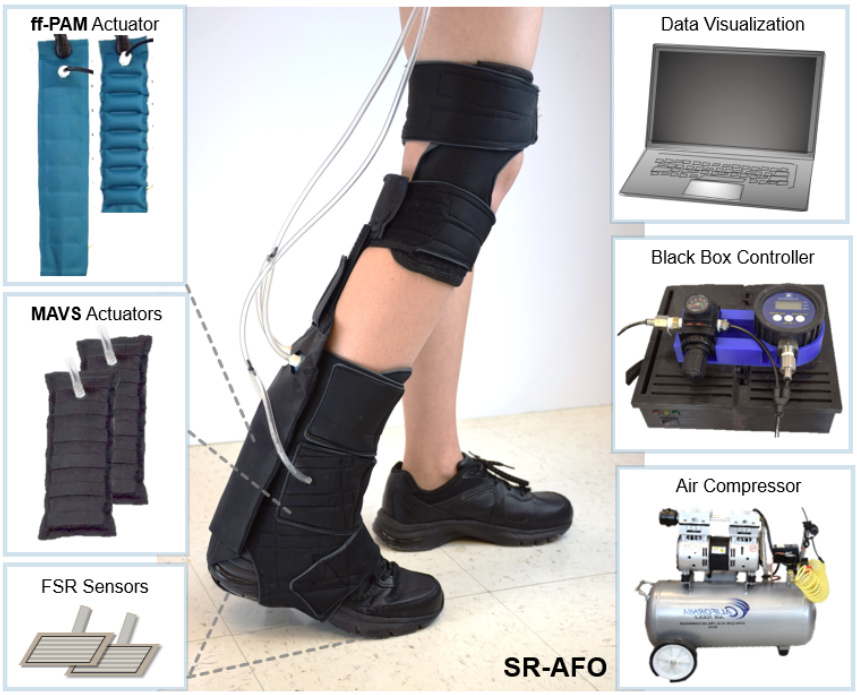

Figure 3.17: The final assembly of the SR-AFO and all components. (Left) Each actuator set and the sensors for gait detection. (Right) The controller, pneumatic source, and connection for user feedback and system information for diagnostics.

terlink 406, Adafruit, New York, USA) which are embedded in the user's shoe to detect gait phase, pressure sensors (ASDXAVX 100PGAA5, Honeywell Sensing and Productivity Solutions, Charlotte, USA) which are used to monitor actuator pressure throughout use, and 3-way, 2-channeled solenoid valves (320 12 VDC, Humphrey, USA) MOSFETs (IRF520 MOSFET Driver Module) which are used to actuate the exosuit at various times. The control pouch connects to a portable air compressor (Model 8010A, California Air Tools, USA), which can be easily placed next to the current test site or facility and provide a pneumatic source for the actuators.

3.4 Actuator Fabrication

The soft actuators were fabricated using thermoplastic polyurethane (TPU) coated nylon fabric (200 Denier Rockywoods Fabrics), which was thermally bonded with a

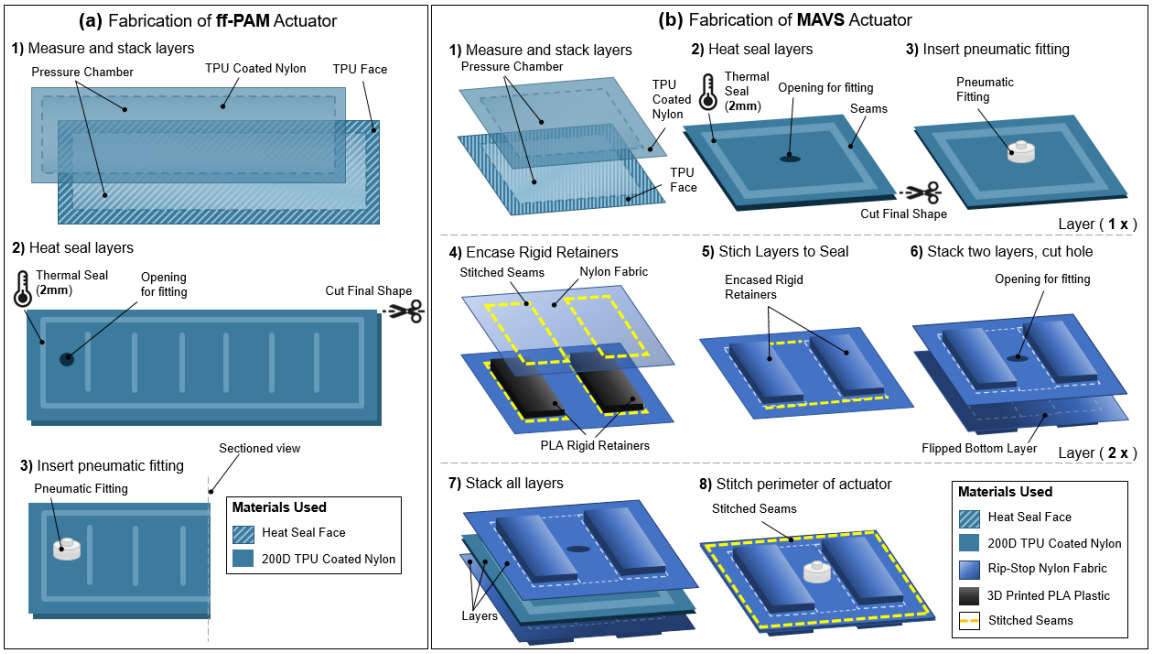

Figure 3.18: (a) The fabrication process for the ff-PAM actuator. The first step shows the formation of the air-tight chamber in a1), a2) shows the creation of the ribs and placement of the pneumatic fitting, while a3) shows the final fitting placement. (b) The fabrication process of the MAVS actuator, from the heal sealing and fitting placement of the soft actuator b1) - b3) and the laying and placement of the rigid retainers in the out layers of the MAVS in b4) - b6). The final final stages of integrating and stacking the MAVS layers in shown in b7) - b8).

2 *mm* heat impulse sealer (AIE-500 2 *mm* Impulse Sealer, American International Electric INC, CA). The heat impulse sealer applied uniform heat and pressure to the seam to create an air-tight seal (Thalman *et al.*, 2019). This fabrication technique was used to fabricate the soft actuators for both the ff-PAM and MAVS actuators when creating the pneumatic chambers of each soft actuator.

3.4.1 Fabrication of ff-PAM

The ff-PAM actuator was fabricated primarily following the procedures for soft fabric actuators listed above, however the ff-PAM has a few additional details that made the actuator design unique to the SR-AFO. Two layers of TPU coated nylon were stacked and sealed as shown in Fig. 3.18a1. Once three sides were sealed, thick

card-stock stencils were placed over the heat sealer with a gap the size of the inner seams shown in Fig. 3.18a2. This ensured that the seal was only formed for the segment in the center and left the gaps open and unsealed on either side of the ff-PAM to allow airflow to the subsequent segments. Each segment was sealed using this technique until the 8 chambers were created. A hole was created in the last chamber as shown in Fig. 3.18a2, and a fitting was inserted as shown in Fig. 3.18a3. The last side was then sealed to create one ff-PAM.

For the dual ff-PAM, two actuators were fabricated using this process and the two actuators were laid out in parallel. Nylon fabric (un-coated) was cut to sew the two actuators to one another along the length of the top and bottom seams. A standard tabletop sewing machine (SE-400 Brother, Bridgewater, NJ) was used to create these seams and stitch the fabric connector onto the ff-PAMs. The nylon fabric connector was cut into a pre-defined pattern that matched the width of the dual ff-PAMs and tapered to a single thin strap. This allowed for the dual ff-PAM to be affixed firmly to the SR-AFO at the base of the heel and at the back of the knee with Velcro.

3.4.2 Fabrication of MAVS

The first of the three layer design is composed of rigid PLA 3D Printer Filament (1.75 mm diameter PLA 3D Printer Filament, HATCHBOX) sewn between two layers of fabric. Two layers of the embedded rigid retainers were used to encase an inflatable actuator in between. A sewing machine was used to create stitching to hold the rigid retainers in place, as well as to hold the layers together.

The MAVS consists of a total of three main layers as shown in Fig. 3.18b: a single fabric-based inflatable actuator and two layers of nylon material with the rigid retainers embedded into the layers. The inflatable chamber was sealed at the designated location to create a rectangular shape using the impulse sealer on three of

the four sides (Fig. 3.18b1). The fourth side was left open for the installation of the pneumatic fitting (Fig. 3.18b2). A small hole was cut into the fabric and the threaded nylon barbed nozzle and nut fitting were secured onto the TPU coated nylon (Fig. 3.18b3). The final side was sealed with the impulse sealer to create an air-tight seal that is the same net shape as the entire actuator.

The additional two layers were fabricated using the same method for each (Fig. 3.18b4 - b6). The rigid retainers were 3D printed using PLA and have a thickness of 2 mm and a width of 40 mm, while the length as well as the placement distance between the rigid retainers were varied for each design of the MAVS actuators (A1-A3). Each of the constraining layers was made from two pieces of nylon fabric, which were stacked with the rigid retainers placed in between at fixed distances. A sewing machine was used to create a stitched seam around the net shape of the rigid retainers, encasing the parts between the two nylon layers. This was done to create the top and bottom constraining layers. A hole was cut into the top constraining layer to allow the tube fitting from the soft actuator to fit in between the rigid retainers.

The sealed soft actuator was placed in between the two constraining layers as shown on the right side of Fig. 3.18b7, with the fitting centered within the hole cut previously into the top constraining layer. A final seam was sewn in a rectangular shape around the rigid retainers, at a 5 mm offset. This seam allowance provided a buffer to avoid sewing into the sealed soft actuator and to provide an offset that constrains vertical expansion during inflation (Fig. 3.18b8).

Chapter 4

HUMAN EXPERIMENTS WITH SR-AFO: LATERAL ANKLE SUPPORT AND PLANTARFLEXION ASSISTANCE

In order to evaluate the effectiveness of the SR-AFO, specifically the MAVS for lateral ankle support and the ff-PAM for plantarflexion assistance, three different human experiments were performed: 1) quiet standing; 2) walking over compliant surfaces; and 3) treadmill walking. A total of 6 healthy participants (N = 6) participated in the experiments (Male = 4, female = 2, Age = 23 - 29 years, height: 1.68 - 1.88 m, weight: 47.6 - 72.9 kg, and leg length: 0.81 - 1.05 m). All the participants gave informed consent prior to participation and the study was approved by ASU Institutional Review Board (STUDY00012099).

4.1 Lateral Ankle Support during Standing: MAVS

4.1.1 Experimental Setup and Protocol

The objective of this experiment was to evaluate the effectiveness of the MAVS of the SR-AFO to support lateral ankle stability during standing. The degree of stiffness increase in the frontal plane with MAVS actuation was quantified and compared with natural frontal plane stiffness without exosuit. Sagittal plane stiffness was also quantified to evaluate the potential impact of MAVS actuation on ankle movement in the sagittal plane.

The subject wore a pair of custom athletic shoes, and a dual-axis goniometer (SG110, Biometrics Ltd, UK) was placed on the right foot-ankle complex to measure 2D ankle kinematics. The dual-axis robotic platform (Fig. 4.1a - b), capable of

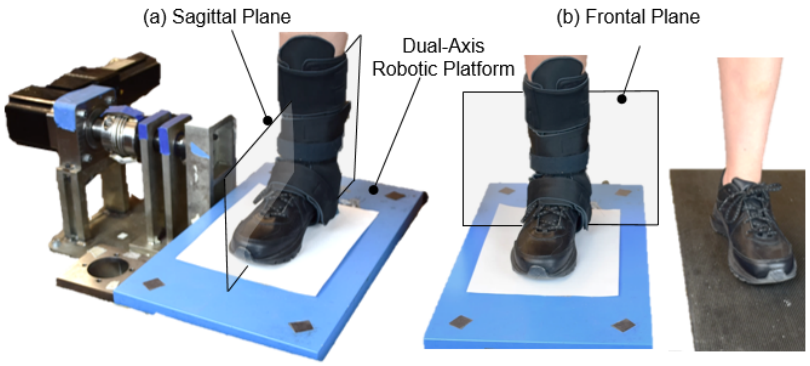

Figure 4.1: The dual-axis robotic platform setup (Nalam and Lee, 2019) is shown with the user wearing the SR-AFO exosuit for the measurement of (a) ankle stiffness in the sagittal plane and (b) ankle stiffness in the frontal plane.

applying position perturbations to the ankle in the sagittal and frontal planes and measuring the corresponding ankle torques, was used to quantify 2D ankle stiffness in the sagittal and frontal planes. The platform was validated to accurately quantify 2D ankle stiffness during upright standing (Nalam and Lee, 2019; Nalam *et al.*, 2020; Adjei *et al.*, 2020; Nalam and Lee, 2018). The subject was asked to stand with the right foot placed on the robotic platform and the left foot on the elevated ground right next to the platform. The right foot was placed in a fashion to ensure that the axes of rotation of the robotic platform were as closely aligned as possible with those of the ankle. Our previous study confirmed that any potential misalignment in the foot placement has minimal impact on the stiffness estimation in the sagittal and frontal planes (Nalam and Lee, 2019).

A fast ramp-and-hold position perturbation of 3° and a duration of 100 ms was randomly applied either in the dorsiflexion direction or the eversion direction to quantify sagittal plane stiffness and frontal plane stiffness, respectively. A total of 30 perturbations was applied in each direction. The experiment was performed under four conditions: (1) No exosuit; (2) Passive exosuit (at 0 kPa); (3) Active exosuit (30 kPa); and (4) Active exosuit (50 kPa).

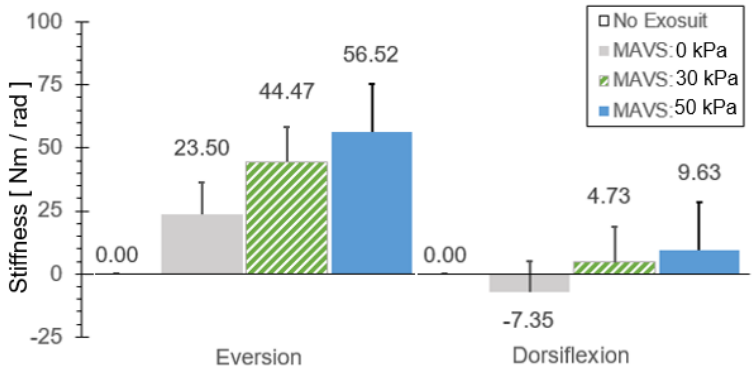

Figure 4.2: The resulting ankle stiffness in the frontal plane (with eversion perturbations) and the sagittal plane (with dorsiflexion perturbations), measured by a dual-axis robotic platform as done in previous work (Thalman and Lee, 2020).

4.1.2 Data Analysis

Ankle stiffness was quantified by fitting a linear 2^{nd} order model, consisting of ankle stiffness, ankle damping, and foot inertia, to the measured ankle kinematics and torques for a window of 100 ms starting from the onset of the perturbation. To check the reliability of stiffness quantification, the percentage variance accounted for (%VAF) between the estimated ankle torque from the best-fit 2^{nd} order model and the measured ankle torque was calculated (Lee *et al.*, 2014a). For each subject, stiffness increase with the exosuit was calculated with respect to the baseline measurement without the exosuit, i.e., No exosuit condition. Group average results of the 6 subjects were reported.

4.1.3 Results

The MAVS of the SR-AFO effectively increased ankle stiffness in the frontal plane with minimal impact on the stiffness in the sagittal plane (Fig. 4.2). Ankle stiffness was reliably quantified in all experimental conditions, evidenced by high %VAF, which was greater than 97.5% in any of the 8 experimental conditions and in any subjects.

In the frontal plane, simply donning the exosuit (passive condition) increased

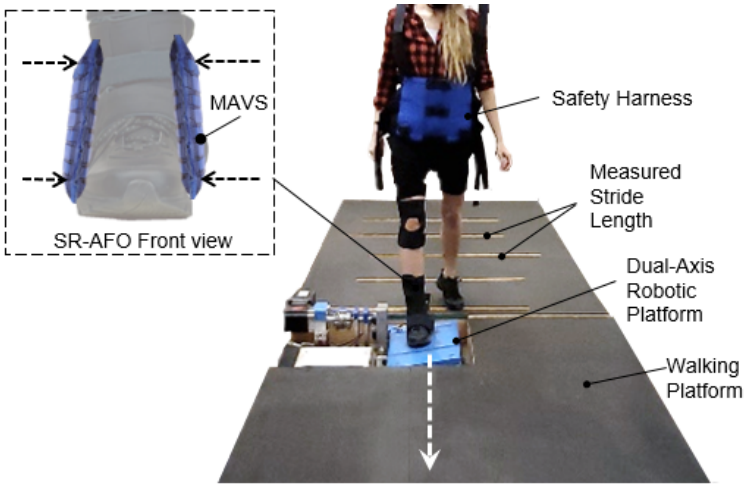

Figure 4.3: Test setup used for walking trials with the MAVS. The dual-axis robotic platform utilized two conditions for compliance in the lateral direction for the ankle as the participant walked across the platform.

ankle stiffness by 23.5 ± 12.6 Nm/rad from the free-foot baseline. Activating MAVS of the exosuit significantly increased the ankle stiffness. At the pressure level of 30 kPa, the increase from the baseline was 44.5 ± 13.8 Nm/rad. The stiffness increased with increasing pressure. At 50 kPa, the increase was 56.5 ± 18.6 Nm/rad. In the sagittal plane, the change in ankle stiffness was minimal. In average across subjects, even activating MAVS increased ankle stiffness less than 10 Nm/rad. At the pressure level of 30 and 50 kPa, the stiffness increase from the baseline was 4.7 ± 14.8 Nm/rad and 9.6 ± 17.4 Nm/rad, respectively.

4.2 Lateral Ankle Support during Walking: MAVS

4.2.1 Experimental Setup and Protocol

The objective of this experiment was to evaluate the effectiveness of the MAVS of the SR-AFO to support lateral ankle stability during walking over compliant surfaces. The degree of lateral ankle deflection with MAVS actuation was quantified and compared with the ankle deflection without exosuit.

The dual-axis robotic platform was used to simulate compliant surfaces in the frontal plane. Our previous study confirmed that the robotic platform was capable of accurately simulating a wide range of stiffness (inverse of compliance) in both the sagittal and frontal planes (Nalam and Lee, 2019). In this experiment, two different compliant surfaces were simulated with stiffness of 100 Nm/rad (compliant) and 50 Nm/rad (more compliant) in the frontal plane, while a rigid surface (stiffness of 10,000 Nm/rad) was simulated in the sagittal plane.

The subject was instructed to walk on the elevated walkway (approximately 6 m in length; Fig. 4.3). A metronome was played at 100 bits per minute to encourage a consistent cadence. In addition, the subject's stride length was measured and marked along the walkway leading up to the platform to ensure consistent foot landing on the platform. The experiment was performed under 6 conditions: 2 surface conditions (compliant and more compliant) $\times$ 3 exosuit conditions (No exosuit, Passive exosuit (at 0 kPa), and Active exosuit (30 kPa)). In each of the 6 experimental conditions, 30 walking trials were completed, resulting in a total of 180 walking trials. The order of the surface conditions was fully randomized.

4.2.2 Data Analysis

Lateral ankle deflection in the frontal plane was measured using the goniometer from the moment of heel strike to toe-off (0 - 60% of the gait cycle). To remove outlier data due to simple human error in foot placement on the platform during walking, only the data with the foot center of pressure within 0 cm (the axis of rotation of the platform) and 5 cm lateral offset were included in data analysis. For each subject, peak-to-peak ankle deflection in the frontal plane was quantified throughout the stance phase, and group average results of the 6 subjects for this measure were compared across the exosuit conditions.

4.2.3 Results

The SR-AFO with MAVS actuation effectively supported lateral ankle stability during walking over the compliant surfaces (Fig. 4.4). Results from a representative subject confirmed a significant reduction in the peak-to-peak ankle deflection in the frontal plane (Fig. 4.4 (a-b)). Group results demonstrated that these trends were consistent across subjects (Fig. 4.4 (c-d)). In the compliant surface condition (100 Nm/rad), the peak-to-peak ankle deflection was 12.5 $\pm$ 4.1° with free-foot, 11.6 $\pm$ 4.7° after donning the SR-AFO (passive exosuit), which was only a minor decrease. However, MAVS actuation with 30 kPa decreased the deflection to 9.7 $\pm$ 3.1°. In the more compliant surface condition (50 Nm/rad), the free foot peak-to-peak ankle deflection was 13.2 $\pm$ 3.7°. After donning the exosuit, the deflection was 11.0 $\pm$ 4.3°. With MAVS actuation at 30 kPa, the deflection decreased to 9.8 $\pm$ 4.2°.

4.3 Plantarflexion Assistance during Walking: ff-PAM

4.3.1 Experimental Setup and Protocol

The objective of this experiment was to evaluate the effectiveness of the ff-PAM of the SR-AFO to assist plantarflexion during walking. Activation of plantarflexor muscles in the push-off phase with and without ff-PAM actuation was compared.

An instrumented treadmill (Bertec Treadmill, Columbus, OH, USA), capable of measuring ground reaction forces (Fig. 4.5a), was used to detect the moment of heel strike and determine the actuation timing of the ff-PAM as shown in Fig. 4.5c, where the valve releases instantaneous pressure from 40% - 60% of the gait cycle. A wireless electromyography (EMG) system (Trigno, Delsys, Natic, MA, USA) was used to monitor activation of two major plantarflexors, soleus (SOL) and medial gastrocnemius (GAS), throughout the experiment. The surface EMG sensors were

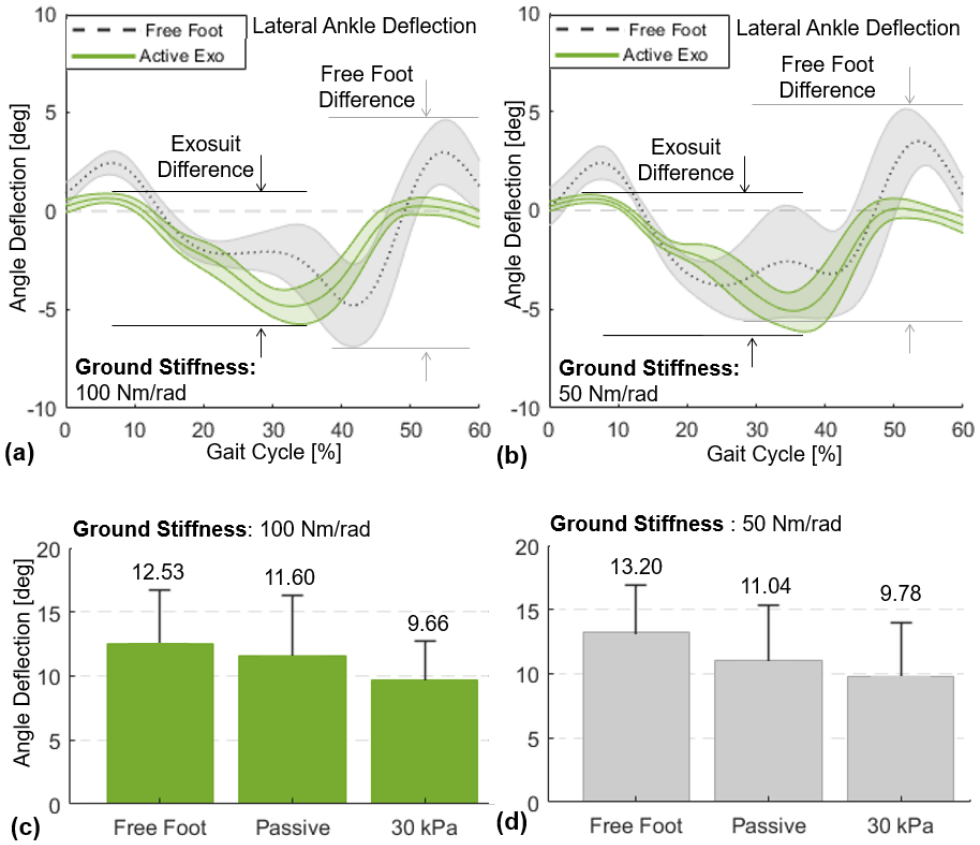

Figure 4.4: Lateral ankle deflection in the frontal plane was recorded and averaged across all trials for 0-60% percent of the gait cycle, from the moment the subjects foot was in contact with the platform (heel strike) to the moment it lost contact (toe off). Results of a representative subject are presented for free foot, passive, and active support (30 kPa) when the platform is set to (a) 100 Nm/rad and (b) 50Nm/rad. Group average results of the lateral ankle deflection are presented for free foot, passive, and active support (30 kPa) when the platform is set to (c) 100 Nm/rad and (d) 50Nm/rad. (c) Total peak-to-peak lateral ankle deflection for the 100 Nm/rad condition averaged across all N = 6 participants, for the duration of time the foot was in contact with the platform. (d) Group averaged peak-to-peak lateral ankle deflection for the 50 Nm/rad condition while the foot was in contact with the platform.

placed and maximum voluntary contraction (MVC) of each muscle was measured as per standard International Society of Electrophysiology and Kinesiology (ISEK) protocols (Merletti and Di Torino, 1999).

Prior to the main walking experiment, the subject was asked to select a preferred walking speed, which was selected by increasing the treadmill speed by 0.1 m/s until

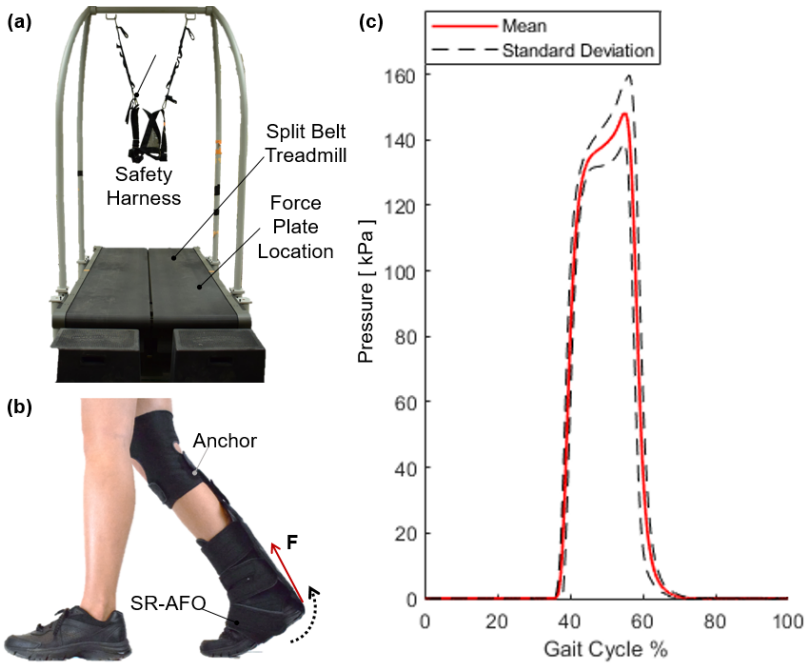

Figure 4.5: (a) The split belt treadmill used throughout this experiment with the safety harness. (b) The ff-PAM placement is shown where the dual actuator setup is paired with the fabric connector to run between the back of the knee and the base of the heel. Tensile force applied to the posterior end of the foot to generate a torque about the ankle. (c) The average pressure levels monitored through the active trials of the ff-PAM while the user was walking.

the subject indicated the pace was too fast for a natural cadence, and then decreased the speed by 0.1 m/s until the pace was determined to feel too slow. This process was repeated one more time and the final preferred walking speed was selected by averaging the two values. For the subjects in this study, this speed ranged from 0.9-1.2 m/s. The subject was then instructed to walk with the selected preferred walking speed for two minutes, which determined the average stride time (i.e., gait cycle duration; T_c).

The main experiment was performed under two conditions: (1) No exosuit and (2) active exosuit. In the active exosuit condition, the ff-PAM was pressurized at 150 kPa in 40-60% of the gait cycle (0.4-0.6T_c) and depressurized in the rest phases of the gait cycle, which was designed to assist push-off in the late stance phase. The subject

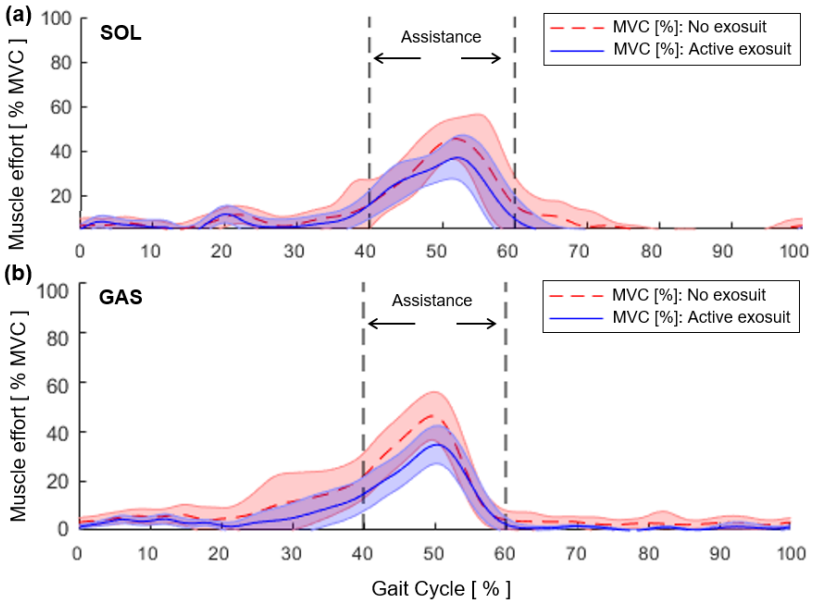

Figure 4.6: The EMG results for the (a) SOL and (b) GAS of a representative subject. The normalized EMG signals show the averaged muscle activity across each gait cycle, with the no exosuit baseline results (dotted red) and the active exosuit results (solid blue). The region of applied assistance is indicated at 40-60% of the gait cycle.

walked for 5 minutes for each experimental condition. A minimum of 3 minute resting period was provided between trials to prevent any potential muscle fatigue.

4.3.2 Data Analysis

Muscle effort was quantified by calculating the normalized EMG amplitude. Surface EMG data was demeaned, rectified, filtered using a low-pass 2^{nd} order Butterworth filter with a cutoff frequency of 5 Hz, and normalized by MVC. The amplitude data was segmented based on successive heel-strikes and each segmented stride data was normalized to the percentage gait cycle (0-100%).

The active region for exosuit assistance (40-60%) was then isolated to evaluate the effectiveness of the ff-PAM for providing assistance to the primary muscles (i.e., SOL and GAS) during push-off (Fig. 4.6). The average reduction of muscle activation in SOL and GAS was quantified by taking the integral of the area under the amplitude

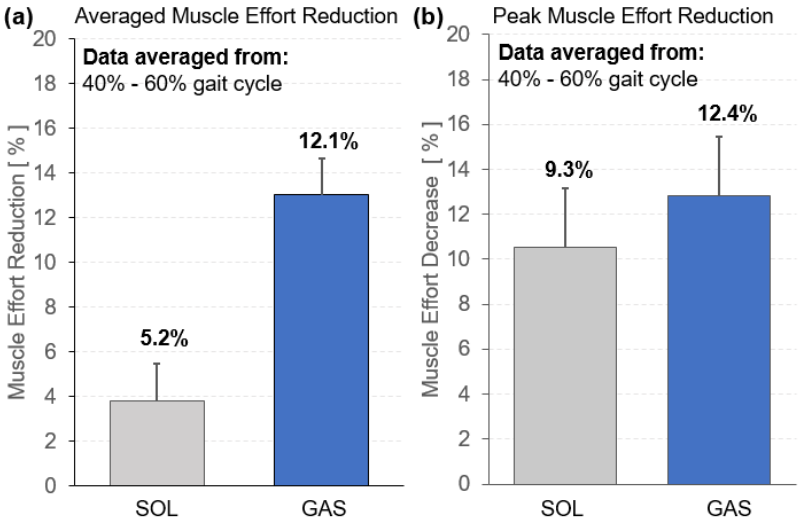

Figure 4.7: Group average results of muscle effort reduction in the 40-60% gait phase are presented. The reduction of the active exosuit condition in reference to the no exosuit condition is shown for (a) the average EMG amplitude and (b) the peak EMG amplitude.

curve between 40-60% of each gait cycle to determine the difference between the no exosuit and active exosuit conditions. In addition, the reduction in peak EMG amplitude within the assistance time window was calculated between the two experimental conditions.

4.3.3 Results

The SR-AFO with ff-PAM actuation effectively reduced muscle effort in plantarflexors in the push-off phase of walking. Results from a representative subject showed a reduction in both the average and peak EMG amplitude within the assistance time window (40-60% of the gait cycle) in both SOL and GAS (Fig. 4.6). Group results demonstrated that this trend was consistent across all subjects (Fig. 4.7). Compared to the no exosuit condition, the active exosuit condition reduced the average EMG amplitude by 5.2 % and 12.1 % in SOL and GAS, respectively (Fig. 4.7a). The peak EMG amplitude was also reduced by 9.3 % and 12.4 % in SOL and GAS, respectively (Fig. 4.7b).

Chapter 5

HUMAN EXPERIMENTS WITH SR-AFO: LOCOMOTION ENTRAINMENT

5.1 Background on Entrainment

Entrainment is the terminology used to describe the phenomenon observed when interacting systems converge into alignment (Ross and Balasubramaniam, 2014). Initially demonstrated in experiments conducted with a system of interacting pendulum clocks, entrainment can specifically refer to when systems with independent periods of oscillation converge and synchronize to a common period (Bennett *et al.*, 2002; Ross and Balasubramaniam, 2014). In regards to a human response, entrainment is defined as the involuntary or voluntary methods in which our neuromuscular system adapts and synchronizes to an external input observed through a behavior or physiological response. A human will respond to external perturbations effectuated by the environment, provided the external stimuli lie within their "basin of entrainment," which is the boundary of cadence increase or decrease to which a human can be entrained (Ahn and Hogan, 2012b). The ankle joint is targeted in gait entrainment as the joint is responsible for 45% of the power behind moving the body forward during walking (Winter, 1983; Farris and Sawicki, 2011). Its contribution is especially significant in the stage of "push-off", where the heel lifts just before the leg swings forward to take the next step (Winter, 1980, 1983). Push-off is a major contributor to forward propulsion during walking, and occurs at roughly between 45% and 60% of the gait cycle (Winter and Sienko, 1988). If external perturbations can be consistently locked in the push-off phase, gait entrainment can be used to assist in forward propulsion.

Human-centered robotics has been used to study the ankle within many research

groups in understanding ankle biomechanics and neuromuscular control behind achieving a regular walking gait (Shi *et al.*, 2019; Kwon *et al.*, 2019; Chung *et al.*, 2018; Park *et al.*, 2014a; Lee *et al.*, 2016; Ren *et al.*, 2017). There is evidence that rigid robots are well-suited for gait rehabilitation due to their ability to manifest human entrainment through the use of controlled periodic perturbations (Ahn and Hogan, 2012b,a; Shi *et al.*, 2019; Ahn *et al.*, 2011). The introduction of soft robotics, a rapidly growing field, could expand the boundaries of human gait entrainment. Soft wearable robots are lightweight, safe and comfortable for the user, and forgo the complex controls and heavy components of many rigid robots, which make soft robots an attractive solution for lower limb studies (Chung *et al.*, 2018; Park *et al.*, 2014a). Gait rehabilitative robotics have rapidly begun implementation of the inherently more compliant and simplistic materials and designs of soft material actuation and robotics.

Previous experimental work on human locomotion demonstrated that a robotic ankle device could be successfully used to reproduce the phenomena of entrainment and phase locking (synchronization of the gait phase to the phase of applied perturbations) during human walking (Ahn and Hogan, 2012b). Entrainment was observed in a majority of human participants when subjected to periodic perturbations caused by a rigid wearable ankle robot. The basin of entrainment was established at $\pm$ 7% of the preferred gait frequency for the rigid and heavy (3.5 kg) robot evaluated (Ahn and Hogan, 2012b). In addition, previous simulations utilizing a simple walking model with a concentrated point body mass and massless legs were able to replicate the experimental results in (Ahn and Hogan, 2012b), suggesting that gait entrainment can be observed even without involvement of supra-spinal control or a contribution of a central pattern generator (CPG) to human walking (Ahn and Hogan, 2012a).

Individuals who exhibit gait abnormalities, such as those suffering from hemiparesis following a stroke, may struggle with the critical motions involved in human loco-

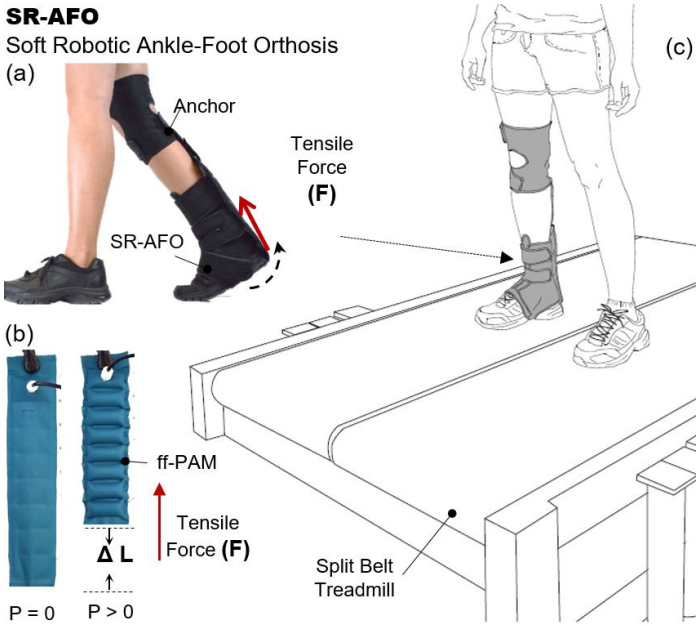

Figure 5.1: (a) A side view of the SR-AFO worn during walking. (b) The soft actuators with a pair of flat fabric pneumatic artificial muscles (ff-PAM) used to provide assistance. (c) A concept on the test conditions and application of the SR-AFO for gait rehabilitation on a treadmill.

motion, including highly asymmetric gait patterns (Sawicki and Ferris, 2009; Merletti and Di Torino, 1999; Mueller *et al.*, 1995). A potential to extend the basin of entrainment is clinically significant since the entrainment paradigm can be better utilized in many gait rehabilitation applications through the use of controlled perturbations (Ahn *et al.*, 2011). For example, the average stroke patient walks at roughly 0.6 m/s (Wing *et al.*, 2012), and a clinically significant increase in rehabilitative walking speeds is measured at an increase of roughly 0.05 m/s. (Hass *et al.*, 2014), Therefore walking speed increase expected from the entrainment at a 7% increase of the gait frequency is not significant enough to have a major impact on gait rehabilitation in the current form.

This study (Thalman *et al.*, 2021) aims to recreate the entrainment achieved in the aforementioned works with a lightweight soft wearable ankle robot (Fig. 6.1a) to determine the effects of a donned robot similar to clothing. The ankle robot, the

Soft Robotic Ankle-Foot Orthosis (SR-AFO), is very light (0.203 kg) and thus has a substantially smaller impact on gait biomechanics due to added mass. Perturbations from the pneumatic actuator (Fig. 6.1b), controlled by a solenoid valve to supply instantaneous pressure, are gentle yet powerful enough to provide assistance to the user (Thalman *et al.*, 2020b). It is predicted that using the lightweight, pneumatically-driven, soft robot will make the entrainment process feel more natural, potentially extending its use in gait adaptation, in place of the heavy, motorized, rigid robots which apply an abrupt force over a smaller window.

The first hypothesis of this study is that participants will be able to achieve entrainment at perturbation frequencies of a significantly higher percentage increase from the baseline (i.e., preferred gait frequency) than the previously reported value with the rigid and heavy ankle robot ($\approx 7\%$) when the treadmill speed is fixed at the preferred walking speed. Secondly, this study hypothesizes that participants will be able to achieve entrainment at perturbation frequencies of a much higher percentage increase from the baseline gait frequency when treadmill speed is scaled up proportionally.

5.2 Methods

5.2.1 Soft Robotic Ankle-Foot Orthosis (SR-AFO)

A critical feature of the SR-AFO exosuit used during this entrainment study is the inherently lightweight nature of the body and actuators of the design, which are all made from compliant soft fabric for a total weight of 0.203 kg (Fig. 5.2). The fabric actuators are pneumatically powered and are used to help assist in ankle plantarflexion. A pair of flat fabric pneumatic artificial muscles (ff-PAM) that contract and generate a pulling force at the heel run along the posterior side of the leg and

Figure 5.2: (a) A side view of the SR-AFO donned by a user in the passive condition, as well as the dual ff-PAM setup prior to inflation. (b) The SR-AFO during the active condition (inflation of the ff-PAM actuators) to assist plantarflexion.

connect to the anchor point just behind the knee. Preliminary studies and earlier developments of this work show the original design and optimization of the ff-PAM actuator (Thalman *et al.*, 2019), as well as further investigation into the dual ff-PAM and final SR-AFO exosuit design (Thalman *et al.*, 2020b). The torque output of the actuators is provided as,

$$\tau = FL_{foot} \tag{5.1}$$

where τ is the torque applied to the ankle joint by the SR-AFO, F is the uniaxial tensile force generated by the actuators during contraction and L_{foot} is the lever arm distance from the center of the ankle joint to the posterior end of the heel. The actuator configuration used in the SR-AFO is the dual ff-PAM design, which consists of two ff-PAM actuators in parallel, connected to two fabric connectors at the top and bottom of each actuator. The fabric connectors affix the actuators to the posterior end of the foot, and the knee brace anchor point just behind the knee joint.

The pressure level of the system is held constant for each trial, while the tensile force generated by the actuators is varied with actuator inflation and deflation. The force output depends on the selected pressure level and the inflation time of the

actuator. The maximum tensile force will increase as the rise time increases as more time is allowed for the actuator to inflate. However, it is also vital that the parameters are optimized to limit the potential of rupture to one or more of the actuator cells.

5.2.2 Actuator Characterization for Entrainment

In order to induce entrainment, the perturbations from the SR-AFO must provide sufficient force in a short time so that users can feel the perturbations at a certain gait phase. The dynamic response of the actuator configuration was evaluated using a universal testing machine (UTM) (Instron 5565, Instron Corp., High Wycombe, United Kingdom). The dual ff-PAM was held in place by two vice clamps at each end, which held the base of the actuator fixed in place by the fabric connector, while the top fabric connector was held by a second vice clamp connecting to the load cell of the UTM. The actuators were fixed at the initial length prior to contraction to measure the maximum force output during isometric contraction. The pressure was set to 200 kPa based on previous studies and evaluations (Thalman *et al.*, 2019), and the valve was released until the actuator reached the stabilized pressure.

The rapid pressurization was recorded as a force output from the load cell to determine how quickly the actuator could reach its maximum force output (Fig. 5.3a). With the displacement held constant throughout the trial, the valve was fully open for 4 iterations, which resulted in a maximum force output of 212.3 $\pm$ 7.7 N in 0.29 seconds. However, for the time window of 0.2 seconds set for the entrainment study, the maximum tensile force that the actuator can yield was 177.8 $\pm$ 2.2 N.

5.2.3 Control and Hardware

One of the benefits of using entrainment as a gait therapy solution is its simplistic control methodologies that have been proven successful in previous studies and thus

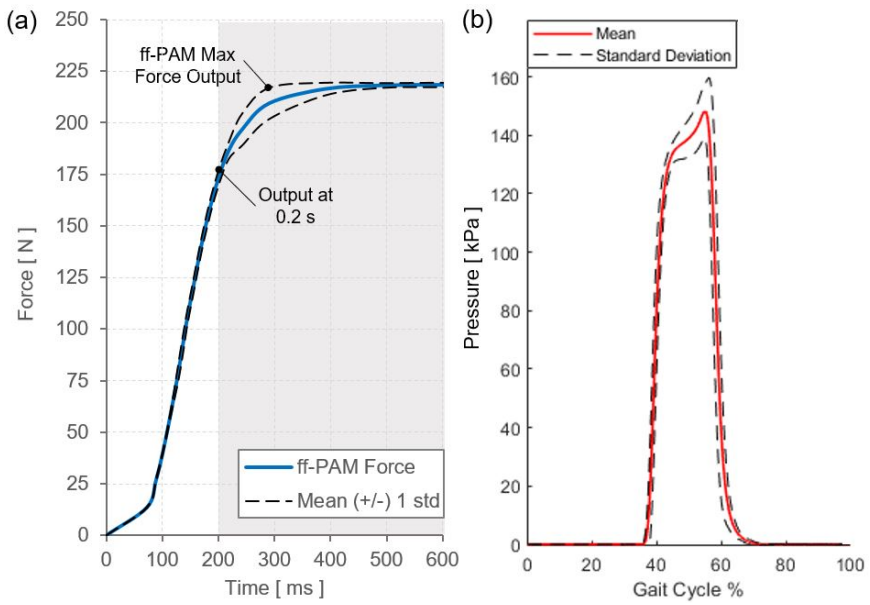

Figure 5.3: (a) The dynamic response of the dual ff-PAM actuator as a force-time curve. The maximum force output at 200 kPa is shown, as well as the force achieved at 0.2 *sec*. (b) The dynamic pressure response of the actuator during walking trials. When the source pressure is set to 200 kPa, the maximum pressure the actuators can achieve within 0.2 seconds is 152.3 kPa and the corresponding force at this pressure is 177.8 N.

have a potential to be easily accessible in rehabilitation facilities. This is in contrast to many lower-limb wearable robots that attempt to predict the user's motions and react in a closed-loop fashion. While effective in many ways, these methods are often extremely costly and complex in terms of computation. By instilling protocol that relies on human entrainment to assist in restoring natural gait patterns, computationally heavy algorithms can be replaced with simple periodic pulses, which are tailored to each individual and contain no closed feedback loop once active.

An open-loop control strategy is used to apply fixed, controlled perturbations to the user by utilizing a portable compressor (Model 8010A, California Air Tools, USA) (Fig. 6.8d) to pressurize the cells of the soft actuators for a specified inflation time. The control strategy, designed in Simulink (Mathworks, MA, USA), contains a modifiable algorithm for updating the frequency of applied perturbations during each

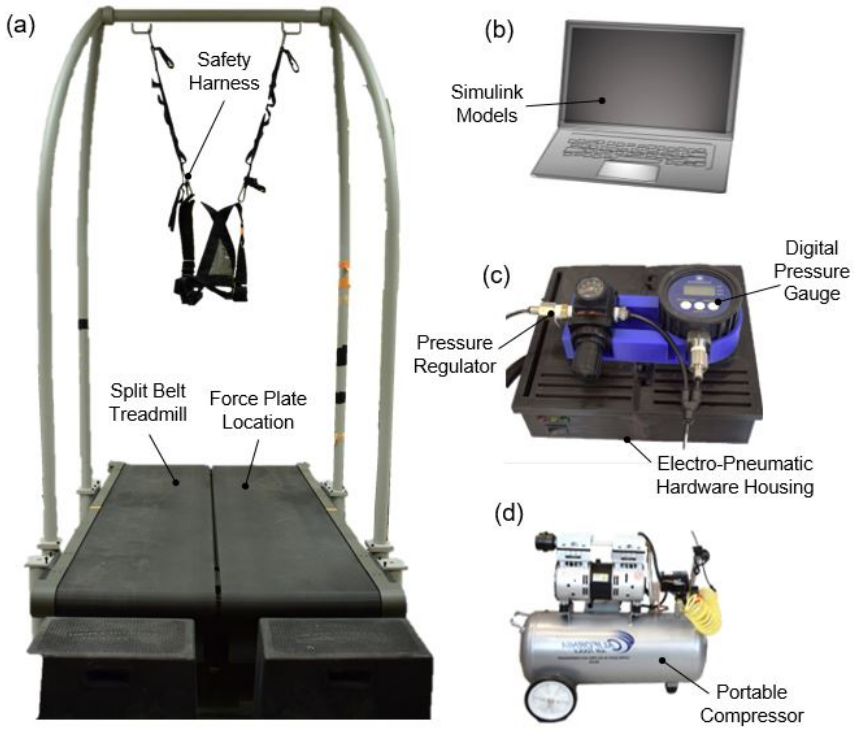

Figure 5.4: (a) The split belt treadmill test setup and safety harness used by participants. (b) A Simulink model for data analysis, programming, and controlling the SR-AFO. (c) The control box which houses all the eletro-pneumatic hardware, pressure gauge, and pressure regulation hardware. (d) The portable compressor used to provide fluidic actuation to the SR-AFO.

trial. The open-loop control strategy involves no feedback of any kind, and provides gentle, heavily-damped, soft perturbations via the pneumatic actuators, which differ from the rigid and abrupt robotic torque pulse used in previous entrainment studies (Ahn and Hogan, 2012b).

Applied perturbations consisted of 0.2-second pulses of inflation for the ff-PAM, at a consistent pressure level of 200 kPa supplied to the valve. During walking trials performed in previous studies where the valve was released for 0.2 seconds (Thalman *et al.*, 2020b) and activated during late stance into push-off, the resulting pressure would reach only 152.3 kPa (Fig. 5.3b). According to Fig. 5.3a, this would yield an average force output of 177.8 $\pm$ 2.2 N on the participant's ankle to assist in plantarflexion if the subject was successfully entrained to the frequency of applied

perturbations. Estimated torque values correspond to roughly 17.8 Nm of torque at the ankle joint to assist plantarflexion, assuming an average L_{foot} length of 10 cm. It is worth to note that the lightweight SR-AFO has a significantly a higher torque density than the rigid heavy ankle robot used in the previous gait entrainment studies. While the SR-AFO is 0.203 kg and can produce 17.8 Nm at the ankle joint, the previous rigid ankle robot weighs 3.6 kg and can produce 23 Nm (Ahn and Hogan, 2012b).

5.3 Experimental Setup and Protocols

The experimental setup of the entrainment study included a split-belt treadmill (Bertec Treadmill, Columbus, OH, USA), a portable air compressor (Model 8010A, California Air Tools, USA), pressure sensor (ASDXAVX 100PGAA5, Honeywell Sensing and Productivity Solutions, Charlotte, USA), and the SR-AFO exosuit and its controller. The force plate embedded into the split-belt treadmill was used to collect ground reaction forces (GRF) for the right foot. This study only aimed to analyze the results of entrainment with the SR-AFO worn on the right foot. The force plate sensors were calibrated prior to data collection for each participant, and zeroed between each trial to reduce the introduction of noise.

This study was conducted with ten (n = 10) healthy participants (age: 21 – 30, height: 1.68 – 1.88 m, weight: 47.6 – 83.9 kg, and leg length: 0.79 – 1.05 m) recruited following the procedures for healthy participants as approved by the Institutional Review Board of Arizona State University (STUDY00012099). Two experimental protocols were implemented, each on a different day, and each subject participated in both experiments.

Two experimental protocols were used to evaluate the efficacy of the SR-AFO exosuit during entrainment tasks. Prior to each protocol, the same setup and calibration process was performed for each subject for Day 1 and Day 2 protocols. The partici-

pants wore a custom pair of athletic shoes, and the knee brace anchor was placed on the right leg. The SR-AFO was donned over the right shoe. Only the right leg was evaluated in this study. A safety harness was donned prior to treadmill use to ensure participant stability and prevent falls. Treadmill speed was increased sequentially in increments of 0.05 m/s, starting at 0.80 m/s and increased until the participant indicated the speed was too brisk for comfortable and natural walking. Speed was then lowered in the same increments until the participant indicated the speed was too slow. These two bound speeds were averaged to determine their preferred walking speed and then noted for use during the trial. Initial preferred walking speed across all participants ranged from 0.90 – 1.25 m/s.

To prevent accidental auditory entrainment throughout the trials, participants were precluded from hearing external noises caused by the experimental setup (e.g., solenoid valve firing, their own steps on the treadmill, etc.). Participants wore a pair of noise canceling wireless headphones, which played white noise over a Bluetooth connection at a high volume. Ear plugs were also worn under the over-ear headphones to protect the participants' ears from elevated volumes of white noise. The participant was always instructed to walk as comfortably as possible, keep their gaze fixed upward away from their feet at a marked spot on the wall in front of the treadmill to prevent any chance of visual entrainment from watching their feet on the treadmill. The participants were asked to keep each foot on its respective belt and avoid crossing their feet from one belt to another during walking. The participant walked first with the passive SR-AFO and noise canceling headphones. The average stride time was obtained using heel strike detection in the force plate of the right leg. This value was used to determine f, the gait frequency at preferred walking speed. Increasing perturbation frequencies were found using the following:

$$f(1 + A_f/100) \tag{5.2}$$

where A_f is the percentage increase in actuation frequency for any given trial. The subject was provided a test trial at the applied perturbation frequency of f to adjust to the device.

During trials with perturbations, the participants were not informed on the process of entrainment or the metrics that would be evaluated as a result of their trials. They were informed that they would feel the pull of the ff-PAM actuator during walking, and that the device would perform the same throughout each walking trial regardless of their input. Each subject was then told that if they felt they were not able to walk comfortably with the device, their step length could be adjusted until they were able to resume comfortable walking with the device. The goal with these instructions was to ensure that the participants were not aware of what this study would be measuring, but also to prevent the participants from feeling they had to fight against the motions of the soft robot as they walked.

5.3.1 Day 1 Protocol: Fixed Walking Speed

The first experimental protocol was performed with the healthy subject walking on the split belt treadmill at a fixed speed throughout the duration of the trials. The treadmill speed was fixed at the subject's preferred walking speed throughout each trial. The experiment included perturbation frequencies of 0 – 15% faster than f in 3% increments. These 6 conditions were broken down into randomized sets of 3 trials, each spanning 3 minutes of walking. The first set contained f+0% – +6%, in randomized order, and the second set contained f+9% – +15%. The trials were structured using this method to first test perturbation frequencies that had been previously used (Ahn and Hogan, 2012b), and evaluate if the participant could successfully get entrained in this frequency range with the SR-AFO. Upon success in the first set of trials, the second set with higher perturbation frequencies were tested.

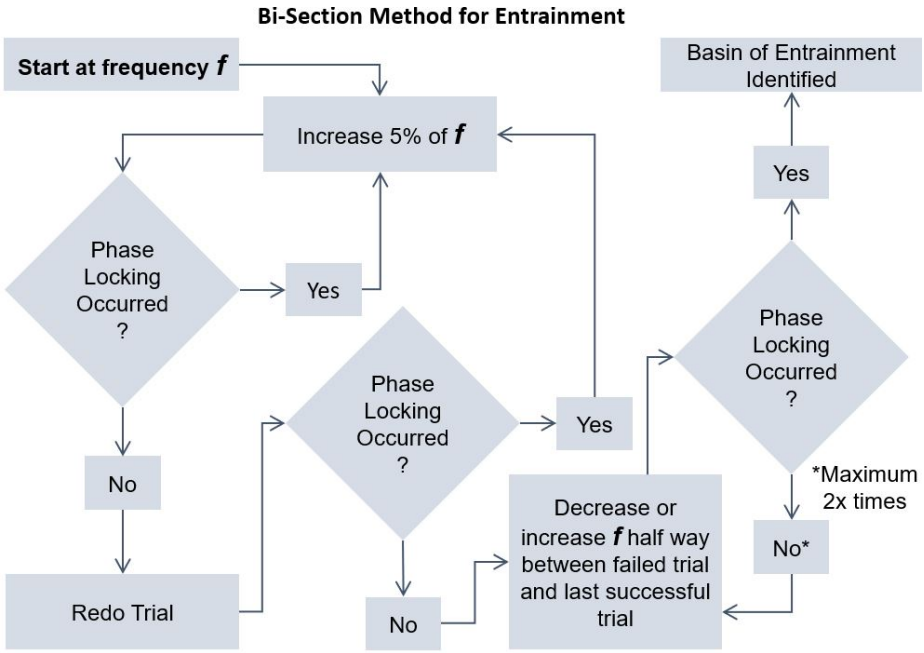

Figure 5.5: The process of the bi-section method is outlined as it was followed during the Day 2 experiment, starting with the baseline periodic perturbations and increasing or decreasing based on passed or failed trials.

5.3.2 Day 2 Protocol: Varying Walking Speed with Bi-Section Method

The second day trials used a varying treadmill speed, which increased the speed proportionally to the increase in the perturbation frequency with each trial. The treadmill speed was adjusted to alleviate a problem of adapting gait in unnatural ways by substantially shortening step length to fast perturbations. Similar to the Day 1 protocol, the participant donned the exosuit and headphones. The participant walked for 2 minutes and the average walking frequency was recorded for the duration of the trial and denoted again as f. The participant was given a 2 minute practice trial at 0% prior to the recorded trials. Each recorded trial ran for a 2 minute duration. Protocols used in Day 2 followed the bi-section method (Fig. 5.5), which initially increased perturbation frequency and treadmill speed by 5% for each trial until entrainment failed at a particular frequency. A successful trial was determined by the participant achieving entrainment and phase locking for at least 50 consecutive

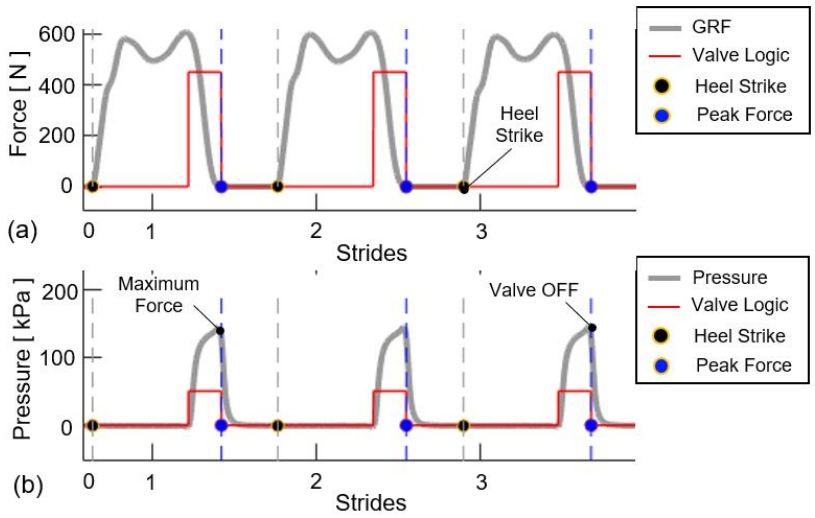

Figure 5.6: (a) The ground reaction forces of the split belt treadmill for the right foot, as well as the valve ON/OFF logic during walking. (b) The pressure-time curve for several steps to ensure proper inflation.

steps throughout the trial. If the subject failed a trial, the trial was repeated and a second failure would begin the bisection method. The trial immediately following the failed trial would be split between the last successful trial and the recently failed trial. Failing a trial would result in a decrease in perturbation frequency by half an increment, and a success would result in an increase in perturbation frequency by half an increment. This method was repeated until the difference of perturbation frequency between the two adjacent trials is less than 1%.

5.4 Data Processing and Analysis

In order to determine the feasibility of the SR-AFO for entrainment and to compare with previous studies, several metrics were evaluated. First, the basin of entrainment, more specifically the upper basin, was calculated for each participant. The timing of perturbations and user's gait were compared to determine if phase locking occurred. Second, the number of steps leading to entrainment were recorded and measured to evaluate how quickly a participant was able to be entrained. Third,

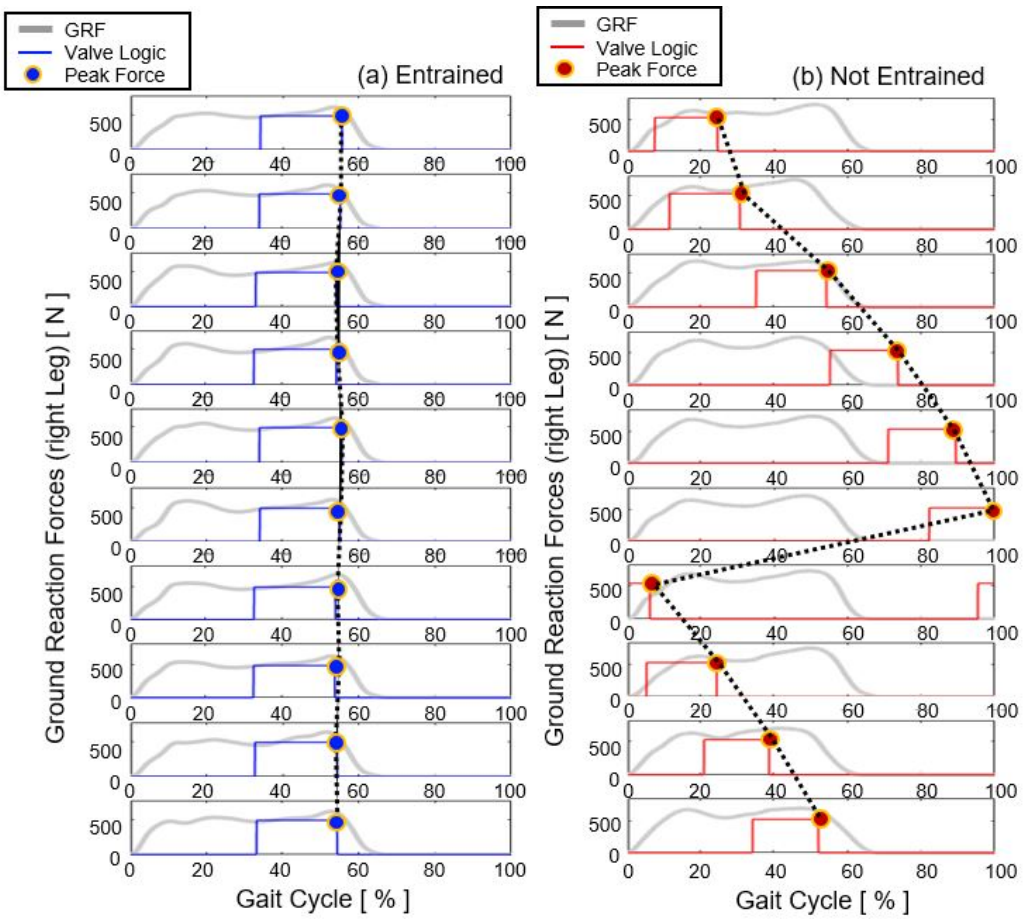

Figure 5.7: (a) Results of a representative subject for a successful phase locking trial from the Day 1 experiment, where the perturbations synchronized with the user's steps in the push-off phase. (b) A non-successful trial, where the perturbation does not line up with a specific gait phase. Rows shown for (a) and (b) represent 10 subsequent strides throughout a trial.

retention of any occurrence of phase locking was also measured to observe trends in the user's ability to maintain phase locking over a period of time. A successful trial of entrainment and phase locking was considered if 50+ consecutive strides fell within 10% of the running average for perturbation timing throughout the gait cycle).

The ground reaction forces were used to determine the heel strike moment during data analysis (examples shown in Fig. 5.6a). This information was used to determine the timing of each stride and the number of strides taken, and was used to normalize each stride into gait cycle percentages from heel strike to heel strike.

The logic state of the valve was recorded and was used to determine the synchronous pattern or lack-thereof for the perturbations during gait. The timing was selected at the instance when the valve switched to the 'OFF' state, where the peak force was obtained by the ff-PAM configuration (Fig. 5.6b). Outliers were determined where multiple perturbations occurred within the same gait cycle, or no perturbation occurred. These steps were truncated from the final data set and in instances where multiple perturbations occurred, the first was selected for the final result.

5.5 Experimental Results

5.5.1 Day 1 Results: Fixed Walking Speed

The percentage of the gait cycle at which the valve shutoff occurred was plotted for each stride across all trials for Day 1 (Fig. 5.7), where the average timing in the gait cycle is reported as a percentage for any trial deemed successful. A successful trial was determined by 50 or more consecutive strides falling within $\pm 10\%$ of the running average value obtained. This window of acceptance criteria was used as a sliding window for each trial, as some participants observed the timing shift from one applied period to another. The mean of the phase locking gait phase was then calculated based on the maximum number of consecutive strides within the selected window.

The overall average timing of the perturbations measured during the Day 1 experiment across all successful trials was $52.2 \pm 5.3\%$ of the gait cycle. The ideal timing for plantarflexion assistance is during push-off, which occurs between 45% and 60% of the gait cycle (Winter and Sienko, 1988). The average timing indicates that participants were able to align with this preferred timing window. The basin of entrainment attained for the Day 1 experiment was determined based on the highest increase in

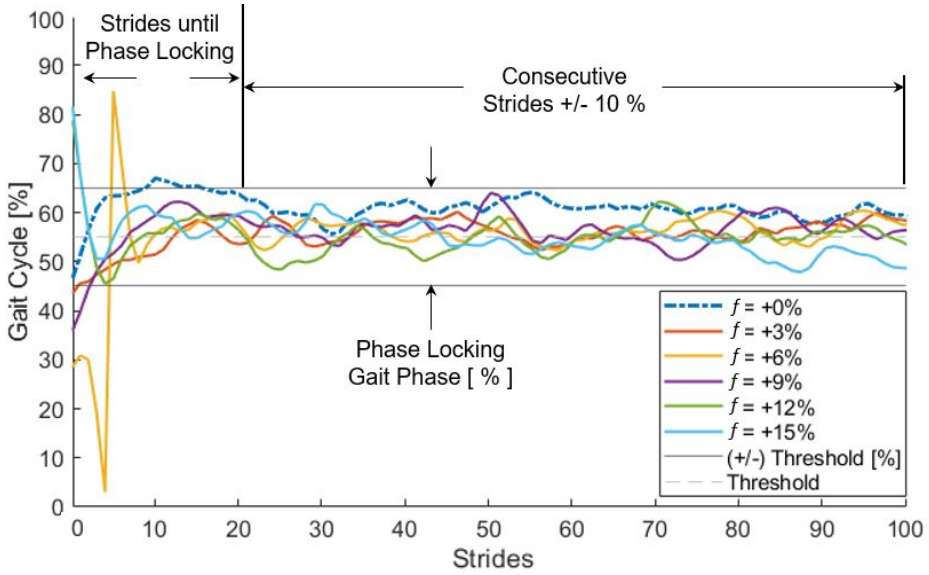

Figure 5.8: Results of a representative subject from the Day 1 experiment, where the subject observed phase locking for each trial and was successful in maintaining this phase locking around the push-off phase throughout the experiment. The y-axis represents the percentage of the gait cycle at which the perturbation occurred. The first 50 steps of these trials are shown for this subject.

Table 5.1: Result Summary of the Day 1 Experiment

Participants	0%	3%	6%	9%	12%	15%
P1	--	--	--	--	--	--
P2	--	--	--	--	--	--
P3	--	--	--	--	--	--
P4	--	--	--	--	--	--
P5	--	--	--	--	--	--
P6	--	--	--	--	--	--
P7	--	--	--	--	--	--
P8	--	--	--	--	--	--
P9	--	--	--	--	--	--
P10	--	--	--	X	X	--

*Successful Trial = -- Unsuccessful Trial = X

frequency that produced a successful trial.

All participants were able to meet the basin of entrainment higher than the 7% threshold. Only one subject was unable to achieve phase locking during the faster applied frequency of perturbations; with observed failed trials at 9 and 12% frequency increases. The summary of passed/failed trials and group average results of performance metrics are shown in Table 5.1 and Fig. 5.9, respectively.

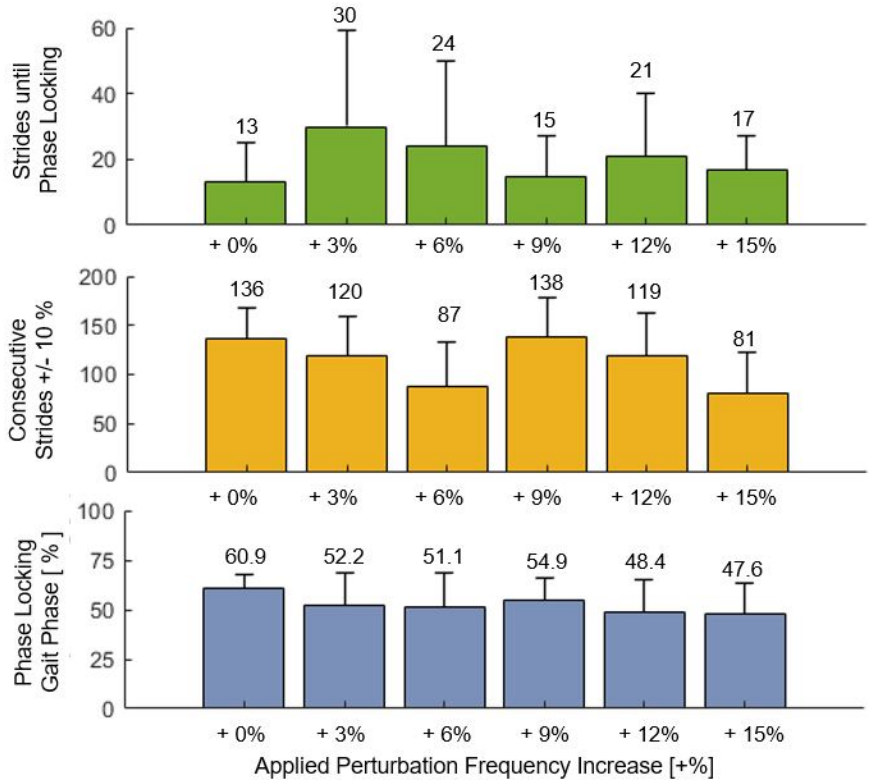

Figure 5.9: A result summary of the Day 1 entrainment study. The number of strides until phase locking (top), the consecutive number of strides within ± 10% of the phase locking value (middle), and the average percentage of gait cycle at which phase locking occurred (bottom) are shown, with the average standard deviation across all participants represented by the error bars.

For the 0% trial, the average timing of phase locking was 60.9 ± 6.6%, with all 10 participants able to achieve phase locking. The +3% trial resulted in a timing of 52.2 ± 16.0%, with all 10 participants able to achieve phase locking. For the +6% trial, the average timing was 51.1 ± 17.3%, with all participants able to achieve phase locking. For the +9% trial, the average timing was 54.9 ± 10.9%, with 9 participants able to achieve phase locking. For the +12% trial, the average timing was 48.4 ± 17.0%, with 9 participants able to achieve phase locking. For the +15% trial, the average timing was 47.6 ± 14.9%, with all participants able to achieve phase locking.

The average amount of steps taken until the mean of successful phase locking was measured at 22±7 steps across all test conditions. For all participants, the average

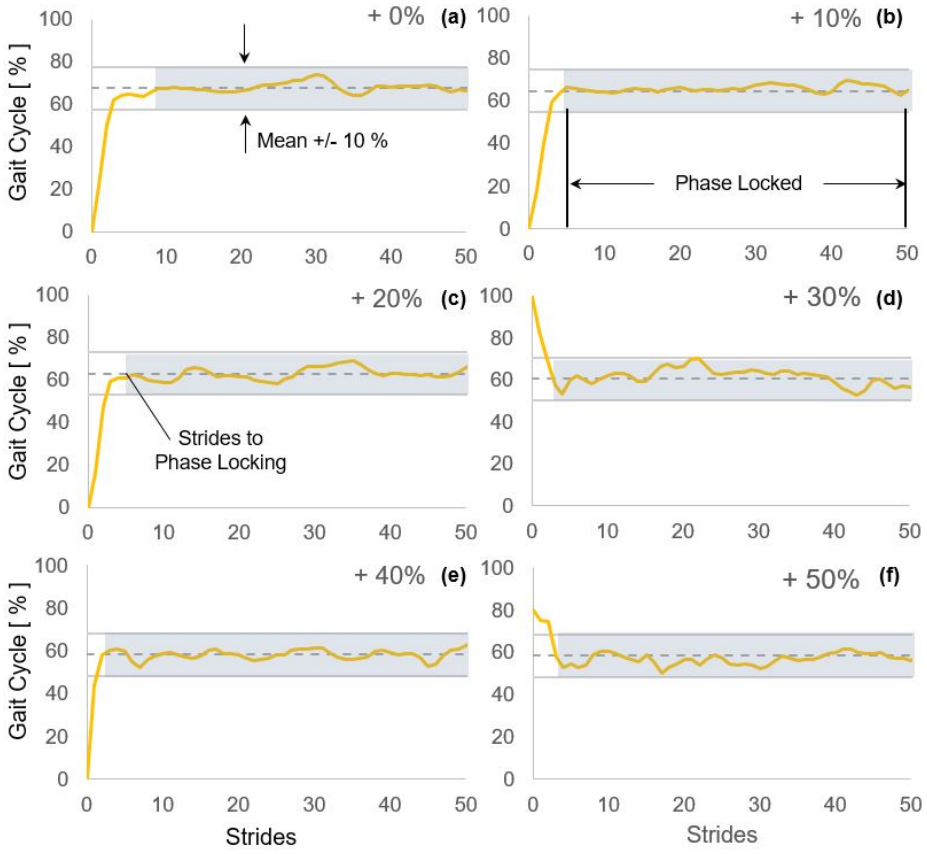

Figure 5.10: Results of a representative subject from the Day 2 experiment, showing phase locking and successful entrainment with the SR-AFO up to +50% frequency increase from the baseline (+0%). Shaded regions indicate successful phase locking.

amount of time the phase locking could be maintained fell at 112±26 strides for all applied perturbation frequencies. Once phase locking was achieved, on average, the timing of the perturbation would drift only 4.1±0.5% from the mean of the phase locked duration of gait.

5.5.2 Day 2 Results: Varying Walking Speed with Bi-Section Method

The overall performance of this protocol far surpassed the performance during Day 1. This could be attributed to several factors, such as familiarity with the SR-AFO exosuit and the protocol and the increased treadmill speed. The highest basin of entrainment observed for any participant in this study was 53.3%, which

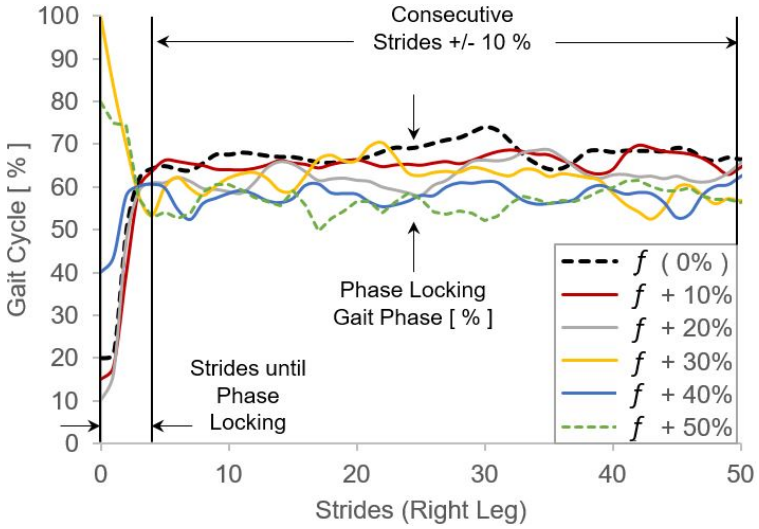

Figure 5.11: Results of a representative subject from the Day 2 experiment, where the subject observed phase locking around the push-off phase for each trial and was successful in maintaining this phase locking throughout the experiment. The first 50 steps of these trials are shown for this subject.

greatly surpasses the previously obtained predictions of an average of 7% with a rigid robot counterpart. As described in Section II.E, a sliding average was used to determine the region of phase locking, and appropriate window of ± 10% from the mean. Fig. 5.10 shows the results of a representative subject with successful entrainment with observable and measurable instances of phase locking (indicated by the shaded regions) across several applied perturbation frequencies ranging from +0% – +50%. A more close-up look at these results is shown in Fig. 5.11, where each trial performed and applied frequency had a similar region within the gait cycle where the participant synchronized to the perturbations.

The overall average basin of entrainment that was achieved across participants for the Day 2 experiment, including all successful trials, was 39.3 ± 9.2%. The basin of entrainment for each participant is provided in Fig. 5.12, with each participant showing the basin of entrainment several magnitudes higher than the previously reported value (+7%) with the heavy and rigid ankle robot. Table 5.2 shows a summary of the performance of each participant throughout the Day 2 experiment. These results

Table 5.2: Result Summary of the Day 2 Experiment

	Steps to PL*	SD	Strides in PL	SD	Gait Cycle Timing [%]	SD	Range of Timing [%]	SD
P1	9	(2)	107	(21)	62.2	(2.8)	3.1	(0.8)
P2	21	(18)	83	(27)	45.3	(8.2)	5.0	(0.7)
P3	16	(5)	152	(46)	48.8	(5.8)	3.8	(1.1)
P4	9	(7)	132	(58)	47.1	(5.2)	3.9	(1.2)
P5	9	(5)	80	(36)	44.4	(6.5)	5.6	(2.1)
P6	23	(20)	80	(31)	47.3	(11.1)	6.2	(1.9)
P7	7	(4)	108	(16)	57.7	(9.1)	3.6	(1.3)
P8	11	(3)	89	(15)	61.3	(1.2)	6.6	(3.6)
P9	7	(4)	93	(18)	49.9	(11.5)	5.3	(5.4)
P10	10	(6)	76	(18)	52.4	(10.6)	9.6	(6.9)
AVG	**12**	**(8)**	**100**	**(29)**	**51.6**	**(7.2)**	**5.2**	**(2.5)**

*** PL**: Phase Locking

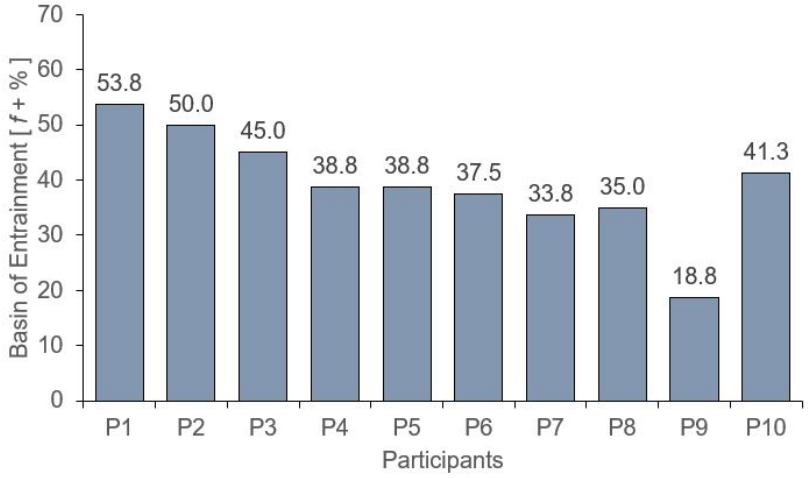

Figure 5.12: The basin of entrainment for each participant in the Day 2 experimental protocol, where each value corresponds to the highest percentage increase in perturbation frequency each participant was able to achieve entrainment and phase locking.

represent the average data for each participant across all successful trials within their basin of entrainment for the Day 2 experiment.

The average steps required for participants to match the mean of the phase locking window was 12 $\pm$ 8 strides. Once phase locking was achieved, participants on average were able to maintain phase locking for 100 $\pm$ 29 strides throughout the 2 minute trials. The average timing of the perturbations applied within the gait cycle was measured to occur at 51.6 $\pm$ 7.2% of the gait cycle, which falls within the targeted

window of 45% and 60% identified as the push-off phase of gait (Winter and Sienko, 1988). During phase locking, the drift of the timing measured was 5.2 ± 2.5%, which stays within the acceptable threshold window of ± 10% set for the acceptance criteria of this study.

Chapter 6

SOFT ROBOTIC HIP EXOSUIT (SR-HEXO)

6.1 Investigation of Hip Assistance

More than 1 million total hip replacements, also known as total hip arthroplasties, are performed each year with over 300,000 performed in the US annually (Ferguson *et al.*, 2018). Following a total hip arthroplasty, patients can incur a decrease of 20% in hip extensor moment of force during early stance phase, a 14% reduction in gait speed and a decrease of 59% in hip extension range at the end of the stance phase (Perron *et al.*, 2000). In addition, stroke is one of the most frequent causes of disability in adults (Kischka and Wade, 2004) in the United States. Almost two-thirds of stroke survivors have initial mobility deficits and cannot walk independently 6 months following a stroke (Jørgensen *et al.*, 1995). The hip joint provides 40-50% of the total average positive power for walking at a variety of rates (Farris and Sawicki, 2012), and injuries to this joint directly or to the spine drastically impact walking capabilities.

As a method of enabling the rehabilitation of gait-deteriorating injuries and procedures, exosuits and exoskeletons for hip flexion and extension assistance have been under development across the world over the past decade (Lewis and Ferris, 2011; Quintero *et al.*, 2011; Wehner *et al.*, 2013; Ding *et al.*, 2014a; Martini *et al.*, 2019; Asbeck *et al.*, 2015b; Ding *et al.*, 2016a; Young and Ferris, 2017; Tefertiller *et al.*, 2018; Thakur *et al.*, 2018). Exosuits, a subsection of soft robotics, employ soft materials as opposed to the rigid linkages found in exoskeletons to improve the comfort and safety of the user, as well as decrease assembly cost (**?**). Exosuits with a variety

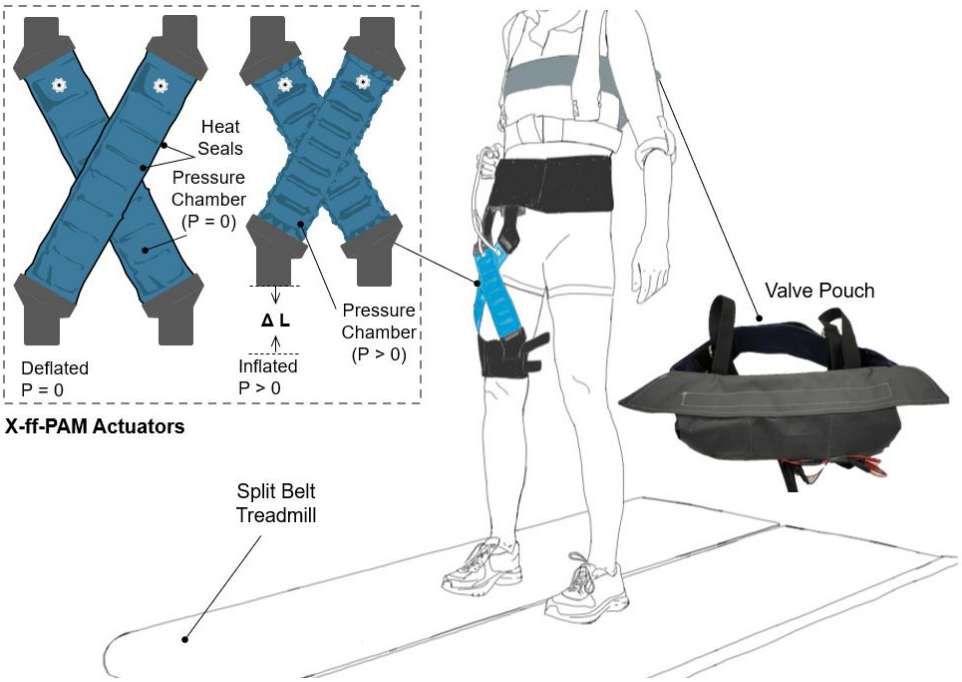

Figure 6.1: X-ff-PAM actuators shown deflated and actuated. The user test setup is shown on a split belt treadmill, wearing the SR-HExo on the right leg just above the knee and wearing the valve pouch on the upper back.

of actuators attempt to replicate the hip joint actuation of flexion and extension. Exosuit actuators have included McKibben actuators (Wehner *et al.*, 2013), Bowden cables (Ding *et al.*, 2014a; Asbeck *et al.*, 2015b; Ding *et al.*, 2016b,a), and pneumatic elastomeric 'muscles' (Thakur *et al.*, 2018). Some exosuits address either extension (Asbeck *et al.*, 2015b) or flexion (Thakur *et al.*, 2018) exclusively with the intention of targeting a particular portion of the gait cycle at the hip.

The proposed design utilizes the flat fabric pneumatic artificial muscle (ff-PAM) actuators introduced by Thalman (Thalman *et al.*, 2019) to assist human walking in hip flexion and extension. In extension, the exosuit mimics the shape and behavior of the Gluteus Maximus (GM), Semimembranosus (SM), and Biceps Femoris (BF) (Webster and Darter, 2019; Dormans, 1993). In flexion, the exosuit mimics the shape and behavior of the Iliacus (IL), Rectus Femoris (RF) and Vastus Medialis (VM) (Webster and Darter, 2019; Dormans, 1993; Winter, 1980). The exosuit uses a pair

of full-length ff-PAMs in an 'X' formation (X-ff-PAM) for both flexion and extension, with different heights of intersection for the actuators. In order to evaluate the effectiveness of the exosuit on user comfort and assistance, hip range of motion (ROM) and muscle activity during walking were monitored using a motion capture system and surface electromyography sensors.

6.2 Design and Characterization of A Soft Robotic Hip Exosuit (SR-HExo)

6.2.1 SR-HExo Design

The SR-HExo is designed to actuate the posterior set of X-ff-PAM actuator from 10-45% of the gait cycle to assist hip extension, and the anterior X-ff-PAM actuator set from 50-90% of the gait cycle to assist hip flexion. The soft robotic hip exosuit (SR-HExo) design is shown in Fig. 6.1. The ff-PAMs cannot be slacked and need to be attached in tension to maximize force output. To allow for this, both the flexion and extension actuators were changed to be in the X orientation referred to as X-ff-PAM, shown for flexion in Fig. 1(b) and for extension in Fig. 1(c). This also hugs the user's thigh more closely than designs that run distally down the back of the leg, such as in (Thakur *et al.*, 2018), and instead mimics the shape of the Iliacus and the Rectus Femoris, the most crucial muscles for hip flexion.

The extension actuator is also in X-ff-PAM formation to guarantee complete ROM in flexion and prevent potential hip abduction generated by force applied to one side of the hip over the other. The final orientation of actuators to assist with extension are shaped like the Adductor Magnus and Vastus Lateralis, hugging the leg more closely than as in (Asbeck *et al.*, 2015b). The horizontal and vertical placements of the actuators are also adjustable given the design features shown in Fig. 6.2a. The length of the actuator attachment to the belt is variable and the placement of that

Table 6.1: Design considerations and criteria (Park *et al.*, 2014a; Browning *et al.*, 2007), motion and Force/Torque Considerations (Neckel *et al.*, 2008; Webster and Darter, 2019; Winter, 1980), and Controls Criteria (Webster and Darter, 2019; Lee *et al.*, 2017b; Thalman *et al.*, 2020b; Winter, 1980) of the SR-HExo

Design Requirements	Characteristics
Design Considerations and Criteria	
Soft, compliant	Neoprene, Spandex and Nylon material
Low profile	~ 5 *mm*
Easy don/doff	≤ 60 s
Light weight	≤ 1.8 kg
Motion and Force/Torque Considerations	
Hip Flexion (Flx.)	0.56 Nm/kg @ 51.6% of gait cycle
Flx. Muscle Assistance	Iliacus (IL), Vastus Medialis (VM), and Rectus Femoris (RF)
Hip Extension (Ext.)	0.66 Nm/kg @ 5.5% of gait cycle
Ext. Muscle Assistance	Gluteus Maximus (GM) and Biceps Femoris (BF)
Minimum ROM	40^o (30^o Flexion, 10^o Extension)
Controls Criteria	
Perturbation Timing	0.2 - 0.3 *sec* actuation time
Flx. Actuator Timing	50-90% of gait cycle
Ext. Actuator Timing	10-45% of gait cycle
Flx. Force (F_{flx})	$\pm$ 10% of 200 N
Ext. Force (F_{ext})	$\pm$ 10% of 100 N
Natural Walking Pace	$\geq$ 1.0 - 1.4 m/s

appendage can be shifted anywhere on the hook-and-loop patch on the belt.

6.2.2 SR-HExo Characterization

The new "X" shape design consists of dual ff-PAM actuators as used in our previous work (Thalman *et al.*, 2019), however rather than being placed in parallel, they are placed at an angle to form an X shape. A universal testing machine (UTM) (Instron 5565, Instron Corp., High Wycombe, United Kingdom) was used to evaluate the effectiveness of the newly proposed orientation of the ff-PAM actuators. Both the parallel and X designs were evaluated to show a comparison between allowing the actuators to work uniaxially vs being positioned off the vertical axis for actuation direction. The actuators were evaluated for maximum force output and dynamic response to demonstrate the proposed design could provide sufficient force output

Figure 6.2: The SR-HExo shown on a user from (a) the side profile, (b) back view, (c) front view, and (d) back view. The actuator anchor points and adjustable leg brace in (a) are highly modular to fit many users. The X-ff-PAM used for actuation in flexion (e) and in extension (f) including the modular knee anchor point.

within a time window that allowed the user to feel each controlled perturbation.

Both actuator orientations were evaluated for a quasi-static fixed lengths at maximum extension to measure the isometric contraction of the actuators as a function of force vs. pressure. The actuators were fixed between two vice clamps, one stationary at the base of the UTM, and the other positioned below the load cell as in Fig. 6.5. A fabric connector interfaced between the actuators and the vice clamps for both orientations to more accurately represent the measured force of the actuators while embedded in the exosuit. The parallel actuators connected to a single point at both

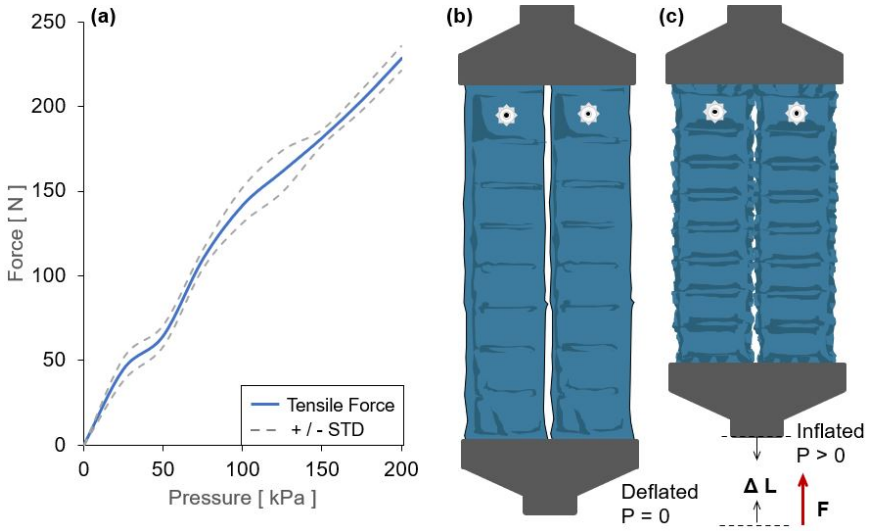

Figure 6.3: (a) The tensile force of the parallel ff-PAM at varying pressures measured in the UTM, from pressures 0 - 200 kPa in 25 kPa increments, and the actuators shown in the deflated (b) and inflated (c) states

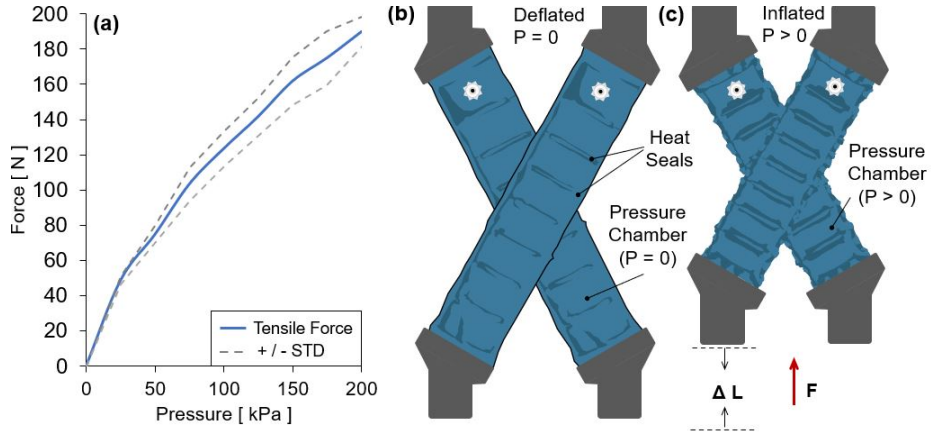

Figure 6.4: The tensile force of the X-ff-PAM at varying pressures, from 0 - 200 kPa (a), and the X-ff-PAM in the deflated (b) and inflated (c) states.

ends, while the X design connected to a beam that was clamped between the vice grips to hold each corner of the X at its fixed position.

A quasi-static force vs. pressure evaluation was performed, where the displacement was fixed at 0 mm and the pressure was increased incrementally from 0 to 200 kPa in steps of 25 kPa. Tensile force was recorded for both the parallel and X designs of the dual ff-PAM across three repeated trials. The resulting force output of the X-ff-PAM at 200 kPa was 190.2 $\pm$ 8.4 N, which falls within $\pm$ 10% of the maximum

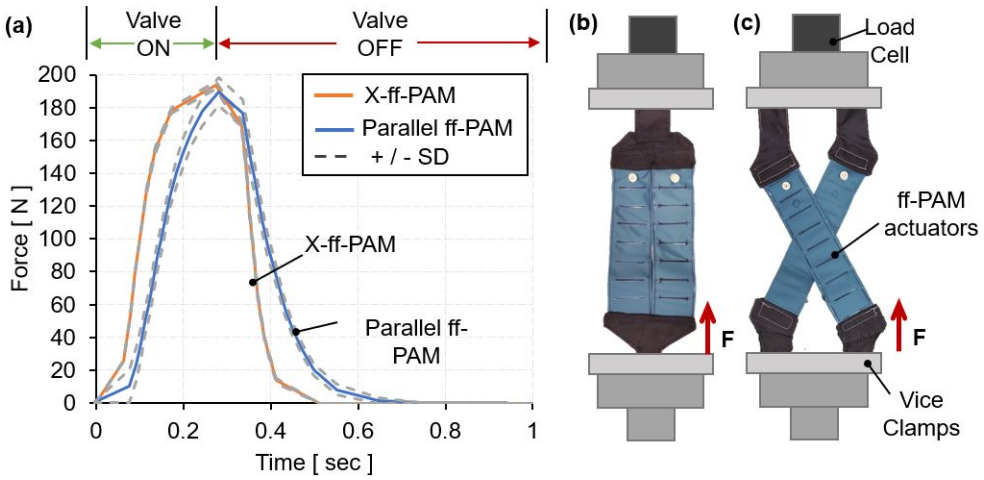

Figure 6.5: (a) The tensile force output parallel ff-PAM (b) compared to the X-ff-PAM (c) recorded as a dynamic response to instantaneous pressure at 200 kPa.

force requirement for hip flexion force (200 N) as shown in Table 1.

A dynamic test was preformed to obtain a force-time relation to measure actuator time response to an impulse of pressure. Fabric connectors were attached to the top and bottom of the ff-PAM to simulate the path along which force is transitioned in the hip exosuit assembly as in the quasi-static evaluation. The dynamic response was induced by quickly opening a 3-way, 2-channeled solenoid valve (320-12 VDC, Humphrey, USA) to rapidly deliver pre-set pressure to the inflate the air chambers of the ff-PAM. This characterization is crucial to ensure the ff-PAM delivers a tensile force through uniaxial contraction to support hip flexion and extension in the correct phases of human gait. Instantaneous pressure from the pressure source were supplied to the valves, and released in a pulse with a period of 1 *sec*, with the valve remaining open for 0.3 *sec* and closed for 0.7 *sec*. The maximum force output and latency in response of each actuator were recorded and are shown in Fig. 6.5 for both actuator configurations.

The parallel actuator orientation and X orientation were able to illicit a similar force response within the same window of actuation time. The parallel actuator (Fig.

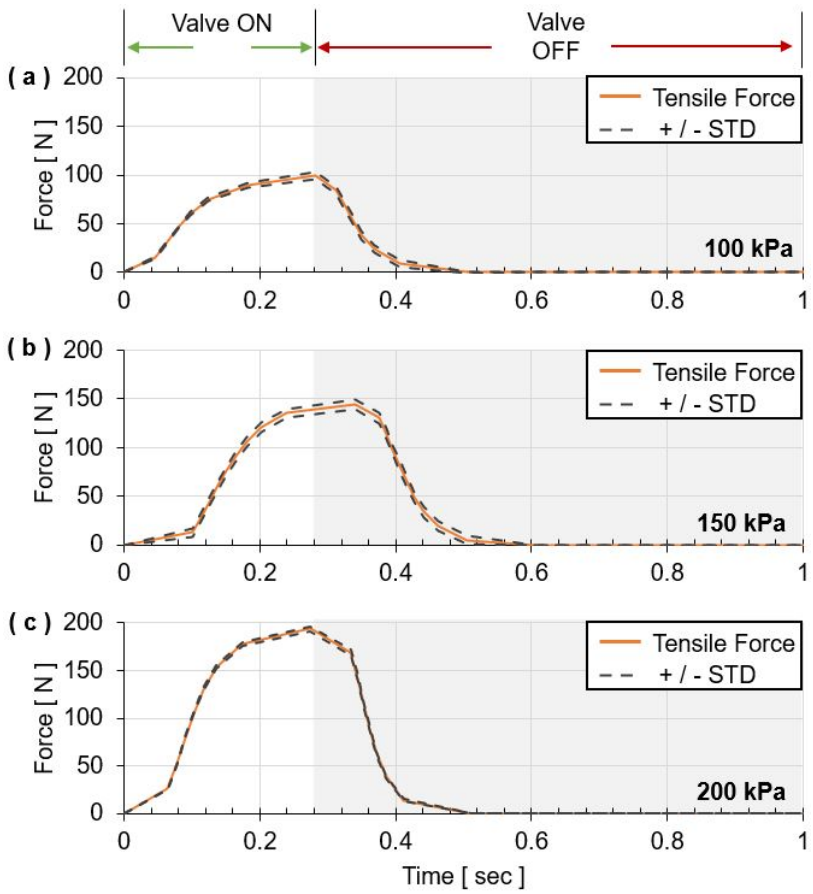

Figure 6.6: The tensile force of the X-ff-PAM recorded as a dynamic response to instantaneous pressure at (a) 100, (b) 150, and (c) 200 kPa.

6.4b) reached a peak force of 189.2 ± 8.2 N at an instantaneous pressure of 200 kPa over a 0.3 *sec* window, with an unloading response time of 0.46 *sec*. The X-ff-PAM orientation (Fig. 6.4c) reached a peak tensile force of 191.2 ± 4.6 N at 200 kPa and an unloading time of 0.25 *sec*. The X-ff-PAM orientation was able to achieve the desired force requirement of 200 N for hip flexion assistance in a short time window that can be scaled within the timing of a typical cadence during healthy walking.

Since the X-ff-PAM operated at a similar level to that of the previous parallel design, the X-ff-PAM was evaluated using the same dynamic test, at varying pressure levels of 100, 150, and 200 kPa. At 100 kPa, the maximum force output was 99.4 ± 3.7 N, with a deflation time of 0.22 *sec*. At 150 kPa the peak force output was 144.1

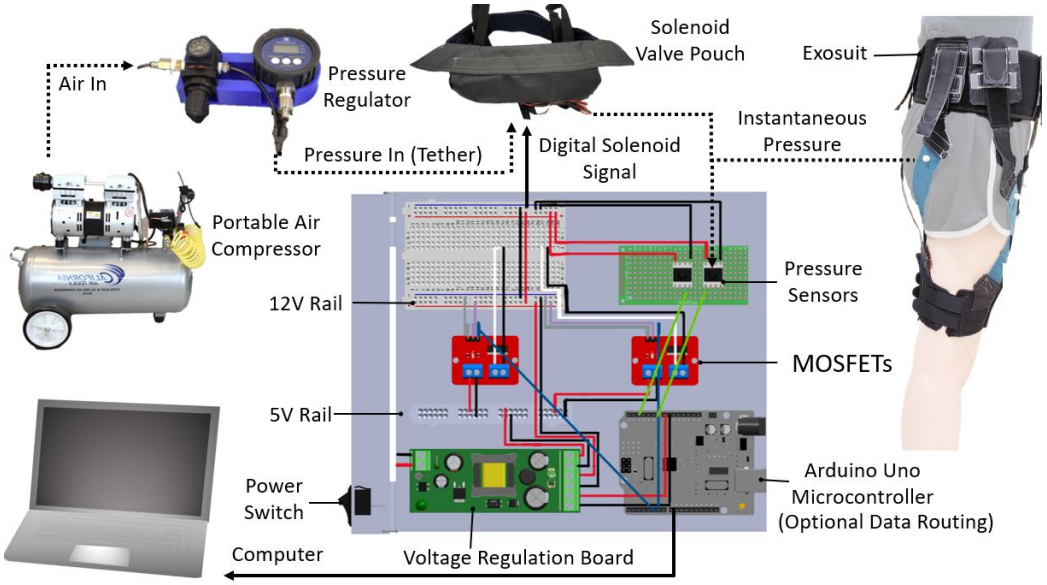

Figure 6.7: High-level overview of sensor, actuator, controller, and air supply integration with the computer. Portable air compressor back-pressure is manually set and pneumatic valves are controlled via MOSFETs located on the control box, which is then monitored via computer or micro-controller.

$\pm$ 5.0 N, with a deflation time of 0.27 *sec.* Peak force at 200 kPa was measured at 193.7 $\pm$ 2.1 N, with a deflation time of 0.24 *sec.* 200 kPa was selected as the final pressure level for this orientation to ensure the 200 N criteria was met during the trials.

6.2.3 Hardware and Control of SR-HExo

The SR-HExo was designed to be worn in rehabilitative contexts utilizing a treadmill setup (Bertec Treadmill, Columbus, OH, USA), and portable air compressor (Model 8010A, California Air Tools, USA) to minimize the necessary on-board components for the user to minimize system weight. This design improved upon the actuation timing of the SR-AFO in (Thalman *et al.*, 2020b) by mounting the pneumatic valves consistently on the user via a low-profile fabric pouch Fig. 6.2d) worn over the SR-HExo. All other hardware was housed in the 3D printed control box (Fig. 6.8c) which sits beside the treadmill and is not on-board the participant. The

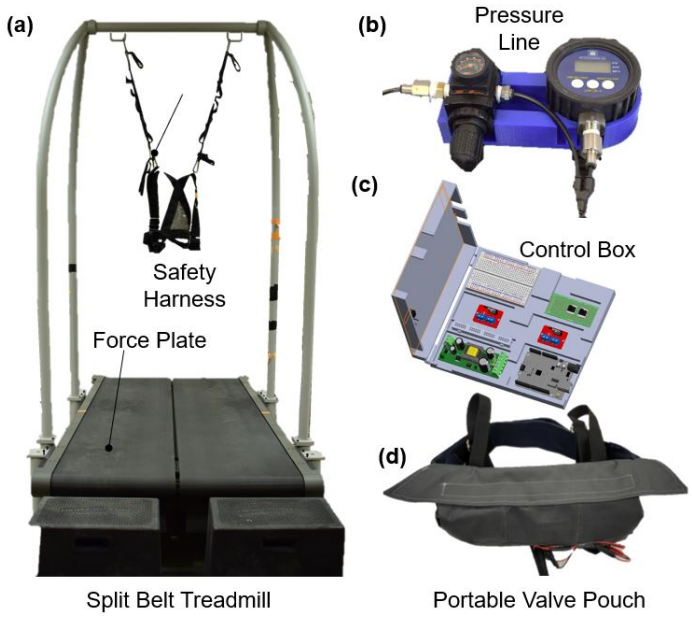

Figure 6.8: (a) The split belt treadmill test setup and safety harness used by participants. (b) The pressure regulator and gauge for consistent pneumatic instantaneous pressure. (c) The control box which houses all the eletro-pneumatic hardware, pressure gauge, and pressure regulation hardware. (d) Wearable pouch for storage of pneumatic valves on the user.

hardware setup utilized pressure sensors (ASDXAVX 100PGAA5, Honeywell Sensing and Productivity Solutions, Charlotte, USA) in each pneumatic line to monitor actuator pressure throughout use, MOSFETs (IRF520 MOSFET Driver Module) for pneumatic valve control, with system control and monitoring of all analog inputs and digital system outputs performed by a speedgoat® (Speedgoat GmbH, Switzerland) through Simulink© (SIMULINK Research License, MATHWORKS, Natick, MA).

The timing of each perturbation was critical to ensure the exosuit was providing proper assistance and not impeding other stages of the gait cycle. In order to do this, the force plate in the treadmill (Fig. 6.8a) was used to determine the user's cadence by taking the average of the last previous five steps and calculating the timing of the next applied perturbation. The extension actuator was activated and deactivated at 10% and 45% of the gait cycle, respectively, while the flexion actuator was activated and deactivated at 50% and 90% of the gait cycle, respectively.

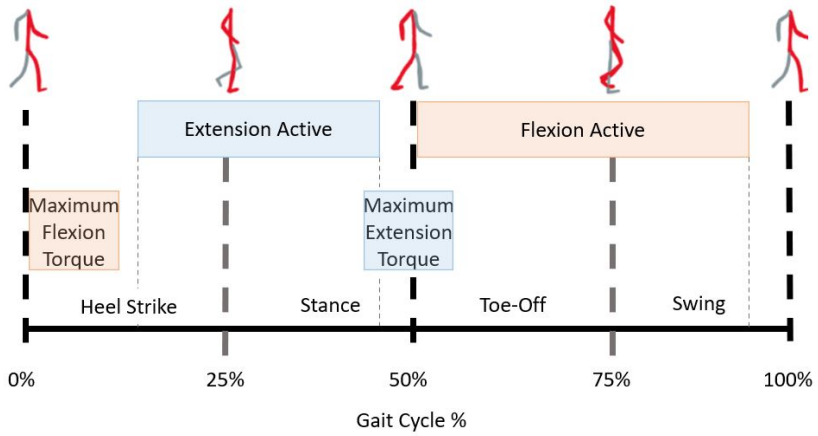

Figure 6.9: System state over a single gait cycle from heel strike to heel strike is primed to assist the moment of greatest torque in flexion and extension separately, resulting in system operation for 70% of the total gait cycle.

6.3 Experiments and Data Analysis

This study was conducted with three (n = 3) healthy participants (age: 21 – 27, height: 1.68 – 1.88 m, weight: 47.6 – 83.9 kg, and leg length: 0.79 – 1.05 m) recruited following the procedures for healthy participants as approved by the Institutional Review Board of Arizona State University (STUDY00012099). Two experimental protocols were implemented, each on a different day, and each subject participated in both experiments.

The objective of this experiment was to assess the effectiveness of the X-ff-PAM to assist in hip flexion and extension during walking. A surface electromyography measurement (EMG) (Delsys Trigno, Delsys, Natick, MA) system recorded the muscle activity of the Iliacus (IL), Rectus Femoris (RF), Biceps Femoris (BF), and Gluteus Maximus (GM), major contributors to successful hip flexion and extension. A motion capture system (T40s, VICON Inc., Los Angeles, CA) allowed for a continuous monitoring of hip angle for comparison to normal ROM at the joint. Reflective markers were placed at the anterior and posterior points of the pelvis, and the center of the thigh to track hip angle in the sagittal plane.

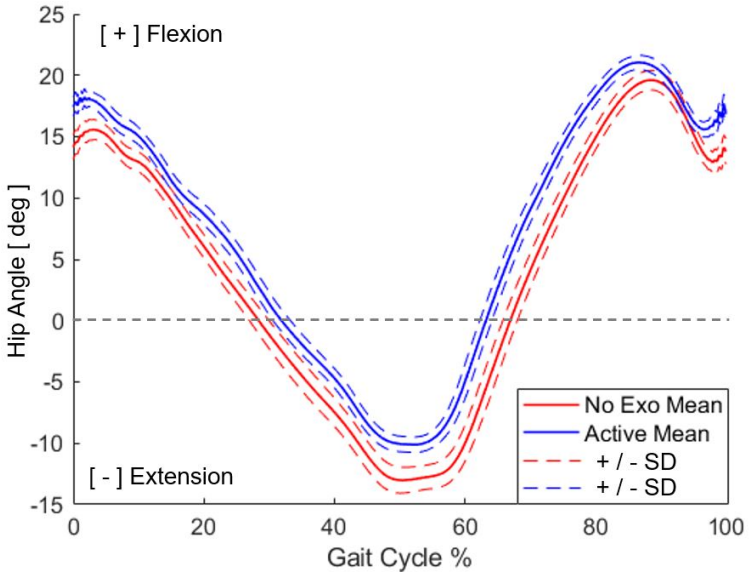

Figure 6.10: Experimental Results of Range of Motion monitoring at the hip joint with and without the SR-HExo for a representative subject.

Prior to the main walking experiment, the surface EMG sensors were placed on the belly of the four muscles described above and maximum voluntary contraction (MVC) of each muscle was measured as per standard International Society of Electrophysiology and Kinesiology (ISEK) protocols (Merletti and Di Torino, 1999). Preferred walking speed was determined by increasing treadmill speeds by steps of 0.1 m/s until the subject indicated the pace was quicker than their natural cadence, then decreased in steps of 0.1 m/s until the subject indicated it too slow. The final preferred walking speed was selected by averaging the two values, and was between 1 and 1.3 m/s for all participants, well within normal bounds of human walking (Farris and Sawicki, 2011).

6.3.1 Experimental Protocol

The main experiment was preformed under 3 conditions (1) no exosuit, (2) passive exosuit, and (3) active exosuit. In the active exosuit condition, the flexion X-ff-PAM was pressurized at 200 kPa for 50-90% of the gait cycle and depressurized

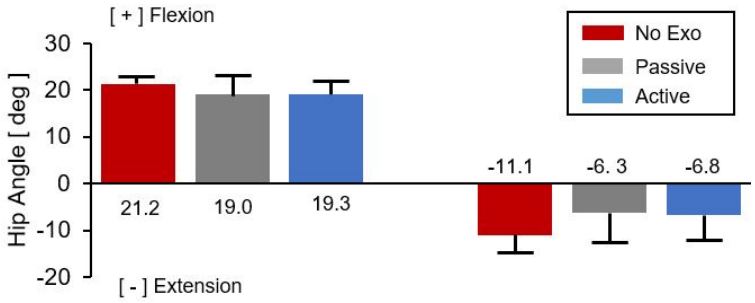

Figure 6.11: Experimental results of hip angle for all participants for all experimental conditions confirm that there is a minimal impact on ROM at the hip during active exosuit usage. Error bars represent mean ± standard deviation (SD) across all three participants.

for the remainder, thus assisting only in the late stance phase. The extension X-ff-PAM was pressurized at 200 kPa for 10-45% of the gait cycle and depressurized for the remainder, assisting only in the terminal swing to loading response. Both actuators were pressurized through valves mounted on the back of the participant. The participant walked for 2 minutes for each experimental condition and a minimum of 3-minute resting period was provided between trial to prevent any potential muscle fatigue. Three active trials were run for each participant, and the cleanest, most consistent data was chosen out of the three.

6.3.2 Data Processing and Analysis

Force plate, motion capture, and EMG data were used to determine gait cycle, kinematics, and muscle activity, respectively. The motion capture system was used to monitor joint angles at a measurement rate of 250 Hz to confirm the SR-HExo did not significantly decrease the hip ROM in the sagittal plane during walking trials. EMG data was collected at 2 kHz and filtered using the second-order Butterworth low-pass filter with a cutoff frequency of 20 Hz and synchronized with kinematic data and force plate data to monitor improvements in muscle expenditure in hip flexion in the IL and RF, and hip extension in the BF and GM muscles. To determine reduction

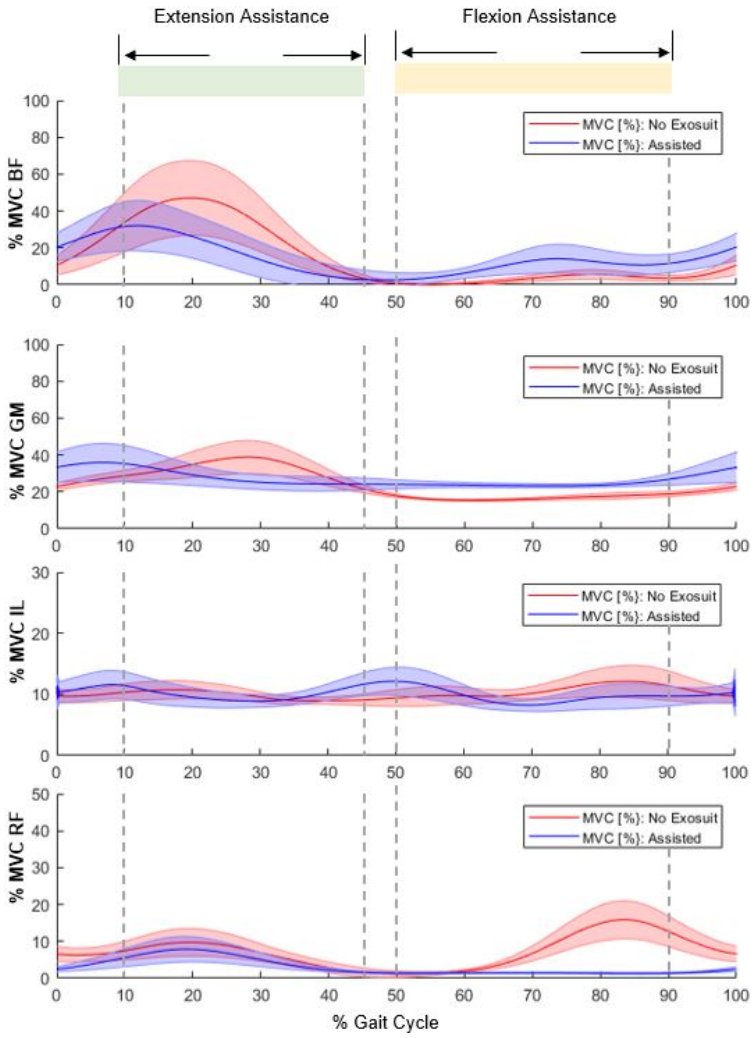

Figure 6.12: Relative EMG reduction for a representative participant across the gait cycle for the BF and GM - to assess extension effort reduction, and the IL and RF - to assess flexion effort reduction.

in muscle activity, the area under the curve was taken between the no exosuit and active conditions from 10-45% of the gait cycle for the hip extensors (GM and BF) and 50-90% of the gait cycle for hip flexors (IL and RF).

6.4 Experimental Results

Preliminary results of this study with three participants showed kinematic data and muscle data to verify the effectiveness of exosuit function in reducing muscle

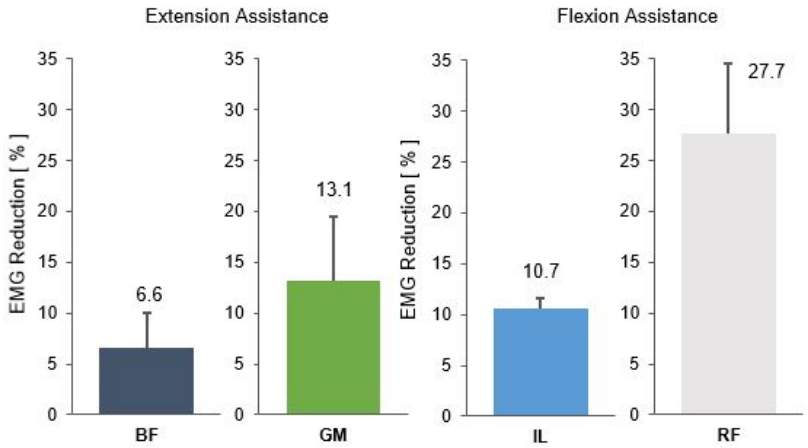

Figure 6.13: EMG area reduction from 50-90% of the gait cycle for flexion assistance of the IL and RF muscles, and 10-45% of the gait cycle for extension assistance of the GM and BF muscles.

activation without significantly altering normal ROM. Each participant showed a hip angle profile that did not drastically alter from their normal ROM in the no exosuit condition (Fig. 6.10). The peak flexion angle at the hip was 21.2 $\pm$ 0.5^o with no exosuit, 19.0 $\pm$ 3.9^o with the passive exosuit, and 19.3 $\pm$ 3.0^o with the active exosuit. The peak extension angle at the hip was measured as -11.0 $\pm$ 2.8^o without the exosuit, -6.3 $\pm$ 5.0^o with the passive exosuit, and -6.8 $\pm$ 3.8^o with the active exosuit. There was some observed reduction in hip ROM with the exosuit passive, however, with the exosuit in the active condition, the ROM was measured at 26.0^o, which is only a 4.0^o reduction from the target ROM of 30^o.

The EMG activity was evaluated for the IL and RF muscles during hip flexion, and showed 10.7 $\pm$ 1.4% and 27.7 $\pm$ 14.2% reduction, respectively. For hip extension, the reduction of muscle activity was 13.1 $\pm$ 5.1% for the GM and 6.6 $\pm$ 3.6% for the BF. No major impact was observed for antagonistic muscle pairings during opposing gait cycle timings.

Chapter 7

DISCUSSION

7.1 SR-AFO Exosuit Design

This paper presents the fully integrated version of the SR-AFO, which is designed to provide medial and lateral ankle support to prevent ankle buckling, as well as plantarflexion assistance to assist the push-off phase during walking. The SR-AFO is made from lightweight materials, entirely fabricated from textile fabrics for a total weight of 0.23 kg. The final design considerations present a novel approach to ankle assistance in both the sagittal and frontal planes using two sets of actuators.

7.2 Dual ff-PAM Actuator Characterization

The first actuator presented was the ff-PAM, which contracts similarly to a muscle when activated. The pneumatic actuation used to create the tensile force generated by the ff-PAM generates a high force-to-weight ratio that showed promising results for assisting ankle plantarflexion. The dual ff-PAM configuration is used for plantarflexion assistance, generating a maximum force output of 337.1 $\pm$ 1.4 N at 200 kPa, which fell within $< 0.5\%$ of the predicted values from the analytical model (336 N) and FEA simulation result (337.5 N).

In previous work Thalman *et al.* (2020b), the ff-PAM was tested for actuation time. During loaded conditions, the dual ff-PAM orientation used in the SR-AFO exosuit could provide peak force output of 118.2 $\pm$ 3.1 N at an interval of 0.3 *sec*. Since the average gait cycles measured for healthy participants in the study ranged from 1.1 - 1.2 *sec*, the actuation time that reached peak force output within a 0.3 *sec*

window would be sufficient to provide plantarflexion assistance with minimal latency. In this study, the dual-ff-PAM actuator was selected due to the higher force output, despite the increased volume of two ff-PAM actuators in parallel. The performance of the improved ff-PAM actuator design was compared to this previous design using a dynamic test to obtain the force-time curves at a fixed pressure of 150 kPa, and the valve was opened to provide rapid pressurization. The actuator was able to provide 212.3 $\pm$ 7.7 N of tensile force in 0.29 *sec*. This configuration and design of the actuator yielded a 79.5% increase in the force output from the previously tested design of the SR-AFO.

7.3 MAVS Actuator Characterization

The MAVS actuator is the second set of actuators featured in the SR-AFO. This design consists of a combination of soft and rigid materials to achieve a design that is compliant when inactive, but retains an increased level of stiffness and resistance to buckling when inflated, fortified by the rigid retainers which constrict outward expansion of the soft materials. This interaction between rigid and soft materials results in the MAVS actuator, which was optimized and characterized for the SR-AFO exosuit. The ratio of rigid to soft material exposed in the final implementation was selected based on the pairing that resulted in the slowest stiffness when deflated, and the highest stiffness when pressurized. The final MAVS design determined to be the best suited for the SR-AFO is the MAVS-A2, with a rigid retainer of L_r = 1 cm and a gap of exposed soft actuator at $L_g = 1$ cm. MAVS-A2 was the second highest stiffness value observed, reaching 26.7 $\pm$ 0.1 N with a calculated stiffness of 1,335.5 N/m and fell within 9.1% of the model predictions, and also showed the lowest stiffness in the passive condition as presented in previous evaluations Thalman *et al.* (2020a).

Six healthy young participants were recruited to perform a series of experiments to validate the overall efficacy of the SR-AFO. The first performance evaluation was conducted using a dual-axis robotic platform, which characterized ankle stiffness as done in previous works Nalam and Lee (2019) with the participant staying in a quiet standing position. The MAVS actuators were evaluated using the platform with the SR-AFO donned on the right foot in a passive condition, and two pressure levels. The group results indicated that the MAVS actuators showed an increase in ankle stiffness in the frontal plane when the MAVS actuators were active, while stiffness in the sagittal plane remained fairly constant. The frontal plane saw an average increase of 56.5 Nm/rad from the baseline free foot stiffness at 50 kPa and 44.5 Nm/rad increase at 30 kPa. The sagittal plane saw an increase in stiffness less than 10 Nm/rad for each pressure level. These results support the proposition that the MAVS actuators can increase ankle stiffness in the medial and lateral directions, with minimal impact on the range of motion in the sagittal plane.

The MAVS actuators were also evaluated in a more dynamic setting, where the participants were asked to walk across the platform while a compliant surface was simulated in the frontal plane. Two compliant surfaces were evaluated, at 50 Nm/rad and 100 Nm/rad. This was done for 30 and 50 kPa conditions for the MAVS actuators, as well as the passive (0 kPa) condition. Results from these trials showed that the overall peak-to-peak ankle deflection in the frontal plane decreases when the MAVS actuators were active compared to the free-foot condition. The decrease in ankle deflection supports the hypothesis that the MAVS actuators would be able to help prevent ankle buckling. By decreasing the overall deflection of the ankle during walking over an unanticipated compliant surface under the foot, the MAVS showed effectiveness in decreasing the range of motion in the medial and lateral direction. With MAVS actuation at 30 kPa, the deflection decreased from 13.2° to 9.8° in the

most compliant condition.

The ff-PAM actuators were evaluated during treadmill walking. EMG sensors were used to monitor muscle activation of the SOL and GAS throughout the trials. The results showed that the SR-AFO was able to reduce the muscle activation of both the SOL and GAS during the 40 – 60 % window of the gait cycle in both average muscle effort and peak muscle effort. These observed changes and reductions in muscle effort suggest that the dual ff-PAM actuator was able to offset some of the effort required from the participant in the free-foot condition and provide assistance from the actuation during the identified range of the gait cycle, i.e., the push-off phase of walking. This result obtained from healthy participants is a promising result that could indicate potential benefits when used with impaired users. With healthy users, the SR-AFO was able to offset existing effort exerted, however, in impaired users, it is predicted that the SR-AFO would instead be able to supplement an otherwise deficient effort that could be exerted from an impaired limb.

7.4 Entrainment Using the SR-AFO

Preliminary results in the ability of the SR-AFO to manifest human entrainment are promising. As indicated in the previous section, all participants recruited for the study exhibited entrainment and phase locking to the gait phase for ankle plantarflexion assistance significantly higher than 7% of their preferred gait frequency. On the Day 1 experiment, all participants were successfully entrained up to the highest perturbation frequency tested, i.e., 15 % higher than the preferred gait frequency. Furthermore, the basin of entrainment of the subjects on the Day 2 experiment ranged from 18.8 – 53.8% from their preferred gait frequency with an average basin of entrainment of 39.3% across all participants.

Motivation for this study was centered around analyzing the rehabilitative ca-

pabilities of the SR-AFO, and the preliminary results suggest strong rehabilitative potential of the SR-AFO. Potential applications of the single-leg mechanical input that will be investigated in future work include correcting asymmetric gait in neurologically impaired patients (e.g., stroke patients) with the entrainment paradigm. These results, coupled with the affordability and accessibility of the SR-AFO, strongly recommend the SR-AFO for rehabilitative applications.

The results of this entrainment study involving the SR-AFO did not match those predicted by the simple state-determined model with afferent feedback proposed in earlier work [2]. The point body mass model with rigid massless legs did not capture the the basin of entrainment observed in this paper. With the SR-AFO donned, human subjects exhibited a basin of entrainment of on average 39.3%, which exceeds the small basin of entrainment predicted by the simple model Ahn and Hogan (2012b,a). These observations indicate that a more detailed model of human locomotor control may be necessary and that human walking cannot be simply modeled with nonlinear dynamics and afferent feedback without higher-level neural contributions.

As suggested in Ahn and Hogan (2012a), the nonlinear dynamic oscillator involved in the participants' ability to be entrained to applied mechanical perturbations could be due to various types of neural control, such as a CPG or supra-spinal control Ahn *et al.* (2011). CPGs are known to be involved in the control of patterned or rhythmic behavior including locomotion Maguire *et al.* (2017); Arya and Pandian (2014); Takakusaki (2013). It is further proposed that supra-spinal control plays an integral role in the context of gait adaptation for purposeful walking, particularly for post-stroke patients Maguire *et al.* (2017). The results of the SR-AFO entrainment study, in particular the participants' ability to adapt their gait patterns, support these ideas, suggesting that higher level supra-spinal control or a greater contribution of a CPG are involved in entrainment during human locomotion.

Extensions of the entrainment study are already underway, including human-SR-AFO interaction characterization to quantitatively establish trends of human adaptability to the soft robotic AFO. In particular, the effect of added mass to the leg during walking on a subject's ability to be entrained with the SR-AFO donned and their corresponding basin of entrainment is under investigation. Another future work will investigate the gait entrainment with the SR-AFO under the condition of adjusting the speed of the treadmill with the user's preference.

7.5 SR-HExo Design

This manuscript presents the design of the SR-HExo for hip flexion and extension assistance, characterization of X-ff-PAM actuator properties and behaviors, and preliminary results of walking trials with healthy participants. The design is lightweight and form-fitting for the user and can be easily worn over pants or shorts. The actuators were characterized for the payload capacity of two actuators in parallel and two actuators in the X formation (X-ff-PAM). The parallel and X-ff-PAM actuator orientations performed similarly in test, as the former delivers a 189.2 $\pm$ 8.2 N payload when inflated to 200 kPa over 0.3 seconds, and the latter 191.2 $\pm$ 4.6 N payload - both well within $\pm$10% of the 200 N desired force requirement for hip flexion. The X-ff-PAM orientation was implemented in this design instead of the parallel ff-PAM to maximize user ROM in flexion and extension and maintain a low profile.

Three healthy individuals participated in a walking study with three different conditions: no exosuit, passive exosuit, and active exosuit. In the active exosuit condition, the flexion actuators were engaged during the window of toe-off to terminal swing, and the extension actuators were engaged between stance phase and toe-off. With the SR-HExo active, the hip ROM was only reduced by 4.0^o from the target ROM of 30^o. EMG data showed a significant reduction in both the hip flexors (IL

and RF) and the hip extensors (GM and BF) during 50-90% and 10-45% of the gait cycle, respectively.

The combination of the SR-HExo's minimal impact on the hip ROM and the reduction in muscle activity during hip flexion and extension stages of the gait cycle indicates a promise for the SR-HExo to provide meaningful assistance without altering natural gait kinematics during human locomotion. The SR-HExo is one of the lightest low-profile lower body exosuits/exoskeletons with potential in gait rehabilitation in the state of the art - an important credential for regular use of the product Lewis and Ferris (2011); Quintero *et al.* (2011); Wehner *et al.* (2013); Ding *et al.* (2014a); Martini *et al.* (2019); Asbeck *et al.* (2015b); Ding *et al.* (2016a); Young and Ferris (2017); Tefertiller *et al.* (2018); Thakur *et al.* (2018). The SR-HExo contains minimal moving parts, preventing most pinching or shear injuries possible with cable-driven systems.

This study was limited to healthy participants and fits most users without major adjustments. However, the exosuit does not properly fit users with legs shorter than 0.71 m and small modifications to the leg brace, point of attachment of the actuators, and expansion of the hip anchor must be made. This study was limited to individuals who‘s leg length exceeded this limitation. Further investigation will be performed during walking protocols for longer durations of time to monitor exosuit integrity over time and transient impact of exosuit use. To properly evaluate exosuit effectively in stroke rehabilitation, the exosuit will need to be tested with stroke patients, and the speed and simplicity of exosuit donning will be assessed by ease of don/doff by patients and their caregivers.

Future work to this design will improve the slight loss in extension ROM and seek to replace the treadmill force plate for data collection with a wearable sensor to make the system portable. Slight modifications to the leg brace and hip anchor will

better fit users with shorter legs. The timing of the system pressurization will be also adjusted to maximize reduction in muscle activity. Further testing will be preformed to assess transient behavior of the exosuit as well as exosuit compatibility with stroke patients.

7.6 Conclusion and Future Work

The SR-AFO showed promising results when evaluated with healthy participants in both standing and walking conditions. Overall evaluation of the SR-AFO exosuit showed a potential for future trials with impaired users to assist in locomotive tasks and serve as a preventative measure to reduce risk of trips or falls due to lateral ankle instability. The ff-PAM actuator design was then implemented for hip assistance with healthy participants, and showed results indicating assistance occurred during hip flexion and extension with minimal impact on the ROM. Overall, the use of the flat fabric pneumatic actuators in the ff-PAM, dual ff-PAM, and x-ff-PAM showed an efficacy in the application of wearable lower body exosuits for gait assistance, and the MAVS actuators provided sufficient dynamics lateral/medial ankle support.

Future work for the SR-AFO will begin to investigate the benefits of the device in clinical trials with users suffering from various gait abnormalities. The combination of the ankle and hip exosuit applications can be investigated for a full lower body robot. Clinical trials will be a critical next step to begin identifying the rehabilitative capabilities of the device. Other future efforts will focus on reducing the size and weight of the control box to provide a more comfortable and low-profile design for increased comfort and portability.

7.7 Contributions of Work

This manuscript presents several novel contributions to the field of soft wearable robotics for assistive and rehabilitative purposes in lower body studies. The design, characterization of the flat fabric pneumatic artificial muscle (ff-PAM) is a design that allow rapid airflow through multiple chamber by allocating gaps on either side of the actuator to allow for faster inflation times, at high tensile forces using a TPU coated nylon, which was optimized using FEA analysis and analytic modeling. The multi-material actuator for variable stiffness (MAVS) is a unique integration of flat fabric inflatables and rigid components. The stacked layers of rigid material and exposed actuator allow for a controllable and easily variable level of stiffness in the actuator to resist transverse loads based on pressure and geometry. The two actuators were integrated into a soft robotic ankle foot orthosis (SR-AFO) which allows for ankle assistance in multiple degrees of freedom. Because of the inherently comfortable and lightweight nature of the SR-AFO, it was also highly effective when used in gait entrainment studies using mechanical perturbations from the ff-PAM actuators. The ff-PAM actuators were also used in hip assistance, for a soft robotic hip exosuit (SR-HExo) which was made from lightweight, compliant materials that provided assistance to the user without impeding natural motion.

"Standards for reporting emg data", Journal of Electromyography and Kinesiology **38**, I – II, URL http://www.sciencedirect.com/science/article/pii/S105064111830035X, neuromechanics of fine hand-motor tasks (2018).

Abe, T., S. Koizumi, H. Nabae, G. Endo and K. Suzumori, "Muscle textile to implement soft suit to shift balancing posture of the body", in "IEEE International Conference on Soft Robotics, (RoboSoft)", (2018).

Abe, T., S. Koizumi, H. Nabae, G. Endo, K. Suzumori, N. Sato, M. Adachi and F. Takamizawa, "Fabrication of "18 Weave" Muscles and Their Application to Soft Power Support Suit for Upper Limbs Using Thin McKibben Muscle", IEEE RA-L, International Conference on Soft Robotics (RoboSoft) **4**, 3, 2532–2538 (2019).

Abouhossein, A., U. Martinez-hernandez, M. I. Awad and A. A. Dehghani-sanij, "Human-activity-centered measurement system : challenges from laboratory to the real environment in assistive gait wearable robotics", in "Mechatronics 2018 - Reinventing Mechatronics, 16th Mechatronics Forum International Conference", (2018).

Abrar, T., F. Putzu, J. Konstantinova and K. Althoefer, "EPAM : Eversive Pneumatic Artificial Muscle", in "IEEE International Conference on Soft Robotics, (RoboSoft)", pp. 2–7 (2019).

Adjei, E., V. Nalam and H. Lee, "Sex differences in human ankle stiffness during standing balance", Frontiers in Sports and Active Living - Biomechanics and Control of Human Movement (2020).

Ahn, J. and N. Hogan, "A simple state-determined model reproduces entrainment and phase-locking of human walking", PloS one **7**, 11, e47963 (2012a).

Ahn, J. and N. Hogan, "Walking is not like reaching: evidence from periodic mechanical perturbations", PloS one **7**, 3 (2012b).

Ahn, J., T. Patterson, H. Lee, D. Klenk, A. Lo, H. I. Krebs and N. Hogan, "Feasibility of entrainment with ankle mechanical perturbation to treat locomotor deficit of neurologically impaired patients", in "2011 Annual international conference of the IEEE engineering in medicine and biology society", pp. 7474–7477 (IEEE, 2011).

Ang, B. W. K. and C. Yeow, "Design and Characterization of a 3D Printed Soft Robotic Wrist Sleeve with 2 DoF for Stroke Rehabilitation", in "IEEE International Conference on Soft Robotics (RoboSoft)", (2019).

Aragane, M., T. Noritsugu, M. Takaiwa, D. Sasaki and S. Naomoto, "Development of Sheet-Like Curved Type Pneumatic RUbber Muscle and Application to Elbow Power Assist Wear", JRSJ **26**, 6, 206–214 (2008).

Arya, K. and S. Pandian, "Interlimb neural coupling: Implications for poststroke hemiparesis", Annals of Physical and Rehabilitation Medicine **57**, 9, 696 – 713, URL http://www.sciencedirect.com/science/article/pii/S187706571401745X (2014).

Asbeck, A., R. Dyer, A. Larusson and C. Walsh, "Biologically-inspired soft exosuit", in "2013 IEEE 13th International Conference on Rehabilitation Robotics (ICORR)", pp. 1–8 (2013).

Asbeck, A. T., S. M. De Rossi, I. Galiana, Y. Ding and C. J. Walsh, "Stronger, smarter, softer: next-generation wearable robots", IEEE Robotics & Automation Magazine **21**, 4, 22–33 (2014).

Asbeck, A. T., S. M. De Rossi, K. G. Holt and C. J. Walsh, "A biologically inspired soft exosuit for walking assistance", International Journal of Robotics Research (2015a).

Asbeck, A. T., K. Schmidt, I. Galiana, D. Wagner and C. J. Walsh, "Multi-joint soft exosuit for gait assistance", in "Proceedings - IEEE International Conference on Robotics and Automation", vol. 2015-June, pp. 6197–6204 (2015b).

Asbeck, A. T., K. Schmidt and C. J. Walsh, "Soft exosuit for hip assistance", in "Robotics and Autonomous Systems", vol. 73, pp. 102–110 (2015c).

Awad, L. N., J. Bae, P. Kudzia, A. Long, K. Hendron, K. G. Holt, K. ODonnell, T. D. Ellis and C. J. Walsh, "Reducing circumduction and hip hiking during hemiparetic walking through targeted assistance of the paretic limb using a soft robotic exosuit", American journal of physical medicine & rehabilitation (2017a).

Awad, L. N., J. Bae, K. O'donnell, S. M. De Rossi, K. Hendron, L. H. Sloot, P. Kudzia, S. Allen, K. G. Holt, T. D. Ellis and C. Walsh, "A soft robotic exosuit improves walking in patients after stroke", Science translational medicine **9**, 400, eaai9084 (2017b).

Babič, J., K. Mombaur, D. Lefeber, J. van Dieën, B. Graimann, M. Russold, N. Šarabon and H. Houdijk, "Spexor: Spinal exoskeletal robot for low back pain prevention and vocational reintegration", in "Wearable robotics: challenges and trends", pp. 311–315 (Springer, 2017).

Babu, S. P., A. Sadeghi, A. Mondini and B. Mazzolai, "Soft sucker shoe for anti-slippage application", in "IEEE International Conference on Soft Robotics, (RoboSoft)", pp. 491–496 (IEEE, 2018).

Bae, J., S. M. M. De Rossi, K. O'Donnell, K. L. Hendron, L. N. Awad, T. R. Teles Dos Santos, V. L. De Araujo, Y. Ding, K. G. Holt, T. D. Ellis and C. J. Walsh, "A soft exosuit for patients with stroke: Feasibility study with a mobile off-board actuation unit", in "IEEE International Conference on Rehabilitation Robotics", pp. 131–138 (IEEE, 2015).

Baiden, D. and O. Ivlev, "Human-robot-interaction control for orthoses with pneumatic soft-actuators - Concept and initial trails", IEEE International Conference on Rehabilitation Robotics pp. 1–6 (2013).

Balasubramanian, S., H. R. Wei, M. Perez, B. Shepard, E. Koeneman, J. Koeneman and J. He, "Rupert: An exoskeleton robot for assisting rehabilitation of arm functions", 2008 Virtual Rehabilitation, IWVR pp. 163–167 (2008).

Baltrusch, S. J., J. H. van Dieën, C. A. van Bennekom and H. Houdijk, "The effect of a passive trunk exoskeleton on functional performance in healthy individuals", Applied ergonomics **72**, 94–106 (2018).

Bao, G., H. Fang, L. Chen, Y. Wan, F. Xu, Q. Yang and L. Zhang, "Soft robotics: Academic insights and perspectives through bibliometric analysis", Soft Robotics **5**, 3, 229–241 (2018).

Bennett, M., M. F. Schatz, H. Rockwood and K. Wiesenfeld, "Huygens's clocks", Proceedings of the Royal Society of London. Series A: Mathematical, Physical and Engineering Sciences **458**, 2019, 563–579 (2002).

Bilodeau, R. A., A. Miriyev, H. Lipson and R. Kramer-Bottiglio, "All-soft material system for strong soft actuators", in "IEEE International Conference on Soft Robotics, (RoboSoft)", pp. 288–294 (2018).

Borboni, A., M. Mor and R. Faglia, "Gloreha—hand robotic rehabilitation: Design, mechanical model, and experiments", Journal of Dynamic Systems, Measurement, and Control **138**, 11 (2016).

Bowers, M. P., C. V. Harmalkar, A. Agrawal, A. Kashyap, J. Tai and M. Popovic, "Design and test of biologically inspired multi-fiber Hydro Muscle actuated ankle", in "Proceedings of IEEE Workshop on Advanced Robotics and its Social Impacts, ARSO", (2017).

Browning, R. C., J. R. Modica, R. Kram and A. Goswami, "The effects of adding mass to the legs on the energetics and biomechanics of walking", Medicine & Science in Sports & Exercise **39**, 3, 515–525 (2007).

Cappello, L., K. C. Galloway, S. Sanan, D. A. Wagner, R. Granberry, S. Engelhardt, F. L. Haufe, J. D. Peisner and C. J. Walsh, "Exploiting Textile Mechanical Anisotropy for Fabric-Based Pneumatic Actuators", Soft Robotics **5**, 5, 662–674 (2018a).

Cappello, L., J. T. Meyer, K. C. Galloway, J. D. Peisner, R. Granberry, D. A. Wagner, S. Engelhardt, S. Paganoni and C. J. Walsh, "Assisting hand function after spinal cord injury with a fabric-based soft robotic glove", Journal of NeuroEngineering and Rehabilitation **15**, 1, 1–10 (2018b).

Center, T. I. S., "Stroke statistics", `http://www.strokecenter.org/patients/about-stroke/stroke-statistics/`, [Online]. Accessed: 22-January-2020 (2020).

Chiaradia, D., M. Xiloyannis, C. W. Antuvan, A. Frisoli and L. Masia, "Design and embedded control of a soft elbow exosuit", in "IEEE International Conference on Soft Robotics, (RoboSoft)", pp. 565–571 (2018).

Chin, R., E. T. Hsiao-Wecksler, E. Loth, G. Kogler, S. D. Manwaring, S. N. Tyson, K. A. Shorter and J. N. Gilmer, "A pneumatic power harvesting ankle-foot orthosis to prevent foot-drop", Journal of NeuroEngineering and Rehabilitation (2009).

Ching-Ping, C. and B. Hannaford, "Measurement and modeling of mckibben pneumatic artificial muscles", IEEE Transactions on Robotics and Automation **12**, 1, 90–102, URL `http://dx.doi.org/10.1109/70.481753` (1996).

Cho, F., R. Sugimoto, T. Noritsugu and X. Li, "Improvement of wearable power assist wear for low back support using pneumatic actuator", in "IOP Conference Series: Materials Science and Engineering", vol. 249, p. 012004 (IOP Publishing, 2017).

Chung, J., R. Heimgartner, C. T. Oneill, N. S. Phipps and C. J. Walsh, "ExoBoot, a Soft Inflatable Robotic Boot to Assist Ankle during Walking: Design, Characterization and Preliminary Tests", in "2018 7th IEEE International Conference on Biomedical Robotics and Biomechatronics (Biorob)", pp. 509–516 (IEEE, 2018).

Cianchetti, M., C. Laschi, A. Menciassi and P. Dario, "Biomedical applications of soft robotics", Nature Reviews Materials **3**, 6, 143–153, URL `http://dx.doi.org/10.1038/s41578-018-0022-y` (2018).

Cogollor, J., J. Rojo-Lacal, J. Hermsdörfer, M. Ferre, M. Waldmeyer, C. Giachritsis, A. Armstrong, J. Martinez, D. Loza and J. Sebastián, "Evolution of cognitive rehabilitation after stroke from traditional techniques to smart and personalized home-based information and communication technology systems: literature review", JMIR rehabilitation and assistive technologies **5**, 1, e4 (2018).

Connelly, L., Y. Jia, M. L. Toro, M. E. Stoykov, R. V. Kenyon and D. G. Kamper, "A pneumatic glove and immersive virtual reality environment for hand rehabilitative training after stroke", IEEE Transactions on Neural Systems and Rehabilitation Engineering **18**, 5, 551–559 (2010).

Connolly, F., P. Polygerinos, C. J. Walsh and K. Bertoldi, "Mechanical programming of soft actuators by varying fiber angle", Soft Robotics **2**, 1, 26–32 (2015).

Cowper, G., "The shear coefficient in timoshenko's beam theory", (1966).

Coyle, S., C. Majidi, P. LeDuc and K. J. Hsia, "Bio-inspired soft robotics: Material selection, actuation, and design", Extreme Mechanics Letters **22**, 51–59 (2018).

Davis, S., N. Tsagarakis, J. Canderle and D. G. Caldwell, "Enhanced modelling and performance in braided pneumatic muscle actuators", The International Journal of Robotics Research **22**, 3-4, 213–227 (2003).

Di Natali, C., T. Poliero, M. Sposito, E. Graf, C. Bauer, C. Pauli, E. Bottenberg, A. De Eyto, L. O'Sullivan, A. F. Hidalgo, D. Scherly, K. S. Stadler, D. G. Caldwell and J. Ortiz, "Design and Evaluation of a Soft Assistive Lower Limb Exoskeleton", Robotica pp. 1–21 (2019).

Ding, Y., I. Galiana, A. Asbeck, S. De Rossi, J. Bae, T. Santos, V. Araujo, S. Lee, K. Holt and C. Walsh, "Biomechanical and Physiological Evaluation of Multi-joint Assistance with Soft Exosuits", IEEE Transactions on Neural Systems and Rehabilitation Engineering **PP**, 99, 1–1 (2016a).

Ding, Y., I. Galiana, A. Asbeck, B. Quinlivan, S. De Rossi and C. Walsh, "Multi-joint actuation platform for lower extremity soft exosuits", in "2014 IEEE International Conference on Robotics and Automation (ICRA)", pp. 1327–1334 (Ieee, 2014a).

Ding, Y., I. Galiana, A. T. Asbeck, S. M. M. De Rossi, J. Bae, T. Santos, V. L. De Araujo, S. Lee, K. G. Holt and C. J. Walsh, "Biomechanical and physiological evaluation of multi-joint assistance with soft exosuits", IEEE Transactions on Neural Systems and Rehabilitation Engineering **25**, 2, 119–130 (2017).

Ding, Y., I. Galiana, C. Siviy, F. A. Panizzolo and C. J. Walsh, "IMU-based iterative control for hip extension assistance with a soft exosuit", Proceedings - IEEE International Conference on Robotics and Automation **2016-June**, 3501–3508 (2016b).

Ding, Y., M. Kim, S. Kuindersma and C. J. Walsh, "Human-in-the-loop optimization of hip assistance with a soft exosuit during walking", Science Robotics (2018).

Ding, Y., M. T. Tolley, Y. Park, R. F. Shepherd, R. J. Wood, M. Wehner, Y. Mengüç, A. Mozeika, C. Onal and G. M. Whitesides, "Pneumatic Energy Sources for Autonomous and Wearable Soft Robotics", Soft Robotics (2014b).

Dinh, B., M. Xiloyannis, L. Cappello, C. Antuvan, S. Yen and L. Masia, "Adaptive backlash compensation in upper limb soft wearable exoskeletons", Robotics and Autonomous Systems **92**, 173–186 (2017).

Dormans, J. P., "Orthopedic management of children with cerebral palsy.", Pediatric Clinics of North America **40**, 3, 645–657 (1993).

Doumit, M., A. Fahim and M. Munro, "Analytical modeling and experimental validation of the braided pneumatic muscle", IEEE Transactions on Robotics **25**, 1282–1291 (2009).

Elliott, G., G. S. Sawicki, A. Marecki and H. Herr, "The biomechanics and energetics of human running using an elastic knee exoskeleton", IEEE International Conference on Rehabilitation Robotics **0**, 4, 1–6 (2013).

Exoskeleton Report (ExR), "Directory of exoskeleton developers", `https://exoskeletonreport.com/exoskeleton-companies-and-organizations-directory/`, [Online]. Accessed: April-2020 (2020).

Ezzibdeh, R., P. Arora and D. F. Amanatullah, "Utilization of a pneumatic exoskeleton after total knee arthroplasty", Arthroplasty Today (2019).

Farris, D. J. and G. S. Sawicki, "The mechanics and energetics of human walking and running: a joint level perspective", Journal of The Royal Society Interface **9**, 66, 110–118 (2011).

Farris, J. and G. S. Sawicki, "The mechanics and energetics of human walking and running: A joint level perspective", Journal of the Royal Society Interface **9**, 66, 110–118 (2012).

Felt, W., M. A. Robertson and J. Paik, "Modeling vacuum bellows soft pneumatic actuators with optimal mechanical performance", in "IEEE International Conference on Soft Robotics, (RoboSoft)", pp. 534–540 (2018).

Ferguson, R. J., A. J. Palmer, A. Taylor, M. L. Porter, H. Malchau and S. Glyn-Jones, "Hip replacement", The Lancet **392**, 10158, 1662–1671 (2018).

Ferris, D. P., K. E. Gordon, G. S. Sawicki and A. Peethambaran, "An improved powered ankle-foot orthosis using proportional myoelectric control", Gait and Posture **23**, 4, 425–428 (2006).

Fraiszudeen, A. and C. Yeow, "Soft actuating sit-to-stand trainer seat", Journal of Mechanisms and Robotics **11**, 1, 014501 (2019).

Funabora, Y., "Flexible Fabric Actuator Realizing 3D Movements Like Human Body Surface for Wearable Devices", in "International Conference on Intelligent Robots and Systems (IROS)", pp. 6992–6997 (2018).

Galiana, I., F. L. Hammond, R. D. Howe and M. B. Popovic, "Wearable soft robotic device for post-stroke shoulder rehabilitation: Identifying misalignments", IEEE International Conference on Intelligent Robots and Systems pp. 317–322 (2012).

Galloway, K. C., P. Polygerinos, C. J. Walsh and R. J. Wood, "Mechanically programmable bend radius for fiber-reinforced soft actuators", in "2013 16th International Conference on Advanced Robotics (ICAR)", pp. 1–6 (IEEE, 2013).

Gao, X., Y. Sun, L. Hao, C. Xiang and H. Cheng, "A new type of soft pneumatic elbow", 2017 IEEE International Conference on Robotics and Biomimetics, ROBIO 2017 **2018-January**, 2681–2686 (2018).

Garrick, J. G., "The frequency of injury, mechanism of injury, and epidemiology of ankle sprains", The American journal of sports medicine **5**, 6, 241–242 (1977).

Gordon, K. E., G. S. Sawicki and D. P. Ferris, "Mechanical performance of artificial pneumatic muscles to power an ankle-foot orthosis", Journal of Biomechanics **39**, 10, 1832–1841 (2006).

Granberry, J., R.and Duvall, L. E. Dunne and B. Holschuh, "An analysis of anthropometric geometric variability of the lower leg for the fit & function of advanced functional garments", in "Proceedings of the 2017 ACM International Symposium on Wearable Computers", pp. 10–17 (ACM, 2017).

Han, K., N. Kim and D. Shin, "A novel soft pneumatic artificial muscle with high-contraction ratio", Soft Robotics **5**, 5, 554–566 (2018).

Hass, C. J., M. Bishop, M. Moscovich, E. L. Stegemöller, J. Skinner, I. A. Malaty, A. W. Shukla, N. McFarland and M. S. Okun, "Defining the clinically meaningful difference in gait speed in persons with parkinson disease", Journal of Neurologic Physical Therapy **38**, 4, 233–238 (2014).

Hassanin, A., D. Steve and N. Samia, "A novel, soft, bending actuator for use in power assist and rehabilitation exoskeletons", in "2017 IEEE/RSJ International Conference on Intelligent Robots and Systems (IROS)", pp. 533–538 (IEEE, 2017).

Heung, K. H., R. K. Tong, A. T. Lau and Z. Li, "Robotic glove with soft-elastic composite actuators for assisting activities of daily living", Soft robotics (2019).

Higuma, T., K. Kiguchi and J. Arata, "Low-profile Two-degree-of-freedom Wrist Exoskeleton Device using Multiple Spring Blade", IEEE Robotics and Automation Letters pp. 1–1 (2017).

Hiramitsu, T., K. Suzumori, H. Nabae and G. Endo, "Experimental Evaluation of Textile Mechanisms Made of Artificial Muscles", in "IEEE International Conference on Soft Robotics (RoboSoft)", (2019).

Holland, D., E. J. Park, P. Polygerinos, G. J. Bennett and C. J. Walsh, "The soft robotics toolkit: Shared resources for research and design", Soft Robotics **1**, 3, 224–230 (2014).

Holland, D. P., C. Abah, M. Velasco-Enriquez, M. Herman, G. J. Bennett, E. Vela and C. J. Walsh, "The Soft Robotics Toolkit: Strategies for Overcoming Obstacles to the Wide Dissemination of Soft-Robotic Hardware", IEEE Robotics and Automation Magazine (2017).

Hong, J., Y. Fukushima, S. Suzuki, K. Yauda, H. Ohashi and H. Iwata, "Estimation of Ankle Dorsiflexion Torque during Loading Response Phase for Spring Coefficient Identification", in "IEEE International Conference on Robotics and Biomimetics", pp. 2237 – 2242 (2017).

In, H., B. B. Kang, M. Sin and K. Cho, "Exo-Glove: A wearable robot for the hand with a soft tendon routing system", IEEE Robotics and Automation Magazine **22**, 1, 97–105 (2015).

Inose, H., S. Mohri, Y. Yamada, T. Nakamura, K. Yokoyama and I. Kikutani, "Development of a lightweight power-assist suit using pneumatic artificial muscles and balloon-amplification mechanism", in "2016 14th International Conference on Control, Automation, Robotics and Vision (ICARCV)", pp. 1–6 (IEEE, 2016).

Irshaidat, M., M. Soufian, A. Al-Ibadi and S. Nefti-Meziani, "A novel elbow pneumatic muscle actuator for exoskeleton arm in post-stroke rehabilitation", in "2019 2nd IEEE International Conference on Soft Robotics (RoboSoft)", pp. 630–635 (IEEE, 2019).

Iwata, H., K. Yasuda, J. Hong, H. Ohashi, S. Suzuki and Y. Fukushima, "Development of High-Dorsiflexion Assistive Robotic Technology for Gait Rehabilitation", in "IEEE International Conference on Systems, Man, and Cybernetics Development", pp. 3801 – 3806 (2018).

Jiang, M. and N. Gravish, "Sliding-layer laminates: a robotic material enabling robust and adaptable undulatory locomotion", in "2018 IEEE/RSJ International Conference on Intelligent Robots and Systems (IROS)", pp. 5944–5951 (IEEE, 2018).

Jiang, Y., D. Chen, P. Liu, X. Jiao, Z. Ping, Z. Xu, J. Li and Y. Xu, "Fishbone-inspired soft robotic glove for hand rehabilitation with multi-degrees-of-freedom", in "IEEE International Conference on Soft Robotics, (RoboSoft)", pp. 394–399 (2018).

Jørgensen, H. S., H. Nakayama, H. O. Raaschou and T. S. Olsen, "Recovery of walking function in stroke patients: the copenhagen stroke study", Archives of physical medicine and rehabilitation **76**, 1, 27–32 (1995).

Kadivar, Z., C. Beck, R. Rovekamp, M. O'Malley and C. Joyce, "On the efficacy of isolating shoulder and elbow movements with a soft, portable, and wearable robotic device", in "Wearable Robotics: Challenges and Trends", pp. 89–93 (Springer, 2017).

Kang, B. B., H. Choi, H. Lee and K. Cho, "Exo-Glove Poly II: A Polymer-Based Soft Wearable Robot for the Hand with a Tendon-Driven Actuation System", Soft Robotics **00**, 00, soro.2018.0006 (2018).

Karavas, N., A. Asbeck, I. Galiana, D. Wagner, C. Siviy, M. Grimmer, S. Lee, B. T. Quinlivan, P. Malcolm, C. J. Walsh and D. M. Rossi, "Assistance magnitude versus metabolic cost reductions for a tethered multiarticular soft exosuit", Science Robotics (2017).

Kawamura, T., K. Takanaka, T. Nakamura and H. Osumi, "Development of an orthosis for walking assistance using pneumatic artificial muscle: A quantitative assessment of the effect of assistance", in "2013 IEEE 13th International Conference on Rehabilitation Robotics (ICORR)", pp. 1–6 (IEEE, 2013).

Kesner, S. B., L. Jentoft, F. L. Hammond, R. D. Howe and M. Popovic, "Design considerations for an active soft orthotic system for shoulder rehabilitation", in "2011 Annual International Conference of the IEEE Engineering in Medicine and Biology Society", pp. 8130–8134 (IEEE, 2011).

Khin, P., H. Yap, M. H. Ang and C. Yeow, "Fabric-based actuator modules for building soft pneumatic structures with high payload-to-weight ratio", IEEE International Conference on Intelligent Robots and Systems **2017-Septe**, c, 2744–2750 (2017).

Kim, D. H. and H. Park, "Cable actuated dexterous (cadex) glove for effective rehabilitation of the hand for patients with neurological diseases", in "2018 IEEE/RSJ International Conference on Intelligent Robots and Systems (IROS)", pp. 2305–2310 (IEEE, 2018).

Kischka, U. and D. T. Wade, "Rehabilitation after stroke", Handbook of Cerebrovascular Diseases, Second Edition, Revised and Expanded pp. 231–241 (2004).

Klute, G., J. Czerniecki and B. Hannaford, "McKibben artificial muscles: pneumatic actuators with biomechanical intelligence", in "IEEE/ASME International Conference on Advanced Intelligent Mechatronics", pp. 221–226 (1999).

Kobayashi, H., H. Suzuki and M. Iba, "Development of a muscle suit for the upper limb motion support - a new shoulder mechanism and posture measurement", 2006 World Automation Congress, WAC'06 (2007).

Koh, T., N. Cheng, H. Yap and C. Yeow, "Design of a Soft Robotic Elbow Sleeve with Passive and Intent-Controlled Actuation", Frontiers in Neuroscience **11**, October, 1–12 (2017).

Koo, I., C. Yun, M. V. Costa, J. V. Scognamiglio, T. A. Yangali, D. Park and K. Cho, "Development of a meal assistive exoskeleton made of soft materials for polymyositis patients", in "2014 IEEE/RSJ International Conference on Intelligent Robots and Systems", pp. 542–547 (IEEE, 2014).

Kwon, J., J. Park, S. Ku, Y. Jeong, N. Paik and Y. Park, "A Soft Wearable Robotic Ankle-Foot-Orthosis for Post-Stroke Patients", IEEE RA-L, International Conference on Soft Robotics (RoboSoft) (2019).

Kwon, J., S. Yoon and Y. Park, "Flat inflatable artificial muscles with large stroke and adjustable force–length relations", IEEE Transactions on Robotics (2020).

Lamers, E. P., A. J. Yang and K. E. Zelik, "Feasibility of a biomechanically-assistive garment to reduce low back loading during leaning and lifting", IEEE Transactions on Biomedical Engineering **65**, 8, 1674–1680 (2018).

Lee, G., Y. Ding, I. G. Bujanda, N. Karavas, Y. M. Zhou and C. J. Walsh, "Improved assistive profile tracking of soft exosuits for walking and jogging with off-board actuation", in "2017 IEEE/RSJ International Conference on Intelligent Robots and Systems (IROS)", pp. 1699–1706 (IEEE, 2017a).

Lee, H., H. I. Krebs and N. Hogan, "Multivariable dynamic ankle mechanical impedance with active muscles", IEEE Transactions on Neural Systems and Rehabilitation Engineering **22**, 5, 971–981 (2014a).

Lee, S., S. Crea, P. Malcolm, I. Galiana, A. Asbeck and C. Walsh, "Controlling negative and positive power at the ankle with a soft exosuit", in "IEEE International Conference on Robotics and Automation (ICRA)", pp. 3509–3515 (IEEE, 2016).

Lee, S. W., K. A. Landers and H. Park, "Development of a biomimetic hand exotendon device (biomhed) for restoration of functional hand movement post-stroke", IEEE Transactions on Neural Systems and Rehabilitation Engineering **22**, 4, 886–898 (2014b).

Lee, Y., S. Roh, M. Lee, B. Choi, J. Lee, J. Kim, H. Choi, Y. Shim and Y. Kim, "A flexible exoskeleton for hip assistance", IEEE International Conference on Intelligent Robots and Systems **2017-Septe**, 1058–1063 (2017b).

Lessard, S., P. Pansodtee, A. Robbins, L. Baltaxe-Admony, J. M. Trombadore, M. Teodorescu, A. Agogino and S. Kurniawan, "CRUX: A compliant robotic upper-extremity exosuit for lightweight, portable, multi-joint muscular augmentation", IEEE International Conference on Rehabilitation Robotics **3**, 1633–1638 (2017).

Lessard, S. R., *The Design, Consturction, and Evaluation of Crux: A Tensegrity-Inspired Compliant Robotic Upper-Extremity Exosuit*, Ph.D. thesis, University of California (2018).

Lewis, C. L. and D. P. Ferris, "Invariant hip moment pattern while walking with a robotic hip exoskeleton", Journal of Biomechanics **44**, 5, URL `http://dx.doi.org/10.1016/j.jbiomech.2011.01.030` (2011).

Li, H., J. Yao, P. Zhou, X. Chen, Y. Xu and Y. Zhao, "High-force soft pneumatic actuators based on novel casting method for robotic applications", Sensors and Actuators A: Physical **306**, 111957 (2020).

Li, N., T. Yang, P. Yu, L. Zhao, J. Chang, N. Xi and L. Liu, "Force point transfer method to solve the structure of soft exoskeleton robot deformation due to the driving force", in "2018 IEEE International Conference on Real-time Computing and Robotics (RCAR)", pp. 236–241 (IEEE, 2018).

Li, S., D. M. Vogt, D. Rus and R. J. Wood, "Fluid-driven origami-inspired artificial muscles", Proceedings of the National Academy of Sciences **114**, 50, 13132–13137 (2017).

Low, F., H. Tan, J. H. Lim and C. Yeow, "Development of a soft pneumatic sock for robot-assisted ankle exercise", Journal of Medical Devices **10**, 1 (2016).

Low, F., R. Yeow, H. Yap and J. Lim, "Study on the use of Soft Ankle-Foot Exoskeleton for Alternative Mechanical Prophylaxis of Deep Vien Thrombosis", in "IEEE International Conference on Rehabilitation Robotics (ICORR)", (IEEE, 2015).

Lusardi, M. M., M. Jorge and C. C. Nielsen, *Orthotics and Prosthetics in Rehabilitation-E-Book* (Elsevier Health Sciences, 2013).

Maciejasz, P., J. Eschweiler, K. Gerlach-hahn, A. Jansen-troy and S. Leonhardt, "A survey on robotic devices for upper limb rehabilitation", Journal of NeuroEngineering and Rehabilitation pp. 1–29 (2014).

Maeder-York, P., T. Clites, E. Boggs, R. Neff, P. Polygerinos, D. Holland, L. Stirling, K. Galloway, C. Wee and C. Walsh, "Biologically inspired soft robot for thumb rehabilitation", Journal of Medical Devices **8**, 2 (2014).

Maguire, C. C., J. M. Sieben and R. A. de Bie, "The influence of walking-aids on the plasticity of spinal interneuronal networks, central-pattern-generators and the recovery of gait post-stroke. a literature review and scholarly discussion", Journal of Bodywork and Movement Therapies **21**, 2, 422 – 434, URL http://www.sciencedirect.com/science/article/pii/S1360859216302029 (2017).

Majidi, C., "Soft robotics: A perspective, current trends and prospects for the future", Soft Robotics **1**, 1, 5–11 (2013).

Malcolm, P., W. Derave, S. Galle and D. De Clercq, "A simple exoskeleton that assists plantarflexion can reduce the metabolic cost of human walking", PloS one **8**, 2 (2013).

Malcolm, P., S. Lee, S. Crea, C. Siviy, F. Saucedo, I. Galiana, F. A. Panizzolo, K. G. Holt and C. J. Walsh, "Varying negative work assistance at the ankle with a soft exosuit during loaded walking", Journal of neuroengineering and rehabilitation **14**, 1, 62 (2017).

Manfredi, L. and A. Cuschieri, "A Wireless Compact Control Unit (WiCCU) for Untethered Pneumatic Soft Robots", in "IEEE International Conference on Soft Robotics (RoboSoft)", (2019).

Martini, E., S. Crea, A. Parri, L. Bastiani, U. Faraguna, Z. McKinney, R. Molino-Lova, L. Pratali and N. Vitiello, "Gait training using a robotic hip exoskeleton improves metabolic gait efficiency in the elderly", Scientific reports **9**, 1, 1–12 (2019).

Meeker, C., S. Park, L. Bishop, J. Stein and M. Ciocarlie, "Emg pattern classification to control a hand orthosis for functional grasp assistance after stroke", IEEE International Conference on Rehabilitation Robotics pp. 1203–1210 (2017).

Merletti, R. and P. Di Torino, "Standards for reporting emg data", J Electromyogr Kinesiol **9**, 1, 3–4 (1999).

Miller-Jackson, T., R. F. Natividad and C. Yeow, "Simplifying soft robots through adhesive-backed fabrics", in "2019 2nd IEEE International Conference on Soft Robotics (RoboSoft)", pp. 834–839 (IEEE, 2019).

Miller-jackson, T., R. F. Natividad and C. Yeow, "Simplifying Soft Robots Through Adhesive-backed Fabrics * Type Type C", in "IEEE International Conference on Soft Robotics, (RoboSoft)", (2019a).

Miller-jackson, T. M., J. Li, R. F. Natividad and R. C. Yeow, "STAS : An Antagonistic Soft Pneumatic Actuator Assembly for High Torque Output *", in "IEEE International Conference on Soft Robotics, (RoboSoft)", (2019b).

Morales, R., F. J. Badesa, N. García-Aracil, J. M. Sabater and C. Pérez-Vidal, "Pneumatic robotic systems for upper limb rehabilitation", Medical and Biological Engineering and Computing **49**, 10, 1145–1156 (2011).

Mosadegh, B., P. Polygerinos, C. Keplinger, S. Wennstedt, R. Shepherd, U. Gupta, J. Shim, K. Bertoldi, C. Walsh and G. Whitesides, "Pneumatic networks for soft robotics that actuate rapidly", Advanced functional materials **24**, 15, 2163–2170 (2014).

Mueller, M. J., S. D. Minor, J. A. Schaaf, M. J. Strube and S. A. Sahrmann, "Relationship of plantar-flexor peak torque and dorsiflexion range of motion to kinetic variables during walking", Physical therapy **75**, 8, 684–693 (1995).

Murphy, P., G. Adolf, S. Daly, M. Bolton, O. Maurice, T. Bonia, C. Mavroidis and S. Yen, "Test of a customized compliant ankle rehabilitation device in unpowered mode", in "International Conference of the IEEE Engineering in Medicine and Biology Society, EMBC 2014", (2014).

Nalam, V., E. Adjei and H. Lee, "Quantification and modeling of 2d human ankle stiffness during standing balance", IEEE Transactions on Biomedical Engineering (TBME) (2020).

Nalam, V. and H. Lee, "Environment-dependent modulation of human ankle stiffness and its implication for the design of lower extremity robots", in "2018 15th International Conference on Ubiquitous Robots, UR 2018", pp. 112–118 (Institute of Electrical and Electronics Engineers Inc., 2018).

Nalam, V. and H. Lee, "Development of a two-axis robotic platform for the characterization of two-dimensional ankle mechanics", IEEE/ASME Transactions on Mechatronics **24**, 2, 459–470 (2019).

Natividad, R. and C. Yeow, "Development of a soft robotic shoulder assistive device for shoulder abduction", in "2016 6th IEEE International Conference on Biomedical Robotics and Biomechatronics (BioRob)", pp. 989–993 (IEEE, 2016).

Neckel, N. D., N. Blonien, D. Nichols and J. Hidler, "Abnormal joint torque patterns exhibited by chronic stroke subjects while walking with a prescribed physiological gait pattern", Journal of NeuroEngineering and Rehabilitation **5**, 1–13 (2008).

Niiyama, R., X. Sun, C. Sung, B. An, D. Rus and S. Kim, "Pouch Motors: Printable Soft Actuators Integrated with Computational Design", Soft Robotics **2**, 2, 59–70 (2015).

Nilsson, M., J. Ingvast, J. Wikander and H. von Holst, "The soft extra muscle system for improving the grasping capability in neurological rehabilitation", in "2012 IEEE-EMBS Conference on Biomedical Engineering and Sciences", pp. 412–417 (IEEE, 2012).

Noritsugu, T., "Pneumatic soft actuator for human assist technology", International Symposium on Fluid Power pp. 11–20 (2005).

Noritsugu, T., M. Takaiwa and D. Sasaki, "Power assist wear driven with pneumatic rubber artificial muscles", 15th International Conference on Mechatronics and Machine Vision in Practice, M2VIP'08 pp. 539–544 (2008).

Noritsugu, T., H. Yamamoto, D. Sasakil and M. Takaiwa, "Wearable power assist device for hand grasping using pneumatic artificial rubber muscle", in "SICE 2004 annual conference", vol. 1, pp. 420–425 (IEEE, 2004).

Nycz, C. J., M. A. Delph and G. S. Fischer, "Modeling and design of a tendon actuated soft robotic exoskeleton for hemiparetic upper limb rehabilitation", in "2015 37th Annual International Conference of the IEEE Engineering in Medicine and Biology Society (EMBC)", pp. 3889–3892 (IEEE, 2015).

Oguntosin, V., W. S. Harwin, S. Kawamura, S. J. Nasuto and Y. Hayashi, "Development of a wearable assistive soft robotic device for elbow rehabilitation", IEEE International Conference on Rehabilitation Robotics (ICORR) **2015-Septe**, 747–752 (2015).

Ohno, A., H. Nabae and K. Suzumori, "Static analysis of powered low-back orthosis driven by thin pneumatic artificial muscles considering body surface deformation", in "2015 IEEE/SICE International Symposium on System Integration (SII)", pp. 39–44 (IEEE, 2015).

O'Neill, C. T., N. S. Phipps, L. Cappello, S. Paganoni and C. J. Walsh, "A soft wearable robot for the shoulder: Design, characterization, and preliminary testing", IEEE International Conference on Rehabilitation Robotics **02129**, 1672–1678 (2017).

Organization, W. H., *The world health report 2002: reducing risks, promoting healthy life* (World Health Organization, 2002).

Panizzolo, F. A., G. M. Freisinger, N. Karavas, A. M. Eckert-Erdheim, C. Siviy, A. Long, R. A. Zifchock, M. E. LaFiandra and C. J. Walsh, "Metabolic cost adaptations during training with a soft exosuit assisting the hip joint", Scientific reports **9**, 1, 1–10 (2019).

Park, H., J. Lan, J. Zhang, K. Chen and C. Fu, "Design of a soft wearable device for hip and knee extension assistance", in "2019 5th International Conference on Control, Automation and Robotics (ICCAR)", pp. 798–801 (IEEE, 2019a).

Park, S. and C. Park, "Suit-type wearable robot powered by shape-memory-alloy-based fabric muscle", Scientific Reports **9**, 1, 9157 (2019).

Park, S., L. M. Weber, L. Bishop, J. Stein and M. Ciocarlie, "Design and development of effective transmission mechanisms on a tendon driven hand orthosis for stroke patients", 2018 IEEE International Conference on Robotics and Automation (ICRA) pp. 2281–2287 (2018).

Park, S., J. Yi, D. Kim, Y. Lee, H. S. Koo and Y. L. Park, "A Lightweight , Soft Wearable Sleeve for Rehabilitation of Forearm Pronation and Supination", in "IEEE International Conference on Soft Robotics (RoboSoft)", (2019b).

Park, Y., B. Chen, N. Pérez-Arancibia, D. Young, L. Stirling, R. Wood, E. Goldfield and R. Nagpal, "Design and control of a bio-inspired soft wearable robotic device for ankle-foot rehabilitation.", Bioinspiration & biomimetics **9**, 1, 016007, URL `http://iopscience.iop.org/article/10.1088/1748-3182/9/1/016007` (2014a).

Park, Y., B. R. Chen, N. O. Pérez-Arancibia, D. Young, L. Stirling, R. J. Wood, E. C. Goldfield and R. Nagpal, "Design and control of a bio-inspired soft wearable robotic device for ankle-foot rehabilitation", Bioinspiration and Biomimetics **9**, 1 (2014b).

Park, Y., B. R. Chen, D. Young, L. Stirling, R. J. Wood, E. Goldfield and R. Nagpal, "Bio-inspired active soft orthotic device for ankle foot pathologies", in "IEEE International Conference on Intelligent Robots and Systems", pp. 4488–4495 (2011).

Park, Y., J. Santos, K. G. Galloway, E. C. Goldfield and R. J. Wood, "A soft wearable robotic device for active knee motions using flat pneumatic artificial muscles", in "Proceedings - IEEE International Conference on Robotics and Automation", pp. 4805–4810 (2014c).

Perez-Ibarra, J. C., A. Alarcon, J. Jaimes, F. Ortega, M. H. Terra and A. A. Siqueira, "Design and analysis of H-force control of a series elastic actuator for impedance control of an ankle rehabilitation robotic platform", in "Proceedings of the American Control Conference", (2017).

Perron, M., F. Malouin, H. Moffet and B. J. McFadyen, "Three-dimensional gait analysis in women with a total hip arthroplasty", Clinical Biomechanics **15**, 7, 504–515 (2000).

Petersen, K. H. and R. F. Shepherd, *Fluid-driven intrinsically soft robots* (Elsevier Ltd., 2018).

Poliero, T., C. Natali, M. Sposito, J. Ortiz, E. Graf, C. Pauli, E. Bottenberg, A. De Eyto and D. G. Caldwell, "Soft Wearable Device for Lower Limb Assistance: Assessment of an Optimized Energy Efficient Actuation Prototype", in "IEEE International Conference on Soft Robotics, (RoboSoft)", pp. 559 – 564 (2018).

Polygerinos, P., N. Correll, S. A. Morin, B. Mosadegh, C. D. Onal, K. Petersen, M. Cianchetti, M. T. Tolley and R. F. Shepherd, "Soft Robotics: Review of Fluid-Driven Intrinsically Soft Devices; Manufacturing, Sensing, Control, and Applications in Human-Robot Interaction", Advanced Engineering Materials **19**, 12 (2017).

Polygerinos, P., K. C. Galloway, E. Savage, M. Herman, K. O'Donnell and C. J. Walsh, "Soft robotic glove for hand rehabilitation and task specific training", Proceedings - IEEE International Conference on Robotics and Automation **2015-June**, June, 2913–2919 (2015).

Quinlivan, B., A. Asbeck, D. Wagner, T. Ranzani, S. Russo and C. J. Walsh, "Force Transfer Characterization of a Soft Exosuit for Gait Assistance", in "ASME International Design Engineering Technical Conferences & Computers and Information in Engineering Conference (IDETC/CIE)", p. V05AT08A049 (2015).

Quintero, H., R. Farris, C. Hartigan, I. Clesson and M. Goldfarb, "A powered lower limb orthosis for providing legged mobility in paraplegic individuals", Topics in spinal cord injury rehabilitation **17**, 1, 25–33 (2011).

Realmuto, J. and T. Sanger, "A robotic forearm orthosis using soft fabric-based helical actuators", in "IEEE International Conference on Soft Robotics (RoboSoft)", (2019).

Ren, Y., Y. Wu, C. Yang, T. Xu, R. L. Harvey and L. Zhang, "Developing a Wearable Ankle Rehabilitation Robotic Device for in-Bed Acute Stroke Rehabilitation", IEEE Transactions on Neural Systems and Rehabilitation Engineering (2017).

Roam, "Roam robotics", `https://www.roamrobotics.com/`, [Online]. Accessed: 18-April-2019 (209).

Robertson, M. and J. Paik, "New soft robots really suck: Vacuum-powered systems empower diverse capabilities", Science Robotics **2**, 9, eaan6357 (2017).

Robertson, M. A., "Modular soft pneumatic actuator system design for compliance matching", p. 236, URL `http://infoscience.epfl.ch/record/265405` (2019).

Robertson, M. A. and J. Paik, "Trunk postural tracking of assistive soft pneumatic actuator belt", in "Dynamic Walking Conference", (2016).

Ross, J. M. and R. Balasubramaniam, "Physical and neural entrainment to rhythm: human sensorimotor coordination across tasks and effector systems", Frontiers in human neuroscience **8**, 576 (2014).

Sankaranarayan, H., A. Gupta, M. Khanna, A. B. Taly and K. Thennarasu, "Role of ankle foot orthosis in improving locomotion and functional recovery in patients with stroke: A prospective rehabilitation study", Journal of neurosciences in rural practice **7**, 04, 544–549 (2016).

Sasaki, D., T. Noritsugu and M. Takaiwa, "Development of Active Support Splint driven by Pneumatic Soft Actuator (ASSIST)", in "IEEE International Conference on Robotics and Automation", (2005a).

Sasaki, D., T. Noritsugu, M. Takaiwa and H. Yamamoto, "Wearable power assist device for hand grasping using pneumatic artificial rubber muscle", in "SICE Annual Conference in Sapporo", pp. 655–660 (2005b).

Sawicki, G. S. and D. P. Ferris, "Powered ankle exoskeletons reveal the metabolic cost of plantar flexor mechanical work during walking with longer steps at constant step frequency", Journal of Experimental Biology **212**, 1, 21–31 (2009).

Schiele, A., "Ergonomics of exoskeletons: Objective performance metrics", in "EuroHaptics conference and Symposium on Haptic Interfaces for Virtual Environment and Teleoperator Systems", pp. 103–108 (IEEE, 2009).

Schiele, A. and F. C. van der Helm, "Influence of attachment pressure and kinematic configuration on phri with wearable robots", Applied Bionics and Biomechanics **6**, 2, 157–173 (2009).

Schmidt, K., M. Duarte, J E.and Grimmer, A. Sancho-Puchades, H. Wei, C. Easthope and R. Riener, "The myosuit: Bi-articular anti-gravity exosuit that reduces hip extensor activity in sitting transfers", Frontiers in Neurorobotics **11** (2017).

Schmitt, F., O. Piccin, L. Barbé and B. Bayle, "Soft Robots Manufacturing: A Review", Frontiers in Robotics and AI **5**, July (2018).

Sedal, A., M. Fisher, J. Bishop-Moser, A. Wineman and S. Kota, "Auxetic Sleeves for Soft Actuators with Kinematically Varied Surfaces", in "IEEE/RSJ International Conference on Intelligent Robots and Systems (IROS)", pp. 464–471 (2018).

Shi, B., X. Chen, Z. Yue, S. Yin, Q. Weng, X. Zhang, J. Wang and W. Wen, "Wearable ankle robots in post-stroke rehabilitation of gait: A systematic review", Frontiers in neurorobotics **13**, 63 (2019).

Shiota, K., S. Kokubu, T. V. Tarvainen, M. Sekine, K. Kita, S. Huang and W. Yu, "Enhanced kapandji test evaluation of a soft robotic thumb rehabilitation device by developing a fiber-reinforced elastomer-actuator based 5-digit assist system", Robotics and Autonomous Systems **111**, 20–30 (2019).

Siviy, C., I. Galiana, K. G. Holt, C. J. Walsh, F. A. Panizzolo, P. Malcolm, S. Crea, S. Lee and F. Saucedo, "Varying negative work assistance at the ankle with a soft exosuit during loaded walking", Journal of NeuroEngineering and Rehabilitation (2017).

Sovero, S., N. Talele, C. Smith, N. Cox, T. Swift and K. Byl, "Initial data and theory for a high specific-power ankle exoskeleton device", in "International Symposium on Experimental Robotics", pp. 355–364 (Springer, 2016).

Spector, W. D. and J. A. Fleishman, "Combining activities of daily living with instrumental activities of daily living to measure functional disability", The Journals of Gerontology Series B: Psychological Sciences and Social Sciences **53**, 1, S46–S57 (1998).

Sun, T., Y. Chen, T. Han, C. Jiao, B. Lian and Y. Song, "A soft gripper with variable stiffness inspired by pangolin scales, toothed pneumatic actuator and autonomous controller", Robotics and Computer-Integrated Manufacturing **61**, 101848 (2020).

Takakusaki, K., "Neurophysiology of gait: from the spinal cord to the frontal lobe", Movement Disorders **28**, 11, 1483–1491 (2013).

Tefertiller, C., K. Hays, J. Jones, A. Jayaraman, C. Hartigan, T. Bushnik and G. F. Forrest, "Initial outcomes from a multicenter study utilizing the indego powered exoskeleton in spinal cord injury", Topics in spinal cord injury rehabilitation **24**, 1, 78–85 (2018).

Teng, C., Z. Wong, W. Teh and Y. Z. Chong, "Design and development of inexpensive pneumatically-powered assisted knee-ankle-foot orthosis for gait rehabilitation-preliminary finding", in "2012 International Conference on Biomedical Engineering, ICoBE 2012", (2012).

Thakur, C., K. Ogawa, T. Tsuji and Y. Kurita, "Soft Wearable Augmented Walking Suit With Pneumatic Gel Muscles and Stance Phase Detection System to Assist Gait", IEEE Robotics and Automation Letters 2018 IEEE/RSJ International Conference on Intelligent Robots and Systems (IROS) **3**, 4, 4257–4264 (2018).

Thalman, C. M. and P. Artemiadis, "A review of soft wearable robots that provide active assistance: Trends, common actuation methods, fabrication, and applications", Wearable Technologies **1** (2020).

Thalman, C. M., M. Debeurre and H. Lee, "Entrainment during human locomotion using a soft wearable ankle robot", IEEE Robotics and Automation Letters (2021).

Thalman, C. M., T. Hertzell, M. Debeurre and H. Lee, "The multi-material actuator for variable stiffness (mavs): Design,modeling, and characterization of a soft actuator for lateral ankle support", in "2020 IEEE/RSJ International Conference on Intelligent Robots and Systems (IROS)", (IEEE, 2020a), [Accepted].

Thalman, C. M., T. Hertzell and H. Lee, "Toward a soft robotic ankle-foot orthosis (sr-afo) exosuit for human locomotion: Preliminary results in late stance plantarflexion assistance", in "2020 3rd IEEE International Conference on Soft Robotics (RoboSoft)", pp. 801–807 (IEEE, 2020b).

Thalman, C. M., J. Hsu, L. Snyder and P. Polygerinos, "Design of a soft ankle-foot orthosis exosuit for foot drop assistance", in "2019 International Conference on Robotics and Automation (ICRA)", pp. 8436–8442 (IEEE, 2019).

Thalman, C. M., Q. Lam, P. H. Nguyen, S. Sridar and P. Polygerinos, "A Novel Soft Elbow Exosuit to Supplement Bicep Lifting Capacity", in "2018 IEEE/RSJ International Conference on Intelligent Robots and Systems (IROS)", pp. 6965–6971 (2018).

Thalman, C. M. and H. Lee, "Design and validation of a soft robotic ankle-foot orthosis (sr-afo) exosuit for inversion and eversion ankle support", in "2019 International Conference on Robotics and Automation (ICRA)", (IEEE, 2020).

Thomas, J. and A. L. VANa, "Inflatable beams subjected to axial forces", (2019).

Tripanpitak, K., T. V. Tarvainen, I. Sonmezisik, J. Wu and W. Yu, "Design a soft assistive device for elbow movement training in peripheral nerve injuries", 2017 IEEE International Conference on Robotics and Biomimetics, ROBIO 2017 **2018-Janua**, 544–548 (2018).

Venesky, K., C. L. Docherty, J. Dapena and J. Schrader, "Prophylactic ankle braces and knee varus-valgus and internal-external rotation torque", Journal of athletic training **41**, 3, 239 (2006).

Wang, X., *Identification for a Class of Soft Pneumatic Actuators*, Ph.D. thesis, University of Surrey (United Kingdom) (2016).

Wearable Robotics Association, "Wearable robots", `http://www.wearablerobotics.com/wearable-robots/`, [Online]. Accessed: April-2020 (2015).

Webster, J. B. and B. J. Darter, "Principles of normal and pathologic gait", in "Atlas of Orthoses and Assistive Devices", pp. 49–62 (Elsevier, 2019).

Wehner, M., Y. Park, C. Walsh, R. Nagpal, R. Wood, T. Moore and E. Goldfield, "Experimental characterization of components for active soft orthotics", in "2012 4th IEEE RAS & EMBS International Conference on Biomedical Robotics and Biomechatronics (BioRob)", pp. 1586–1592 (IEEE, 2012).

Wehner, M., B. Quinlivan, P. M. Aubin, E. Martinez-Villalpando, M. Baumann, L. Stirling, K. Holt, R. Wood and C. Walsh, "A lightweight soft exosuit for gait assistance", in "Robotics and Automation (ICRA), 2013 IEEE International Conference on : date 6-10 May 2013.", p. 5863 (2013).

Whiteside, S., M. Allen, W. Barringer, W. Beiswenger, M. Brncick, T. Bulgarelli, C. Hentges and R. Lin, "Practice analysis of certified practitioners in the disciplines of orthotics and prosthetics", Alexandria (VA): American Board for Certification in Orthotics, Prosthetics, and Pedorthics (2007).

Wielgosz, C., J. Thomas and A. Le Van, "Mechanics of inflatable fabric beams", in "International Conference on Computational & Experimental Engineering and Sciences Honolulu, Hawaii, USA", (2008).

Wielgosz, C. and J.-C. Thomas, "Deflections of inflatable fabric panels at high pressure", Thin-walled structures **40**, 6, 523–536 (2002).

Wilkening, A., H. Stoppler and O. Ivlev, "Adaptive assistive control of a soft elbow trainer with self-Alignment using pneumatic bending joint", IEEE International Conference on Rehabilitation Robotics **2015-September**, 729–734 (2015).

Wing, K., J. V. Lynskey and P. R. Bosch, "Walking speed in stroke survivors: considerations for clinical practice", Topics in Geriatric Rehabilitation **28**, 2, 113–121 (2012).

Winter, A. and S. Sienko, "Biomechanics of below-knee amputee gait", Journal of Biomechanics **21**, 5, 361–367 (1988).

Winter, D. A., "Overall principle of lower limb support during stance phase of gait", Journal of biomechanics **13**, 11, 923–927 (1980).

Winter, D. A., "Energy generation and absorption at the ankle and knee during fast, natural, and slow cadences.", Clinical orthopaedics and related research , 175, 147–154 (1983).

Wirekoh, J. and Y.-L. Park, "Design of flat pneumatic artificial muscles", Smart Materials and Structures **26**, 3, 035009 (2017).

Wu, Q., X. Wang, F. Du and X. Zhang, "Design and control of a powered hip exoskeleton for walking assistance", International Journal of Advanced Robotic Systems (2015).

Xiloyannis, L., M.and Cappello, K. D. Binh, C. W. Antuvan and L. Masia, "Preliminary design and control of a soft exosuit for assisting elbow movements and hand grasping in activities of daily living", Journal of Rehabilitation and Assistive Technologies Engineering **4** (2017).

Yandell, M. B., B. T. Quinlivan, D. Popov, C. J. Walsh and K. E. Zelik, "Physical interface dynamics alter how robotic exosuits augment human movement: implications for optimizing wearable assistive devices", Journal of NeuroEngineering and Rehabilitation **14**, 1, 40 (2017).

Yandell, M. B., J. R. Tacca and K. E. Zelik, "Design of a low profile, unpowered ankle exoskeleton that fits under clothes: Overcoming practical barriers to widespread societal adoption", IEEE Transactions on Neural Systems and Rehabilitation Engineering (2019).

Yandell, M. B., D. M. Ziemnicki, K. A. McDonald and K. E. Zelik, "Characterizing the comfort limits of forces applied to the shoulders, thigh and shank to inform exosuit design", Plos one **15**, 2, e0228536 (2020).

Yang, H. D., *Modeling and Analysis of a Novel Pneumatic Artificial Muscle and Pneumatic Arm Exoskeleton*, Ph.D. thesis, Virginia Tech (2017).

Yang, H. D. and A. T. Asbeck, "A new manufacturing process for soft robots and soft/rigid hybrid robots", in "2018 IEEE/RSJ International Conference on Intelligent Robots and Systems (IROS)", pp. 8039–8046 (IEEE, 2018).

Yang, X., T. Huang, H. Hu, S. Yu, S. Zhang, X. Zhou, A. Carriero, G. Yue and H. Su, "Spine-inspired continuum soft exoskeleton for stoop lifting assistance", IEEE Robotics and Automation Letters **4**, 4, 4547–4554 (2019).

Yap, H., J. Goh and R. Yeow, "rehabilitation applications", in "6th European conference of the International Federation for Medical and Biological Engineering", pp. 367–370 (Springer, 2015a).

Yap, H. K., P. M. Khin, T. Koh, Y. Sun, X. Liang, J. H. Lim and C. Yeow, "A fully fabric-based bidirectional soft robotic glove for assistance and rehabilitation of hand impaired patients", IEEE Robotics and Automation Letters **2**, 3, 1383–1390 (2017).

Yap, H. K., J. H. Lim, F. Nasrallah, J. C. Goh and R. C. Yeow, "A soft exoskeleton for hand assistive and rehabilitation application using pneumatic actuators with variable stiffness", in "2015 IEEE international conference on robotics and automation (ICRA)", pp. 4967–4972 (IEEE, 2015b).

Yariott, J. M., "Fluid actuator", US Patent 3,645,173 (1972).

Yeung, M., K.-M. Chan, C. So and W. Yuan, "An epidemiological survey on ankle sprain.", British journal of sports medicine **28**, 2, 112–116 (1994).

Young, A. J. and D. P. Ferris, "State of the art and future directions for lower limb robotic exoskeletons", IEEE Transactions on Neural Systems and Rehabilitation Engineering **25**, 2, 171–182 (2017).

Zhang, X., A. Shtarbanov, J. Zeng, V. K. Chen, M. Bove, P. Maes and J. Rekimoto, "Bubble: Wearable assistive grasping augmentation based on soft inflatables", in "Extended Abstracts of the 2019 CHI Conference on Human Factors in Computing Systems", pp. 1–6 (2019a).

Zhang, Y., R. J. Kleinmann, K. J. Nolan and D. Zanotto, "Preliminary validation of a cable-driven powered ankle–foot orthosis with dual actuation mode", IEEE Transactions on Medical Robotics and Bionics **1**, 1, 30–37 (2019b).

Zhao, H., J. Jalving, R. Huang, R. Knepper, A. Ruina and R. Shepherd, "A helping hand: Soft orthosis with integrated optical strain sensors and emg control", IEEE Robotics and Automation Magazine **23**, 3, 55–64 (2016).

Zhu, M., W. Adams and P. Polygerinos, "Carpal Tunnel Syndrome Soft Relief Device for Typing Applications", in "ASME Design of Medical Devices Conference (DMD 2017)", p. V001T03A003 (2017).